ANALYSIS OF COHESIVE AND FRICTIONAL RESISTANCE OF SOIL AS RELATED TO THE GEOMETRICAL CONFIGURATION OF THE PARTICLES

By

T. J. CHUNG

Engineering Diploma
Seoul National University
Seoul, Korea
1949

Master of Science
Oklahoma State University
Stillwater, Oklahoma
1962

Submitted to the Faculty of the Graduate School of
the Oklahoma State University
in partial fulfillment of the requirements
for the degree of
DOCTOR OF PHILOSOPHY
May, 1965

ANALYSIS OF COHESIVE AND FRICTIONAL RESISTANCE OF SOIL AS RELATED TO THE GEOMETRICAL CONFIGURATION OF THE PARTICLES

Thesis Approved:

L. V. Parker
Thesis Adviser

John F. Stone

Roger L. Handlers

J. W. Gillespie

J. W. Bragg
Dean of the Graduate School

Dedicated

to

My Mother

ACKNOWLEDGEMENT

The writer, in completing the final phase of his work, could never express in mere words his deep appreciation to his adviser, Professor J. V. Parcher, for his untiring assistance throughout the course of this research investigation. Gratitude is expressed also to Professor Parcher for his valuable suggestions in editing of the final manuscript.

Appreciation is further extended to Professors J. F. Stone, R. L. Flanders, J. W. Gillespie, and all Civil Engineering faculty members for their helpful interest during his academic work.

The writer wishes to thank P. G. Wilson and A. L. Harris for their efficient and timely assistance in providing modifications of the equipment used in this research.

The writer, finally, acknowledges his thanks to Mrs. Grayce S. Wynd for her careful typing of this dissertation.

TABLE OF CONTENTS

Chapter		Page
I.	INTRODUCTION	1
II.	SHEAR STRENGTH AND STRUCTURE OF SOILS	
	Mechanics of Interparticle Forces	5
	Activating Force under Applied Loads . . .	7
III.	EXPERIMENTAL PROCEDURES AND DATA	
	Principles of Cohesion-Friction-Strain Tests	20
	Preparation of Specimens	23
	Description of Equipment	26
	Placement of Specimens	28
	Mathematical Solutions	28
	Presentation of Data	31
IV.	DISCUSSION OF RESULTS	
	Summary of Experimental Data	33
	Evaluation of Cohesive and Frictional Forces	35
V.	CONCLUSIONS AND RECOMMENDATIONS	
	Conclusions	46
	Recommendations	56
	A SELECTED BIBLIOGRAPHY	57

LIST OF TABLES

Table		Page
I.	Load Increments, Anisotropic Consolidation	59
II.	Summary of Specimens, Anisotropically Consolidated	60
III.	Computation Sheet for CFS Triaxial Test.	61
IV.	Specimen Data, Anisotropically Consolidated	62
V.	Specimen Data, Isotropically Consolidated.	63
VI.	Specimen Data, Harvard-Mold Compacted.	64
VII.	Summary of c and ϕ at Selected Strains, Anisotropically Consolidated Specimens.	65
VIII.	Summary of c and ϕ at Selected Strains, Isotropically Consolidated Specimens.	66
IX.	Summary of c and ϕ at Selected Strains, Harvard-Mold Compacted Specimens	67
X.	CFS Test Data Sheet, AN-H-1-1.	68

LIST OF PLATES

Plate		
1.	Anisotropic Consolidation Apparatus.	70
2.	Isotropic Consolidation Apparatus.	71
3.	Modified CFS Test Equipment.	72

LIST OF FIGURES

Figure			Page
1.	Potential Energy Barrier with and without Shearing Force		8
2.	Grain Size Distribution of Permian Red Clay (Hydrometer Analysis)		29
3.	Modified CFS Test Equipment, Schematic Diagram		73
4.	Geometry of Mohr Circle at Any Strain		74
5.	Stress-Strain, CFS Test,	AN-H-1-1	75
6.	" "	AN-H-1-2	76
7.	" "	AN-H-1-3	77
8.	" "	AN-H-2-1	78
9.	" "	AN-H-2-2	79
10.	" "	AN-M-1-1	80
11.	" "	AN-M-1-2	81
12.	" "	AN-M-2-1	82
13.	" "	AN-M-2-2	83
14.	" "	AN-L-1-1	84
15.	" "	AN-L-1-2, 3	85
16.	" "	AN-L-2-1	86
17.	" "	AN-L-2-2	87
18.	" "	AN-L-2-3	88
19.	" "	IS-H-1-1	89

Figure			Page
20.	Stress-Strain, CFS Test,	IS-H-1-2	90
21.	" "	IS-H-1-3	91
22.	" "	IS-H-2-1	92
23.	" "	IS-H-2-2, 3	93
24.	" "	IS-M-1-1	94
25.	" "	IS-M-1-2	95
26.	" "	IS-M-2-1	96
27.	" "	IS-M-2-2	97
28.	" "	IS-M-2-3	98
29.	" "	IS-L-1-1	99
30.	" "	IS-L-1-2	100
31.	" "	IS-L-2-1	101
32.	" "	IS-L-2-2	102
33.	" "	IS-L-2-3	103
34.	" "	HC-H-1	104
35.	" "	HC-H-2	105
36.	" "	HC-H-3	106
37.	" "	HC-M-1	107
38.	" "	HC-M-2	108
39.	" "	HC-M-3	109
40.	" "	HC-L-1	110
41.	" "	HC-L-2	111
42.	" "	HC-L-3	112
43.	c and ϕ versus Strain	AN-H-1	113
44.	" "	AN-M-1	114

Figure Page

45. c and ϕ versus Strain AN-L-1 115
46. " " AN-H-2 116
47. " " AN-M-2 117
48. " " AN-L-2 118
49. " " IS-H-1 119
50. " " IS-M-1 120
51. " " IS-L-1 121
52. " " IS-H-2 122
53. " " IS-M-2 123
54. " " IS-L-2 124
55. " " HC-H 125
56. " " HC-M 126
57. " " HC-L 127
58. c and ϕ versus Water Content, Anisotropic, 1% Strain 128
59. " " " 5% " 129
60. " " " 10% " 130
61. " " Isotropic, 1% " 131
62. " " " 5% " 131
63. " " " 10% " 132
64. " " Compacted, 1% " 132
65. " " " 5% " 133
66. " " " 10% " 133
67. c and ϕ versus Dry Density, Anisotropic 1% " 134
68. " " " 5% " 135
69. " " " 10% " 136

Figure Page

70. c and ϕ versus Dry Density, Isotropic, 1% Strain . 137

71. " " " 5% " . 137

72. " " " 10% " . 138

73. " " Compacted, 1% " . 138

74. " " " 5% " . 139

75. " " " 10% " . 139

TABLE OF SYMBOLS USED

B	$\ln\left(s\lambda'\frac{KT}{h}\right)$
c	Cohesion, in Kg/sq.cm.
D	Energy required for dilation expressed as distance displaced under the action of a unit interparticle normal force, in cm.
E	Energy that must be supplied to cause rupture or sliding of an interparticle contact (commonly termed "activation energy"), in dyne-cm.
e	Void ratio.
f	Shearing force applied to interparticle contact, in dynes.
h	Planck's constant, in dyne-cm-sec.
k	Boltzman constant, in dyne-cm/°K.
P	Mean interparticle normal force.
p(E)	Probability of an energy state equal to or greater than E.
S	Soil structure as represented by the number of particle contacts per unit cross-sectional area.
s	Number of interparticle contacts per unit length along a chain of particles in the axial direction.
T	Temperature, in °K.
u	Pore pressure, in Kg/sq.cm.
W	Water content, in %.
ϵ	Strain, in mm.
$\dot{\epsilon}$	Strain rate, in mm/min.
λ	Distance between successive interparticle equilibrium position, in cm.
λ'	Component in axial direction of displacement due to a single bond rupture, in cm.
ν	Frequency of bond activation.

σ Normal stress at failure, in Kg/sq.cm.

$\bar{\sigma}$ Effective normal stress, in Kg/sq.cm.

σ_1 Total axial stress in triaxial compression, in Kg/sq.cm.

$\bar{\sigma}_1$ Effective axial stress in triaxial compression, in Kg/sq.cm.

σ_3 Total lateral stress in triaxial compression, in Kg/sq.cm.

$\bar{\sigma}_3$ Effective lateral stress in triaxial compression, in Kg/sq.cm.

τ Shearing resistance, in Kg/sq.cm.

Φ $\frac{D}{\lambda}$

ϕ Angle of internal friction, in deg.

CHAPTER I

INTRODUCTION

The most fundamental properties of soil in the practice of soil mechanics and foundation engineering are probably the ability of the soil to resist shear and the characteristics which it exhibits when undergoing deformation under applied loads. These properties are important in the design of foundation structures, sloping embankments, and highway subgrades.

The basic equation that governs the shear strength of the soil was first proposed by C. A. Coulomb, and is expressed:

$$\tau = c + \sigma \tan \phi \qquad (1)$$

where τ is the shearing resistance, c represents the cohesion, σ denotes the normal stress on the shearing plane, and ϕ is usually called the angle of internal friction.

In the presence of water which carries a part of the applied pressure, it has been established by Terzaghi (1) that the applied normal stress σ must be corrected for the pressure in the pore water such that the effective stress

$$\bar{\sigma} = \sigma - u \qquad (2)$$

in which u represents the pore pressure.

It becomes obvious from the Coulomb equation that the shear strength of the soil is related to two components, the cohesion and the angle of internal friction. Unfortunately, however, these two components of the shear strength of the soil are not constants for a given type of soil but are so greatly influenced by numerous environmental conditions that investigation of the fundamental nature of the cohesion and friction is of vital importance in understanding the strength and stress-deformation characteristics of soil.

The conventional viewpoint generally adopted by engineers supposes that a clay owes most of its strength to cohesion and little to internal friction, and that the reverse is true in the case of sand.

A very nearly isotropic material such as metal derives its strength from strong bonds between the atoms of which it consists. A closely knit network or array of atoms in the metal establishes strong bonds due to the electrostatic forces operating between them. Under applied stress the atoms normally will be displaced relative to each other by the resulting shearing deformations. During this process resistance is entirely due to the bonds of the atoms, not to the physical interference between individual atoms undergoing displacement.

In the case of soil, however, interest is centered on the interaction of discrete, crystalline particles, each

of which consists of an orderly array of strongly bonded atoms and molecules. The physico-chemical forces operating between these discrete particles are similar in nature to those bonding the molecules of the crystals, but are generally much weaker. Thus, in soils, resistance to shear under normal stress results not only from the bonds in the double layer between the particles, but also from the interference of the particles with respect to each other. One of these two components may have negligible effects, depending on the gradation, mineralogical composition, or various environmental conditions. Therefore, it is reasonable to assume that there are essentially two different sources of energy being simultaneously activated during deformations: the cohesion due to the physico-chemical forces, and the resistance due to interference between the individual particles as influenced by dilatancy and the normal stress acting on the shearing planes. Finally, these two factors are, to a great extent, believed to be dependent upon the geometrical orientation of the particles as the soil mass is being sheared.

The purpose of this dissertation is, therefore, to attempt to clarify the relationships between the structure (or the geometric orientation of the soil grains) and the two components of the shear strength of the soil.

A special technique convenient to evaluate magnitudes of the cohesion and the angles of internal friction at all

desired ranges of strain has been developed by Schmertmann and Osterberg (2). This procedure, called the cohesion-friction-strain (or CFS) triaxial compression test, has been adopted for this study, and necessary modifications of the equipment and test procedures worked out.

The triaxial specimens were prepared from the Permian Red Clay which has been anisotropically and isotropically consolidated or compacted with a kneading tamper.

The formulation of theories based on the physico-chemical viewpoints and the rate processes, presentation of the experimental data and comparison of theories with the experimental results follow in the subsequent chapters.

CHAPTER II

SHEAR STRENGTH AND STRUCTURE OF SOILS

Mechanics of Interparticle Forces

The crystalline structure of clay particles is such that the particles usually occur in nature as tiny platelets, either flat or curled, or as small needle-like crystals. It is a generally accepted theory that these particles possess negative charges on their lateral surfaces, and that the edges of the particles are positively charged. A surface electrical charge is common for almost all materials naturally occurring as colloidal size particles. Because of this surface charge, a swarm of ions of opposite charge is attracted toward the surface. These ions along with the dipolar water molecules take up positions in the space adjacent to the surface, forming the diffuse part of the double layer.

Verwey and Overbeck (5) attribute attraction between particles to Van der Waals-London forces. London (5) (1930) explained on the basis of wave mechanics that universal attractive forces act between all atoms, molecules, ions, etc. They are the result of the mutual influence of

the electronic motion between the atoms. The charge fluctuations in one atom induce a temporary dipole in the second atom, and vice versa, resulting in a mutual attraction. It has been shown (5) that the force of this attraction between atoms is proportional to d^{-7}, where d is the distance between two atoms. The attraction between two flat plates then consists of the summation of the attractive forces for all atomic pairs formed by two atoms belonging to different particles. Equations developed through this summation process have shown (5) that the repulsive force due to ionic diffusion tendencies dissipates much more slowly with increasing distance between particles than does the force between two atoms. The resulting Van der Waals force of attraction may be shown to be approximately proportional to d^{-3}.

It is well known that the electrostatic attractive force between two charges of opposite sign varies as d^{-2}. For the case of attraction between a particle surface and a particle edge, each containing many charges, the attractive force will dissipate much more slowly with distance than do the Van der Waals forces. Once flocculation has set in, however, and particles are arranged in an edge-to-face orientation, the electrostatic edge-to-face attractive forces will not increase appreciably as the clay is consolidated. This is because initially the edges are about as close to the faces as they can get. The effect of

volume decreases after flocculation is gradually to shift the particles into a more efficient packing. When this occurs, the spacing and the arrangement becomes more favorable for attraction by Van der Waals forces and other attractions, such as cation linkages, water dipole linkages and hydrogen bonding.

Rutledge (12) (1948) and Leonards (12) (1955) demonstrated that, other things being equal, the closer the average particle spacing, the greater the shear strength. In the closer particle spacing the attractive force is greater. If two clay particles are spaced some distance apart, the effect of a reduction in spacing on the shear strength would depend on whether the net increase in the electric potential is positive or negative. For a given average particle spacing (given void ratio) it may be concluded that the more nearly parallel the adjacent particles are, the weaker the soil, due to the fact that attractive forces dissipate with powers of the distance between them. This may be illustrated by observing that when one particle is tilted with respect to another, the gain in attractive force between the near halves more than offsets the loss of force between the far halves.

Activating Force under Applied Loads

The shear strength of the soil may be mathematically correlated with the physico-chemical forces operating be-

tween the particles. It is assumed (7) that an activation energy is required to displace the particles from their equilibrium positions to new positions. Sources of this energy are the externally applied loads and the thermal energy present in the material. The displacement progresses at a rate determined by the frequency with which particles may acquire sufficient energy to overcome the energy barriers between equilibrium positions. To explain the energy-displacement relation, the theory of rate processes (7) is used, and Fig. 1 was reproduced from Ref. 7 (p. 482).

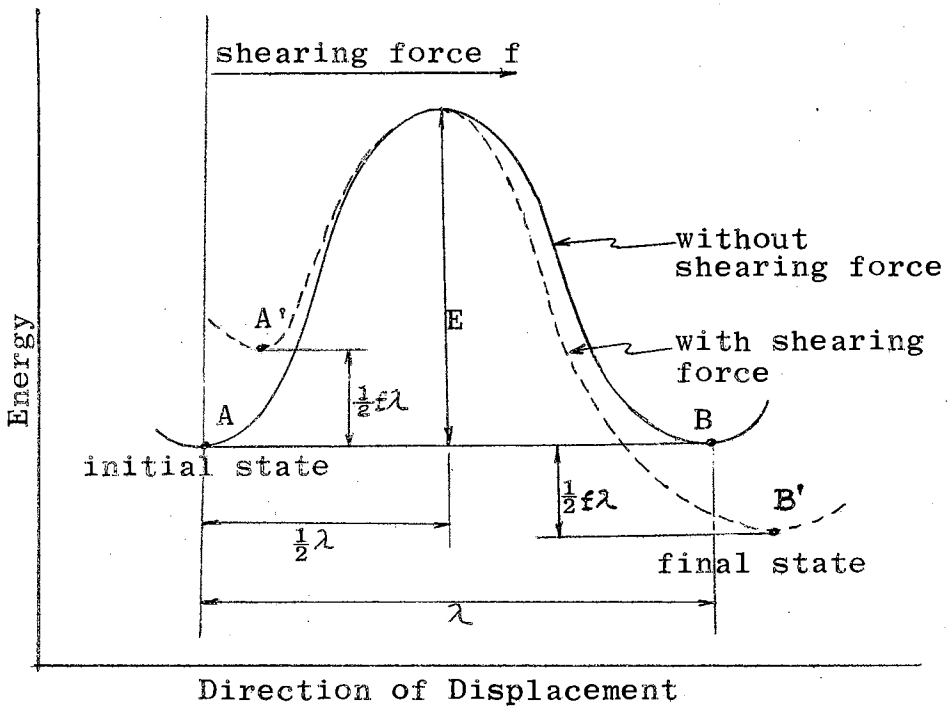

Fig. 1 - Potential Energy Barrier with and without Shearing Force

The shearing force, f, is applied to the system in which E represents energy (commonly termed the activation energy)

that must be supplied to cause rupture or sliding along an interparticle contact from an initial position of equilibrium, A, in the direction of the shearing force. The energy necessary to cause the displacement from A to A' is $f\frac{\lambda}{2}$ where λ represents the distance between two successive equilibrium positions. In this process the force, f, has lowered the potential barrier by an amount $f\frac{\lambda}{2}$ in the direction of the force and raised it an amount $f\frac{\lambda}{2}$ in a direction opposite to the force.

In order to determine the frequency of activation for movement to the right, an introduction of the Maxwell-Boltzman equation (7) is necessary. It states that the probability of an energy state equal to or greater than E, denoted by P(E), assumes the form

$$P(E) = (\text{const}) \exp\left(\frac{-E}{KT}\right) \tag{3}$$

where

K = Boltzman constant

T = Absolute temperature

KT = Average thermal energy of the interparticle contact zone atoms

The quantity $\exp\left(\frac{-E}{KT}\right)$ represents, at any instant, either the probability of any one interparticle bond being activated for rupture or the fraction of the total number of bonds that would provide sufficient energy to surmount the energy barrier for rupture. The work of Glasstone, Laidler and Eyring (7) indicates that the constant in Eq. 3 may be taken as unity.

It may also be shown (7) that the mean frequency of thermal oscillations at normal temperature is

$$\frac{KT}{h} \simeq 6 \times 10^{12} \text{ sec}^{-1}$$

where h is Planck's constant.

Thus the frequency of activation, ν , per second is

$$\nu = \frac{KT}{h} \exp \left(- \frac{E}{KT}\right) \tag{4}$$

Referring then to Fig. 1, the frequency of activation for movement to the right becomes

$$\nu_{(R)} = \frac{KT}{h} \exp \left[\frac{-\left(E - \frac{f\lambda}{2}\right)}{KT}\right] \tag{5}$$

and to the left

$$\nu_{(L)} = \frac{KT}{h} \exp \left[\frac{-\left(E + \frac{f\lambda}{2}\right)}{KT}\right] \tag{6}$$

The net frequency of displacements to the right is therefore

$$\nu_{(R)} - \nu_{(L)} = \frac{KT}{h} \left\{ \exp \left[\frac{-\left(E - \frac{f\lambda}{2}\right)}{KT}\right] - \exp \left[\frac{-\left(E + \frac{f\lambda}{2}\right)}{KT}\right] \right\}$$

or

$$\nu_{(R)} - \nu_{(L)} = \frac{KT}{h} \left\{ \exp \left(\frac{-E}{KT}\right) \left[\exp \left(\frac{f\lambda}{2KT}\right) - \exp \left(\frac{-f\lambda}{2KT}\right)\right] \right\}$$

or

$$\nu_{(R)} - \nu_{(L)} = \frac{2KT}{h} \exp \left(\frac{-E}{KT}\right) \sinh \left(\frac{f\lambda}{2KT}\right) \tag{7}$$

On the basis of Eq. 7, which represents the frequency of rupture of a single bond, Mitchell related the deformation rate under a triaxial state of stress to the frequency of bond ruptures per unit length along a chain of particles.

Denoting

σ_1, $\bar{\sigma}_1$ = total and effective major principal stress, respectively;

σ_3, $\bar{\sigma}_3$ = total and effective minor principal stress, respectively;

ϵ = axial compressive strain;

$\dot{\epsilon}$ = axial compressive strain rate;

λ' = component, in the axial direction, of displacement due to a single bond rupture (average value);

S = a structural factor equal to the number of interparticle contacts per unit area of cross section; and

s = a structural factor equal to the number of interparticle contacts per unit length along a chain of particles in the axial direction;

and assuming, on the average, that a displacement λ' occurs in the axial direction each time a bond ruptures, the total displacement per unit time per unit length or the rate of axial strain, $\dot{\epsilon}$, becomes

$$\dot{\epsilon} = s\lambda' \left(\nu_{(R)} - \nu_{(L)} \right) \tag{8}$$

Substituting Eq. 7 in Eq. 8,

$$\dot{\epsilon} = 2s\lambda' \frac{KT}{h} \exp\left(- \frac{E}{KT} \right) \sinh\left(\frac{f\lambda}{2KT} \right) \tag{9}$$

It appears reasonable to assume that the mean value of f is proportional to the deviator stress and inversely pro-

portional to the number of interparticle contacts per unit of area on which the deviator stress acts.

Therefore,

$$f = \text{const} \frac{\sigma_1 - \sigma_3}{S} \tag{10}$$

Since the maximum displacement occurs along a plane on which the shearing stress is almost equal to the maximum shearing stress, which is $\frac{\sigma_1 - \sigma_3}{2}$, the constant in Eq. 10 may be taken as $\frac{1}{2}$. Eq. 10 thus becomes

$$f = \frac{\sigma_1 - \sigma_3}{2S} \tag{11}$$

Let us assume that the lowest typical value of deviator stress which would cause a significant deformation may be approximately .5 Kg/ sq cm or about $.5 \times 10^6$ dynes/sq.cm. At a given void ratio, the number of particles per unit volume of soil should decrease with about the third power of the mean particle diameter. The number of contacts should be approximately in proportion to the number of particles. For pure montmorillonites, the number of particles per gram approximates (8) between 4.5×10^{13} and 55×10^{13}. Therefore, 50×10^{13} particles per gram of clay will be assumed for the probable maximum value of S, producing the probable minimum value of f. Under stresses normally encountered it is unlikely that such a material would have a void ratio much less than 2.0. At this void ratio one cubic centimeter of soil would contain .33 cu cm or .89 grams of clay (assuming the specific gravity to be 2.70). Use of these assumptions indicates that there would be about 45×10^{13}

clay particles per cubic centimeter.

Assuming the particles to be uniformly distributed throughout the volume, the number contacting any unit area would be the two-thirds power of the number of particles per unit volume, or 5.9×10^9. If each clay particle develops four stress carrying contacts with adjacent particles, then the average number of interparticle contacts per unit area, S, becomes approximately 25×10^9. Therefore f may be calculated as follows:

$$f = \frac{\sigma_1 - \sigma_3}{2S} = \frac{.5 \times 10^6}{2(25 \times 10^9)}$$

The surfaces of silicate minerals are composed of oxygen atoms, and the distance between successive equilibrium positions separated by an energy barrier, λ, would be approximately 2.8 Å if it is assumed that a bond ruptures or slips following the displacement of one oxygen atom whose diameter is 2.8 Å. The distance between successive interatomic valleys is also 2.8 Å.

Values of K and T are

$K = 1.38 \times 10^{-16}$ dyne-cm per ^oK

$T = 300\ ^oK\ (27^oC)$

thus

$$\frac{f\lambda}{2KT} = \frac{(1 \times 10^{-5})(2.8 \times 10^{-8})}{(2)(1.38 \times 10^{-16})(300)} = 3.36$$

The value of $\frac{f\lambda}{2KT}$ is probably a lowest possible value. Therefore,

$$\sinh \frac{f\lambda}{2KT} = \frac{1}{2}\left[\exp\left(\frac{f\lambda}{2KT}\right) - \exp\left(\frac{-f\lambda}{2KT}\right)\right] \simeq \frac{1}{2}\exp\left(\frac{f\lambda}{2KT}\right)$$

Since $\exp\left(\frac{-f\lambda}{2KT}\right)$ cannot exceed $\exp^{-3.36} = 0.035$, it may be neglected. Under practical conditions $\frac{f\lambda}{2KT}$ could be far greater than 3.36, but never less. Therefore,

$$\dot{\epsilon} = s\lambda'\frac{KT}{h}\exp\left(\frac{-E}{KT}\right)\exp\left(\frac{f\lambda}{2KT}\right) \qquad (12)$$

If the mean interparticle contact normal force is P, the dilatancy contribution is assumed to be proportional to P. Denoting

E_o = Physico-chemical component of bond energy,

D = Energy required for dilation expressed as distance displaced under the action of a unit interparticle normal force,

the mean activation energy that is required to cause contact failure may be expressed as

$$E = E_o + P\,D \qquad (13)$$

For any plane through the soil the average interparticle contact normal force, P, is equal to the normal effective stress divided by the number of contacts per unit area. Unfortunately, however, the normal stresses vary for planes of different orientation. It will be assumed that the average interparticle contact normal force is given by the mean effective stress, which is

$\frac{\bar{\sigma}_1 + 2\ \bar{\sigma}_3}{3}$ for the triaxial condition.

Thus P becomes

$$P = \frac{\bar{\sigma}_1 + 2\bar{\sigma}_3}{3S} \tag{14}$$

Substituting Eq. 13 in Eq. 12 gives

$$\dot{\epsilon} = s\lambda' \frac{KT}{h} \exp\left[-\frac{(E_o + P\,D)}{KT}\right] \exp\left(\frac{f\lambda}{2KT}\right) \tag{15}$$

If logarithms are taken of both sides of Eq. 15,

$$\ln\dot{\epsilon} = \ln\left(s\lambda' \frac{KT}{h}\right) - \frac{E_o}{KT} - \frac{PD}{KT} + \frac{f\lambda}{2KT} \tag{16}$$

Solution of Eq. 16 for f gives

$$f = \frac{2KT}{\lambda} \ln\dot{\epsilon} + \frac{2E_o}{\lambda} - \frac{2KT}{\lambda} \ln\left(s\lambda' \frac{KT}{h}\right) + \frac{2PD}{\lambda} \tag{17}$$

Substituting for f and P from Eqs. 11 and 14 yields

$$\sigma_1 - \sigma_3 = \frac{4SKT}{\lambda} \ln\dot{\epsilon} + \frac{4SE_o}{\lambda} - \frac{4SKT}{\lambda} \ln\left(s\lambda' \frac{KT}{h}\right) + \frac{4}{3\lambda}\left(\bar{\sigma}_1 + 2\bar{\sigma}_3\right)D \tag{18}$$

The following substitutions are used for simplification:

$$B = \ln\left(s\lambda' \frac{KT}{h}\right) \simeq \text{constant}$$

$$\Phi = \frac{D}{\lambda}$$

The final form for the shearing resistance then becomes

$$\zeta = \frac{\sigma_1 - \sigma_3}{2} = \frac{2}{\lambda} S\left(E_o + KT\ln\dot{\epsilon} - KTB\right) + \frac{2\left(\bar{\sigma}_1 + 2\bar{\sigma}_3\right)}{3}\Phi \tag{19}$$

Inspection of Eq. 19 indicates that the shearing resistance consists of two major parts. The evaluation of each item is given below.

(1) $\frac{2}{\lambda} S \quad (E_o + KT \ln\dot{\epsilon} - KT\,B)$

For constant conditions of λ, S, E_o, K, T, $\dot{\epsilon}$ and B, the above expression assumes a constant value and may be considered as analogous to the term c in the Coulomb equation.

Since the variation in cohesion appears to depend on the numerous explicit factors of the above expression, the contribution of these factors to the cohesion should be analyzed by suitable evaluation of each term.

(a) $\frac{2}{\lambda}$ - the cohesive resistance is inversely proportional to the distance between successive interparticle equilibrium positions.

(b) S - the main contributor appears to be the soil structure as represented by the number of interparticle contacts per unit cross-sectional area.

(c) E_o - the cohesive resistance is proportional to the physico-chemical forces.

(d) $KT\ln\dot{\epsilon}$ - this term becomes negative when the axial rate of strain is less than 1 cm per cm per second. As the strain rate increases $KT\ln\dot{\epsilon}$ becomes less negative, leading to increased resistance. For a constant rate of strain, however, an increase in temperature causes a decrease in resistance because of the generally negative character of $\ln\dot{\epsilon}$.

(e) -KTB - this term represents a temperature dependent modification or correction to terms (c) and (d). It is obvious that the cohesive resistance decreases as the temperature rises.

(2) $$\frac{\bar{\sigma}_1 + 2\,\bar{\sigma}_3}{3}\,\Phi$$

This term appears similar to $\sigma \tan \phi$ in the Coulomb equation. It represents the effective stress dependent or

frictional contribution to shearing resistance. This quantity is inversely proportional to λ, the distance between successive interparticle equilibrium positions. The influence on the dilatancy component D, together with λ, would suggest some effects of structure on the frictional resistance. It should be noted that the frictional resistance is independent of the strain rate (9) and temperature, except for possible temperature influence on the friction coefficient Φ.

If it is assumed that the shear stress is applied at constant temperature, structure and strain rate, and since the mean normal effective stress, $\frac{\bar{\sigma}_1 + 2\bar{\sigma}_3}{3}$, is not appreciably different from the effective stress on the failure plane, Eq. 19 may be rewritten as

$$\tau = \frac{\sigma_1 - \sigma_3}{2} = C + \bar{\sigma}_m \tan\phi \qquad (20)$$

where

$$C = \frac{2}{\lambda} S\,(E_o + KT \ln\dot{\epsilon} - KT\,B)$$

$$\bar{\sigma}_m = \frac{\bar{\sigma}_1 + 2\,\bar{\sigma}_3}{3}$$

$$\tan\phi = \Phi$$

Eq. 20 is practically the same as Eq. 1

$$\tau = C + \sigma \tan\phi \qquad (1)$$

which is the Coulomb equation.

In summary, it is reasoned that the activating forces under applied loads as analyzed by the rate process theory consist of cohesive and frictional resistance. The acti-

vating forces depend on:

(1) S, the soil structure as represented by the number of interparticle contacts per unit cross-sectional area, (2) E_o, the physico-chemical contribution to bond energy, or the true cohesion expressed as an energy, in dyne - cm, (3) $\dot{\epsilon}$, the axial strain rate in triaxial compression, (4) D, the energy required for dilation, expressed as distance displaced under the action of a unit interparticle normal force, (5) λ, the distance between successive interparticle equilibrium positions, (6) λ', the axial component of displacement due to a single bond rupture, (7) $\mathbf{S}$, number of interparticle contacts per unit length along a chain of particles in the axial direction, (8) K, Boltzman constant, (9) T, temperature, and (10) h, Planck's constant.

It is further reasoned that, for a given soil, all variables with the exceptions of strain rate and temperature, are influenced by the geometrical configuration of the soil particles, hence the soil structure or fabric. The orientation of the individual particles (parallel or random) and the denseness of their packing would, therefore, exert decisive influences on the shearing resistance of the soil. With the present state of knowledge, a satisfactory numerical calculation of each term in Eq. 19 is difficult, if not impossible. The two major components, c and ϕ, of the shear strength of the soil as character-

ized in Eq. 20 (the Coulomb equation) can, however, be experimentally determined not only at failure but also at all desired ranges of strain. A correlation of the structure of the soil with activating forces under applied loads based on Eq. 20 constitutes the main part of the research which comprises this dissertation. The results are presented in Chapters III and IV.

The effects of chemical additives on the cohesive and frictional resistance are beyond the scope of this dissertation.

CHAPTER III

EXPERIMENTAL PROCEDURES AND DATA

Principles of Cohesion-Friction-Strain Tests

The CFS tests employed in this research are based on the validity of the Mohr-Coulomb failure criteria and were first demonstrated by Schmertmann and Osterberg (2).

The CFS tests may be accomplished using either one or two soil specimens. In either case, by adjustment of the pore pressure, a set of two stress-strain curves is obtained, one representing a preassigned high value of the major effective principal stress and the other representing a preassigned low value. The minor total principal stress and the rate of axial strain are held constant throughout the test.

In each of the tests conducted during this study the specimen was consolidated in a triaxial cell under a hydrostatic pressure of 5 Kg/sq.cm. prior to application of a deviator stress. For the first 8 hr. period of the consolidation a back pressure of .5 Kg/sq.cm. was applied through a burette connected to the specimen through porous stones at the top and bottom to insure a high degree of saturation (hopefully, 100%). The back pressure was then removed and the hydrostatic pressure allowed to remain for the rest of the period of consolidation. Approximately 24 hours were considered

adequate for 100% consolidation. After this time no rise of the water level in the burette was observed, which would indicate that the excess pore pressure inside the specimen had dissipated. Except for a few cases, the one specimen test procedure was adopted for the entire research program, and the major effective principal stress high curve and low curve were obtained simultaneously by a curve hopping technique (2).

To insure an initial uniform distribution of the pore pressure in the one specimen test employing the curve hopping technique, a pore pressure of 1 Kg/sq.cm. was applied for about an hour prior to application of the deviator stress. An axial load was then applied at a constant rate of strain of such low magnitude that only a negligible rise of pore pressure due to the strain occurs within the drained specimen. At low strains the deviator stress increased very rapidly. As the strain developed, the pore pressure was increased to maintain a major effective principal stress of 4 Kg/sq.cm. Guidance for the control of $\bar{\sigma}_1$ was provided by the equation

$$\bar{\sigma}_1 = \sigma_d + \bar{\sigma}_3 - u$$

where $\bar{\sigma}_1$ represents the major effective principal stress, σ_d indicates the deviator stress, and $\bar{\sigma}_3$ is the minor total principal stress. The continuous adjustment of the pore pressure to maintain a constant value of $\bar{\sigma}_1$, in accordance with the preceding equation assures that the

locus of all points of the deviator stress represents the $\bar{\sigma}_1$ high curve. When the $\bar{\sigma}_1$ low curve was obtained in the single specimen test, the pore pressure was increased after the strain reached about 0.5%. The increase was that required to reduce $\bar{\sigma}_1$ to 3 Kg/sq.cm., the preassigned low value. As soon as pore pressure equilibrium is reached, the locus of all points of the deviator stress coincides with the $\bar{\sigma}_1$ low curve. After sufficient points were obtained to establish a portion of the $\bar{\sigma}_1$ low curve, the pore pressure was then decreased by 1 Kg/sq.cm. so that the deviator stress again would represent the $\bar{\sigma}_1$ high curve.

At each stage of the test, after the establishment of pore pressure equilibrium corresponding to either the $\bar{\sigma}_1$ high or low curve, the pore pressure was continuously adjusted to produce a portion of one of the two curves of the preassigned $\bar{\sigma}_1$ values. Thus, by hopping back and forth between the two curves coinciding with the $\bar{\sigma}_1$ high and low conditions, it was possible to obtain enough points on both curves to permit the relationship between deviator stress and axial strain to be plotted for both conditions. When the strain reached approximately 12%, the test was discontinued and computations were carried out to determine the values of the cohesion and the angle of internal friction at all desired ranges of strain. A description of the procedural details of the work, including preparation of specimens, description of the equipment, placement of

specimens, and the mathematical solutions of the test results are given in the following sections.

Preparation of Specimens

The soil used in this research was Permian Red Clay, pulverized and screened through a #50 sieve. The grain size distribution is shown in Fig. 3. The liquid limit is 40.5 and the plastic limit 15, giving a plasticity index of 25.5. The specific gravity of the Permian Red Clay is 2.72.

Since the correlation of the orientation of the soil particles with the strength characteristics of the specimens had to be established, the specimens were prepared in such ways as to produce various fashions of particle arrangements. In this manner it was possible to provide specimens having quite different initial orientations of the particles comprising the soil structure.

In this research the specimens consisted of three major categories of soil particle arrangement corresponding to three different methods of sample preparation. The three methods used were anisotropic consolidation, isotropic consolidation, and kneading compaction.

(1) Group I - Specimens Anisotropically Consolidated

A quantity of dry soil weighing 1400 grams was thoroughly mixed with 910 grams of distilled water. The slurry (water content 65%) was poured into a Proctor mold (with collar) having an inside diameter of 4" and a height of 7".

A vacuum of 12" mercury or .37 Kg/sq.cm. was applied to accelerate initial drainage of water through the bottom porous stone over a period of two days. The Proctor mold was then placed in the consolidation loading machine as shown in Plate 1. Loads were applied through a wooden block (weighing 0.47 Kg) bearing on the top porous stone. Approximately 100% consolidation was attained for each increment of load prior to application of the next increment. The incremental magnitudes shown in Table I were selected to produce the desired final water contents of 20% for Group I specimens, 15% for Group II specimens, and 10% for Group III specimens.

At the end of the final increment of loading, the consolidated specimens were extruded by use of a hydraulic jack. From each Proctor mold sample blocks were removed from which triaxial test cylinders 2.816" in height and 1.375" in diameter were prepared using a trimming lathe. Four of these were cut parallel to the direction of drainage, and two of them perpendicular to this direction. Enough Proctor molds were used so that at least three nearly identical specimens were prepared, as identified in Table II. All specimens were wrapped with aluminum foil and coated with micro-crystalline wax to prevent moisture loss during storage in the humid room.

(2) Group II - Specimens Isotropically Consolidated

The soil-water mixtures were prepared in the same way as for the specimens anisotropically consolidated. The slurry was placed in a rubber membrane 0.0085" thick, made of liquid latex. The membrane was manufactured using a glass bottle $3\frac{1}{2}$" in diameter and 10" in height as a dipping mandrel. The open end of the rubber membrane containing the slurry was then fitted and secured to a drained pedestal 4" in diameter, which rested at the bottom of a triaxial cell 8" in diameter and 13" high. A photograph of the arrangement is shown in Plate 2. Drainage was provided through a drilled hole leading from a porous stone recessed in the pedestal. Compressed air was introduced inside the triaxial cell, acting on the surface of the water which nearly filled the cell. The rubber membrane containing the specimen slurry was held upright by supporting rods. Pressures of 4 Kg/sq.cm., 5 Kg/sq.cm., and 7 Kg/sq.cm. were variously applied in an effort to produce water contents of about 20%, 15%, and 10% at the end of the consolidation period. However, under the highest pressure and longest duration of pressure application the lowest water content obtained was 13.9%. The water content of each sample was roughly judged by the amount of water collected in a container connected to the drainage tube. The number of specimens and the methods of trimming were the same as for the specimens anisotropically consolidated, except that the specimens cut perpendicular to the

direction of drainage were 2.79" long instead of 2.816". Specimen identification and storage were the same as for Group I except that the prefix IS was used instead of AN in the specimen number.

(3) Group III - Compacted Specimens

The Harvard miniature compaction apparatus was employed to produce the specimens of Group III. The molding water contents used were 20%, 15%, and 10%. The compaction mold was 2.816" in height and 1.375" in diameter. Compaction was performed by placing the soil in three layers, each of which was subjected to 25 blows of a $\frac{1}{4}$" diameter plunger which was spring-loaded to produce a 20 pound load. The extruded specimens were wrapped and stored in the same way as were those of Groups I and II. The Group III specimens were identified by the Prefix HC, and the codes for specimens cut parallel or perpendicular to the direction of drainage were omitted.

Description of Equipment

The equipment used for the cohesion-friction-strain triaxial tests consisted of two parts, the unconfined compression test machine and the triaxial compression cell. A Karol-Warner Model KW550 unconfined compression machine, of 500 pounds capacity, was modified to accommodate a triaxial cell 4" in diameter and 8.2" in height between the loading

table and the proving ring. A separate strain gage was used instead of the automatic recording device. The loading table was powered by a Karol-Warner Model DV2 electric variable speed drive (1/6 hp A.C. motor). Because of loss of power at low motor speeds, a gear reductor with a ratio of 900:1 was connected between the motor and the main gear train of the unconfined compression machine. With this arrangement a constant rate of strain of about .0061 mm per minute could be maintained during the compression of the specimens. For this rate of strain the motor was operated at approximately 550 rpm. The force exerted by the motor with this angular velocity was believed to be sufficient to overcome disadvantages due to deformation of the proving ring as the specimen was compressed during loading. This belief was substantiated by frequent spot checks for the rate of strain throughout the compression period. The rate of strain was found to be uniform at all ranges of strain when the 900:1 ratio gear reductor was used. On the other hand, when a gear reductor of 50:1 ratio was tried, the rate of strain was found to vary slightly, being lower at small strains than at large strains.

Two triaxial cells were employed in these tests, one being used for the 24 hour consolidation under hydrostatic pressure, while the other was being used for the axial loading phase of the CFS test. A photograph of the combined apparatus is shown in Plate 3, and a schematic diagram of the setup is given in Fig. 4.

Placement of Specimens

The specimen ready to be tested was removed from the waxed aluminum foil. In order to facilitate drainage, a maximum of three wicks of saturated wool threads were installed longitudinally through the cylindrical specimen by using a high-carbon steel needle 3/32" in diameter. Four pieces of filter paper about $\frac{1}{2}$" in width were also placed longitudinally on the surface of the specimen to expedite drainage. The cylinder was then enclosed in a rubber membrane approximately 0.0065" in thickness to prevent contact of the specimen with the water in the triaxial compression cell. The ends of the rubber membrane were fitted to the cap and pedestal of the triaxial cell, and secured with elastic bands. The pore pressure was applied by admitting compressed air to a burette containing water. The water in the burette formed a continuous system with the pore water of the specimen, being linked by drainage lines leading from porous stones in the cap and pedestal at either end of the specimen.

Mathematical Solutions

The two curves representing the high and low values of $\bar{\sigma}_1$ were drawn by connecting those points on the stress-strain plots which corresponded to an equilibrium condition of the pore pressure. These two curves were used in calcu-

lating the values of cohesion and the angles of internal friction at all desired ranges of strain. The known values from the tests include the magnitudes of the deviator stress on both the $\bar{\sigma}_1$ high and low curves at any desired strain (σ_{d1} and σ_{d2} respectively), and the major effective principal stresses at higher and lower ranges ($\bar{\sigma}_{1(H)}$ and $\bar{\sigma}_{1(L)}$ respectively).

The geometry of the Mohr circle at any strain is shown in Fig. 2:

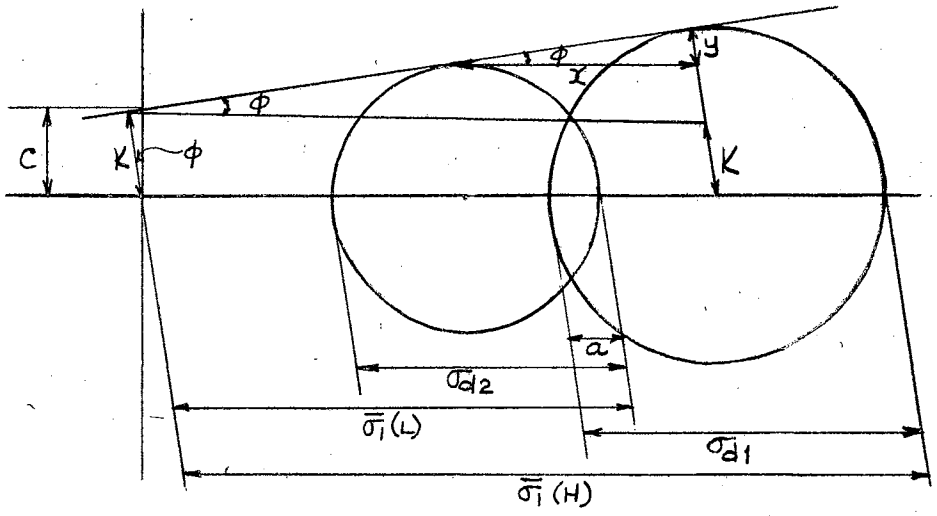

Fig. 2 - Geometry of Mohr Circle at Any Strain

Let $\Delta\sigma_d = \sigma_{d1} - \sigma_{d2}$

and $\Delta\bar{\sigma}_1 = \bar{\sigma}_{1(H)} - \bar{\sigma}_{1(L)}$

then, from the geometry, the angle of internal friction at any strain is

$$\phi = \sin^{-1}\frac{y}{x} = \sin^{-1}\frac{\frac{1}{2}(\sigma_{d1} - \sigma_{d2})}{\frac{1}{2}(\sigma_{d1} + \sigma_{d2}) - a}$$

$$= \sin^{-1}\frac{\frac{1}{2}\Delta\sigma_d}{\frac{1}{2}(\sigma_{d1} + \sigma_{d2}) - (\sigma_{d1} - \Delta\bar{\sigma}_1)}$$

$$= \sin^{-1}\frac{\frac{1}{2}\Delta\sigma_d}{\frac{1}{2}(\sigma_{d2} - \sigma_{d1}) + \Delta\bar{\sigma}_1} = \sin^{-1}\frac{\frac{1}{2}\Delta\sigma_d}{-\frac{1}{2}\Delta\sigma_d + \Delta\bar{\sigma}_1}$$

or

$$\phi = \sin^{-1}\frac{\Delta\sigma_d}{2\Delta\bar{\sigma}_1 - \Delta\sigma_d} \tag{21}$$

The cohesion c at any strain using the $\bar{\sigma}_1$ high curve can be calculated as follows:

$$C = \frac{K}{\cos\phi} = \frac{\frac{\sigma_{d1}}{2} - (\bar{\sigma}_1(H) - \frac{\sigma_{d1}}{2})\sin\phi}{\cos\phi}$$

$$= \frac{\sigma_{d1}}{2\cos\phi} - (\bar{\sigma}_1(H) - \frac{\sigma_{d1}}{2})\tan\phi$$

If the angular functions are derived from Eq. 21

$$C = \frac{\sigma_{d1}}{2}\frac{2\Delta\bar{\sigma}_1 - \Delta\sigma_d}{\sqrt{(2\Delta\bar{\sigma}_1 - \Delta\sigma_d)^2 - (\Delta\sigma_d)^2}}$$

$$-(\bar{\sigma}_1(H) - \frac{\sigma_{d1}}{2})\frac{\Delta\sigma_d}{\sqrt{(2\Delta\bar{\sigma}_1 - \Delta\sigma_d)^2 - (\Delta\sigma_d)^2}}$$

$$= \frac{2\Delta\bar{\sigma}_1\sigma_{d1} - \Delta\sigma_d\sigma_{d1} - 2\bar{\sigma}_1(H)\Delta\sigma_d + \sigma_{d1}\Delta\sigma_d}{2\sqrt{(2\Delta\bar{\sigma}_1 - \Delta\sigma_d)^2 - (\Delta\sigma_d)^2}}$$

or

$$C = \frac{\Delta\bar{\sigma}_1\sigma_{d1} - \bar{\sigma}_1(H)\Delta\sigma_d}{2\sqrt{\Delta\bar{\sigma}_1(\Delta\bar{\sigma}_1 - \Delta\sigma_d)}} \tag{22}$$

If the $\bar{\sigma}_1$ low curve is used, the expression for the cohesion at any strain becomes

$$c = \frac{\Delta\bar{\sigma}_1 \ \sigma_{d2} - \bar{\sigma}_{1(L)} \ \Delta\sigma_d}{2\sqrt{\Delta\bar{\sigma}_1 \ (\Delta\bar{\sigma}_1 - \Delta\sigma_d)}} \tag{23}$$

An illustration of the use of test data in computing c and ϕ for different magnitudes of strain is given in Table III, for specimen No. AN-H-1-1.

Presentation of Data

In most of the laboratory tests the one specimen curve hopping technique was utilized on specimens prepared as previously described. Additional tests were performed in which the longitudinal drainage conditions were varied by omitting both the wicks and the external filter strips. The technique was varied to include some tests in which no pore pressure was applied during the axial loading, and some for which the preliminary consolidation period was extended well into the range of secondary compression. As a check on results obtained using the curve hopping technique, other tests were made using two nearly identical specimens to provide the high and low curve data independently.

The basic data for all specimens, including rate of strain used, number of drains, water content, dry density, void ratio and degree of saturation, are presented in Tables IV, V, and VI.

Computed values of c and ϕ at selected strains are given in Tables VII, VIII and IX, along with summaries of certain other properties of the specimens.

The step-by-step procedure for recording the data of the one specimen test for specimen No. AN-H-1-1 is shown in Table X as an illustration.

The stress-strain curves for all specimens are presented in Figures 5 through 42.

Calculations similar to those shown in Table III were carried out for all specimens, and the values of cohesion and the angles of internal friction plotted against the strain. These results are given in Figures 43 through 57.

The values of cohesion and the angles of internal friction were averaged for identical samples and plotted against the water content. These relationships are shown in Figures 58 through 66.

Similar plots were prepared in which the abscissal water content was replaced by the dry density. The results are presented in Figures 67 through 75.

CHAPTER IV

DISCUSSION OF RESULTS

Summary of Experimental Data

An inspection of the cohesion and friction versus strain plots presented in Figures 43 through 57 reveals that all specimens attain peak values of cohesion at about 1 - 2% strain, and that a decrease of cohesion after 1 - 2% strain is accompanied by an increase of the friction angle.

Wide variations in values of the cohesion and friction angles corresponding to a given strain were produced by different water contents and by different dry densities or void ratios. These variations are graphically illustrated in Figures 58 through 75.

For anisotropically consolidated specimens of low water content the cohesion is high at low strain, but is drastically reduced at high strain (see Figures 58 through 60). As the water content increases, the cohesion gradually decreases at low strain, but increases at high strain. At an intermediate strain of about 5% the variations of cohesion are negligible for all water contents ranging from about 12% to 22%.

For compacted specimens (Figures 64 to 66) the highest cohesion and friction occur at water contents of about 13%, although for a given strain there is little variation in c and ϕ over a range of water contents from 10% to 16%.

Since anisotropically or isotropically consolidated saturated specimens have dry densities inversely proportional to the water contents, the cohesion-dry density curves or the friction angle-dry density curves (Figures 67 to 72) are essentially of the same character as the cohesion-water content curves or the friction angle-water content curves. However, in the case of the compacted specimen (Figures 73 to 75) because of the intermediate water contents at which the maximum dry density results, the curves based on dry density bear no resemblance to those based on water content.

The anisotropically consolidated specimens which were oriented with their axes perpendicular to the direction of drainage produced higher cohesion and lower friction angles than those whose axes were oriented parallel to the direction of drainage. This effect was more pronounced at higher strains with specimens of higher water contents or lower dry densities. The isotropically consolidated specimens do not show such differences to any significant degree.

Evaluation of Cohesive and Frictional Forces

(1) Cohesive Forces

Since the electrostatic forces decrease with the square of distance and the Van der Waals forces with about the third power of the distance between particles, the bond energy which is responsible for cohesion is governed chiefly by the points of nearest proximity of particles rather than by the average spacing. It should be expected, then, that denser packing of the soil particles would result in greater cohesive forces; and that for a given density the greater cohesion would be associated with a random orientation of the particles. Experimental evidence obtained during this investigation supports the theoretical predictions given above as follows:

(1) Compacted specimens exhibited their greatest cohesion at water contents slightly less than optimum. If it were not for the effect of the more random orientation at lower water contents, the maximum cohesion would be expected to correspond with the optimum, where the density is greatest.

(2) Both isotropically and anisotropically consolidated specimens have more cohesion at the lower water contents (higher densities), illustrating the effect of denseness of packing.

(3) The anisotropically consolidated specimens tested with their axes perpendicular to the direction of

drainage (or direction of applied load) during consolidation exhibited higher cohesion than did those whose axes were oriented parallel to the direction of consolidation loading. This is believed to reflect the fact that some parallelism of particle arrangement tends to develop along planes perpendicular to the consolidating load, resulting in a closer particle spacing perpendicular to planes which are more nearly parallel with the failure surfaces of specimens sheared with their axes oriented along these planes.

(4) The isotropically consolidated specimens indicate little effect on the cohesion of axis orientation with respect to direction of drainage during consolidation. Since the particle orientation is random in these specimens, the cohesion is apparently an isotropic property. This is in contrast with its apparent anisotropy in anisotropically consolidated specimens.

The above factors are associated with denseness of packing, orientation of the particles, and the edge-to-planar surface attraction. It is reasonable to assume that it would not take much strain to activate the bond energy due to the edge-to-planar surface attraction forces, and that the resulting cohesive resistance would be greater at low water contents for which the particle spacings are comparatively small.

As the strain develops, the cohesive forces are rap-

idly reduced for specimens of initially low water content. For specimens of high water content the decrease in cohesion with increasing strain is not nearly so pronounced. This is probably due to the fact that the initial cohesion is lower, due to the increased particle spacing, than that of low water content specimens; and that the edge-to-planar surface contacts may be partly restored as deformation takes place.

A difference in orientation of particles between isotropically and anisotropically consolidated specimens exists, such that the greater degree of orientation or more parallelism is produced in anisotropically consolidated specimens. It is postulated that, even at high water contents, a random orientation of the particles may persist when the specimen is subjected to the isotropical consolidation. Drainage of the water, of course, would not appreciably affect the degree of orientation, but would result in a closer packing of the particles with a random orientation still maintained. This is probably the reason that the isotropically consolidated specimens do not exhibit variations of cohesion and the friction angles with changes in the water contents as appreciably as do anisotropically consolidated specimens.

(2) Frictional Forces

The frictional forces are activated by physical contacts of grains and depend upon the effects of dilatancy and the normal stress acting on the shearing planes. It

seems likely that such forces cannot be very effective until the bond energy has been exhausted or reduced during the initial ranges of the strain. Individual particles must be displaced over relatively great distances in order to bring about any significant increases in the number of physical contacts of the particles. These conditions can be achieved more favorably at low water contents and at greater densities, and this fact has been demonstrated by the experimental data. Whenever the bond energy is predominant (for whatever reason) the frictional forces are retarded. An inspection of Fig. 58 - Friction-Water Content, and Fig. 67 - Friction-Dry Density, indicates that at low water contents and low strains the cohesion is predominant. The particles are prevented from moving into contact and, therefore, the frictional forces are small. An increase of water at this low strain would cause a reduction of the bond energy, thus creating more favorable conditions for the particles to move under applied load. However, significant frictional resistance will not develop until activated by sufficient strain. A further increase of water gradually reduces the cohesion except for the case of the specimens consolidated anisotropically. At the present time no reason can be advanced for the apparently anomalous behavior of these latter specimens.

There is no compensating increase in frictional resistance corresponding to the general decrease in cohesion at high water contents. Within those ranges of strain

where frictional resistance is substantial the effect of additional water is to reduce the friction angle. Since these higher water contents are associated with lower dry densities, the reduction of the friction angle is probably explained by the lesser energy of dilation.

Validity of Curve Hopping Technique

The locus of points representing the magnitudes of the deviator stress, σ_d, is controlled by changes in the rate of strain $\dot{\epsilon}$, pore pressure u, permeability k, minor total principal stress σ_3, and major effective principal stress $\bar{\sigma}_1$. This relation is expressed generally as

$$\sigma_d = f(\dot{\epsilon}, u, k, \sigma_3, \bar{\sigma}_1) \tag{24}$$

With the rate of strain, permeability, and minor total principal stress held constant, a partial differentiation of Eq. 24 with respect to time gives

$$\frac{\partial \sigma_d}{\partial t} - \frac{\partial f}{\partial u}\frac{\partial u}{\partial t} - \frac{\partial f}{\partial \bar{\sigma}_1}\frac{\partial \bar{\sigma}_1}{\partial t} = 0 \tag{25}$$

Eq. 25 expresses the stress paths without the limitations of maximum and minimum values of the preassigned major effective principal stresses as the specimen undergoes deformations with constant rate of strain, permeability, and minor total principal stress.

In order that changes of the deviator stress with respect to strain, ϵ, may be specified along with the pore pressure and the major effective principal stress, the

quantities, $\frac{\partial \sigma_d}{\partial \epsilon}$, $\frac{\partial \sigma_d}{\partial u}$, and $\frac{\partial \sigma_d}{\partial \bar{\sigma}_1}$ can be related with some values P, Q, R, and S indicating functions of all variables of ϵ, u, $\bar{\sigma}_1$, and σ_d. A consideration of all these values would lead to the following quasi-linear partial differential equation:

$$P(\epsilon, u, \bar{\sigma}_1, \sigma_d)\frac{\partial \sigma_d}{\partial \epsilon} + Q(\epsilon, u, \bar{\sigma}_1, \sigma_d)\frac{\partial \sigma_d}{\partial u} + R(\epsilon, u, \bar{\sigma}_1, \sigma_d)\frac{\partial \sigma_d}{\partial \bar{\sigma}_1} = S(\epsilon, u, \bar{\sigma}_1, \sigma_d) \qquad (24)$$

It should be noted that any or all of P, Q, R, and S are functions of the dependent variable σ_d in addition to the independent variables ϵ, u, and $\bar{\sigma}_1$. For this reason either an increase or decrease in pore pressure must be restricted to maintain $\bar{\sigma}_1$ within the limited ranges of the preassigned effective major principal stresses in order that the influence of the quasi-linearity may be kept minimum.

The magnitudes of the two values of $\bar{\sigma}_1$, high and low, should be selected so that the deformation of the specimen will attain a reasonable magnitude within a practicable time of testing. Since adjustment of the pore pressure is the operation used for manipulation between the high and low values of $\bar{\sigma}_1$, the difference between the two preassigned $\bar{\sigma}_1$ values must be set at some fraction of σ_3.

In this research σ_3 was 5 Kg/sq.cm., $\bar{\sigma}_{1(H)}$ 4 Kg/sq.cm., and $\bar{\sigma}_{1(L)}$ 3 Kg/sq.cm., providing the difference between $\bar{\sigma}_{1(H)}$ and $\bar{\sigma}_{1(L)}$ equal to 1 Kg/sq.cm., which is 20% of σ_3. For satisfactory

results the pore pressure changes must be restricted to a limited range, operating along relatively small segments of the rebound and recompression branches. This precaution assures that the time dependent stress paths will remain more closely linear, with any gross change of structure reasonably minimized.

With this requirement met, the additional experiments conducted to evaluate further the validity of the curve-hopping technique consisted of:

(1) two specimen tests

(2) tests with external longitudinal filter strips, but without drainage threads

(3) tests without both filter strips and drainage threads

(4) tests without application of pore pressure

(5) tests with consolidation having been advanced well into the secondary stage.

Evaluations of these special tests are given in the following sections:

(1) Two specimen tests

The two groups of specimens used for these tests are AN-L-1-2 and AN-L-1-3 (anisotropically consolidated, low water content, parallel to drainage), and IS-H-2-2 and IS-H-2-3 (isotropically consolidated, high water, perpendicular to drainage). Test results are shown in Figures 45 and 52.

Two specimen tests for AN-L-1 resulted in slightly increased values of cohesion and decreased values of the friction angles for all ranges of strain as compared with those obtained by one specimen tests. However, in view of the magnitudes of deviations of these properties for any two supposedly identical specimens, it is considered that the results of the two specimen tests for AN-L-1 have sufficiently validated the results of one specimen tests dealing with specimens of similar low water contents (about 13%).

In the case of IS-H-2, the two specimen test results are in very close agreement with the results of one specimen tests, probably due to the favorable conditions available for more rapid distribution of the pore pressure changes throughout the pore spaces of the specimens.

In the two specimen tests, the deviator stress paths are operated on only one preassigned value of the major effective stress. This, of course, would imply that errors originating from quasi-linearity of the stress paths are much smaller than in the case of the one specimen tests. If the pore pressures are continuously adjusted to maintain $\bar{\sigma}_1$ constant, all error due to quasilinearity would disappear.

(2) Tests with external longitudinal filter strips, but without drainage threads

These tests were performed on specimens, AN-L-2 (anisotropically consolidated, low water, perpendicular to

drainage), and IS-L-2 (isotropically consolidated, low water, perpendicular to drainage). See Figures 48 and 54.

It was found to be possible to use the curve hopping technique on specimens without drainage wicks, even for the denser, low water content (about 13%) specimens. However, the results obtained are not at all dependable. Without the drainage wicks the values of cohesion are extremely high and the friction angles unreasonably low as compared with tests in which wicks were used. This, of course, indicates that the pore pressure would never reach equilibrium (for the rate of strain employed) within soil specimens of such low permeability as those tested.

(3) Tests without filter strips and drainage threads

Specimen No. IS-H-1 (isotropically consolidated, high water content, parallel to drainage) was used in this test, for which the results are given in Fig. 49.

The results of this test demonstrate that the Permian Red Clay passing a #50 sieve is sufficiently permeable for the curve hopping technique to be employed without the use of either filter paper or drainage threads, provided that the density is about as low as that corresponding to a water content of 21%.

At large strain, the values of cohesion and the angle of internal friction were slightly larger and smaller, respectively, than those values obtained from tests employing both the filter paper and drainage threads. In general,

the differences are not great enough to be of serious, practical concern.

(4) Tests without application of pore pressure

The triaxial test was performed with the same axial rate of strain as in the CFS tests, approximately .006 mm/min. In order to determine whether or not any appreciable pore pressure would develop for such low rates of strain, specimen No. IS-M-2-3 (isotropically consolidated, medium water, perpendicular to drainage) was tested. The results are shown in Fig. 28. Attempts were made to measure the pore pressure by observing the rise of water level in the capillary tube inside the burette and equalizing the pressure below and above the water level. Such attempts, even if unsuccessful, indicated that the magnitude of the pore pressure which develops under the stated rate of strain is negligible when drainage threads are used.

(5) Tests with consolidation having been advanced well into the secondary stage

Any effect on the results of the CFS test due to the consolidation period having been extended beyond 24 hours would be related to the effects of secondary consolidation. If such effects exist, they would probably be present even if 100% primary consolidation had not been quite attained during a 24 hour period.

Specimen No. IS-H-1 (isotropically consolidated, high water content, parallel to drainage) was used to determine

the influence, if any, of the secondary consolidation. The result of this test is shown in Fig. 43. Slightly higher values of cohesion and lower values of friction were obtained at large strain (about the same effects observed in the tests without the drainage threads), suggesting that slight hardening due to further consolidation simulated the condition of lower permeability. Again, the effects are too small to be of practical importance, in routine testing, though the differences do emphasize the necessity for consistent procedures in research investigations.

CHAPTER V

CONCLUSIONS AND RECOMMENDATIONS

Conclusions

1. General

Effects of water contents, dry density, void ratio, anisotropic consolidation, isotropic consolidation, and kneading compaction of the Permian Red Clay on the cohesive and frictional resistance have been investigated. Effects of these factors are closely related to the geometrical configurations of the soil particles. A summary of knowledge as evidenced both theoretically and experimentally concerning the cohesive and frictional resistance correlated to the various environmental conditions leads to a confirmation of the results of other investigators (2)(3)(4)(14), but also establishes new concepts previously unknown to the writer in view of all publications available to this date. The summarized conclusions are given in the following subsections.

a. Relation between the Cohesion and the Friction Angles

During shearing deformations the cohesive and frictional resistance develop independently. In general, the cohesion attains a peak value at low strain, about

1 - 2%, whereas the angle of internal friction increases steadily as the strain develops. These results support the theoretical approach based on the rate process, which leads to an equation analogous to the Coulomb equation. The equation contains the two components of shearing resistance, cohesion and friction, expressed in fundamental and rather complex forms. According to this equation the cohesive force, derived mainly from bond energy, should be strongest at the points of shortest distance between the particles, thus requiring very small strain for activation. The activation of the frictional force, on the other hand, is associated with particle interference, which would develop progressively with increasing ranges of strain. Other things being equal, the degree of such interference is proportional to the magnitude of the normal stress on the shearing plane and to dilatancy. Hence, the greater the normal stress and dilatancy, the more vigorous the interference of particles and consequently the greater the frictional resistance.

b. Specimens anisotropically consolidated

(1) Cohesion

(a) If the soil is anisotropically consolidated, it is believed that the soil particles tend to be oriented perpendicular to the direction of the consolidation pressure or the drainage. This tendency would be accen-

tuated as the magnitude of the consolidation pressure increases, producing a correspondingly lower water content. Inversely, it may be reasoned that the degree of orientation must be small for smaller vertical consolidation pressure and for greater water contents. These conclusions seem to be verified by the experimental data (Fig. 58 through 60) obtained during this investigation. It has been shown that the specimens oriented perpendicular to the direction of drainage possess higher values of cohesion than do those oriented parallel to that direction.

(b) At low water contents and low strain the soil particles of specimens oriented both perpendicular and parallel to drainage are predominated by edge-to-planar surface attraction due to the extremely reduced particle spacings. It is, therefore, reasonable to expect the cohesive resistance under these conditions to be very high. As the water contents increase, however, the edge-to-face attraction becomes rapidly reduced — a condition which was clearly evidenced by a decrease in the cohesion. An increase in the water content of the Permian Clay beyond about

16% produced little additional effect on cohesion. It may be reasoned that the cohesion is a predominant factor only at very small particle spacings, and that once these small interparticle distances are exceeded, then the cohesion remains almost constant with further increase in water content (possibly up to about 20%).

(c) As the strain develops, the cohesion at low water content decreases sharply, almost disappearing at 10% strain for specimens whose water content is about 13%. The cohesion at 10% strain increases with an increase in water content, whereas at the 1% strain the opposite effect is produced. This may possibly be explained in terms of differences in particle orientation at low and high strains in the two cases. For example, it may be hypothesized that the more or less random orientation which exists at low water contents may be altered during strain to one in which parallelism to the multitudinous shear surfaces predominates. On the other hand, because of the greater interparticle distances associated with higher water contents, the drag along shear surfaces would probably be less efficient in reorienting

the particles than would be the case for low water contents. The phenomenon can also, perhaps, be explained by the difference in dilatancy in the two cases.

(2) Friction Angles

The effects of dilatancy and the magnitude of the normal stress on the friction angles (as expressed in the second term of Eq. 19) were experimentally demonstrated. For higher strains and lower water contents the effects of both normal stress on the shearing planes and structural dilatancy are greater. The greatest magnitudes of frictional resistance were exhibited under these conditions. The angles of internal friction decreased with an increase of water content, since the effect of dilatancy is reduced. The friction angles are small at low strains because, regardless of the magnitude of the normal stress, these angles depend principally upon particle interference and the usual dilatancy which accompany larger displacements. The low frictional resistance is also associated with the low normal stresses on the shearing planes at small strains.

Because there is a fixed relationship between the water content and dry density of saturated soils, the dependency of cohesion and friction

angle on dry density is essentially of the same character as their dependency on water content.

c. Specimens Isotropically Consolidated

The basic difference in the particle orientation between the specimens anisotropically consolidated and those isotropically consolidated is that a random orientation is thought to be predominant for all water contents and densities if the soil is consolidated isotropically. This supposition has been verified by the results presented in Figures 61 through 63, and Figures 70 through 72, in which the cohesion and the angles of internal friction are shown not to vary appreciably with change of the water content or dry density. Because the cohesion and friction angles vary mainly with strain alone it appears that such results must be attributed to negligible changes in initial particle orientation over the range of water contents investigated.

d. Specimens Compacted by Kneading Action

The behavior of the compacted specimens as compared with those anisotropically or isotropically consolidated serves to explain more decisively the role of the structure of the soil in determining its shear strength and stress-deformation characteristics. With the maximum dry density occurring at water contents of about 16 - 17%, and because the water contents bear no

fixed relationship to the dry densities, the fact that the highest values of the cohesion and friction angle do not necessarily occur at the lowest water contents or the greatest densities is of paramount importance. The cohesion is greatest for water contents appreciably below the optimum. It seems probable that for this "dry side" condition a random structure combined with a reasonably high density is produced, thus increasing the intrinsic forces or the physico-chemical forces to their maximum possible magnitude. For reasons already mentioned, this trend becomes pronounced only after the strain has exceeded about 1%. The frictional resistance at 1% strain is greatest at about the optimum water content (maximum dry density); but at larger strains, where the frictional forces have been more fully developed, the maximum values occur at lower water contents.

Compacted specimens presumably have a random orientation of particles at low water contents and a relatively parallel orientation at high water contents. Thus the maximum shearing resistance is not produced at the maximum dry density, but at water contents slightly less than the optimum where particle orientation is more nearly random.

It is believed to have been convincingly demonstrated that the cohesive and frictional resistance (shearing resistance) of the soil depends greatly on

the structure of the soil. Structure, in turn, is closely associated with the terms in the expression analogous to the Coulomb equation

$$\tau = \frac{2}{\lambda} S \left(E_o + KT \ln \dot{\epsilon} - KTB\right) + \frac{2(\bar{\sigma}_1 + 2\bar{\sigma}_3)}{3} \Phi \qquad (19)$$

or $$\tau = C + \bar{\sigma}_m \tan \phi \qquad (20)$$

e. Coulomb Equation by Rate Processes

The cohesive resistance depends also on the strain rate and temperature. The greater the rate of strain and the lower the temperature, the greater the cohesive resistance.

The frictional resistance increases as the influence of the dilatancy associated with lower void ratios becomes greater. For large strains, where particle interference during displacement has achieved its maximum, the normal stress exerts its greatest influence.

It is finally concluded that the theory developed by rate processes has been thoroughly analyzed and its validity properly demonstrated by experimental evidence.

2. Practical Applications in Engineering

The primary importance of this research is in its contribution to an understanding of those theoretical aspects of soil behavior associated with the cohesive and frictional resistance and the geometrical configuration of the soil grains. Given a type of soil under various environmental conditions, the design of earth structures depends largely on the shear strength and the stress-deformation characteristics

of the soil. In the conventional practice of civil engineering, the values of cohesion and the angles of internal friction used in design are based on the failure concitions of laboratory test specimens.

Because of the fact that the cohesion and the angle of internal friction vary independently according to the magnitude of strain, the values of these two strength components at failure are not necessarily their maximum values. A superposition of the c and ϕ components of shearing resistance corresponding to a given normal stress would produce a curve representing the shear strength versus strain, from which one may obtain the magnitude of strain at which the maximum shear strength occurs. Such data have not been presented in this dissertation, since the designation of the working range of the normal stress in design is an arbitrary matter, consideration of which falls outside the scope of this study.

It seems worthwhile, however, to consider the load-carrying capacity of foundation soils and the stability of the sloping embankments in respect to the manner in which natural and imposed variations of the soil affect those numerous factors upon which the strength parameters c and ϕ depend. The laboratory test results, based on specimens having controlled particle arrangements, may approximately represent soil behavior under some of the field conditions imposed by methods of deposit, stress history, and (perhaps) leaching action. Under natural conditions most soils are

anisotropically consolidated under vertical stresses which are greater than those acting horizontally. However, the ratio of these stresses varies; under some conditions the ratio may approach unity, corresponding to the hydrostatic state of stress which produces isotropic consolidation. Layers of soil compacted with a roller would have properties resembling those obtained in the laboratory by kneading compaction.

It follows, therefore, that the results of the laboratory experiments may be applicable under various corresponding field conditions. With this fact in mind, the design values of c and ϕ can be selected with reference to the nature and magnitude of the pre-shear consolidation stress, and in accordance with the strain anticipated under working loads. Because the variations of the values of c and ϕ with strain may be appreciable, detailed agreement between laboratory and field should include type of soil, water content, dry density or void ratio, nature of consolidation pressures, and mode of compaction, all of which influence the relationship of c and ϕ with strain. For field loading conditions (which usually involve a substantial factor of safety) it seems more reasonable to use the values of c and ϕ corresponding to strain conditions considerably less severe than those which produce failure. Since, for low strains, the cohesion is relatively higher and the friction angle relatively smaller, the Coulomb equation would probably yield a higher value of τ because of the decimal character of the

term tan ϕ . The precise influence of the use of this procedure would, of course, depend upon the relative magnitudes of cohesion and the normal stresses on the slip surfaces.

Recommendations

The experiments performed in this research made use of cohesion-friction-strain triaxial tests employing a curve hopping technique, and during which the rate of strain and the temperature were held constant. It would appear to be advantageous to include variations of the strain rate and temperature in order to ascertain the effects of these variables on the cohesive resistance. It is further recommended that the magnitudes of the minor total principal stress and the preassigned values of the high and low limits of the major effective principal stress be varied in order to establish definite ranges of validity associated with the quasi-linear character of the data produced by the curve hopping technique.

Finally, the writer feels that tests performed on a variety of soil types would serve to bring out additional information concerning the nature of the shear strength and stress-deformation characteristics of soils insofar as these are related to soil mineralogy and to the widely extended environmental conditions encountered in the practice of engineering.

A SELECTED BIBLIOGRAPHY

1. Terzaghi, K., "From Theory to Practice in Soil Mechanics," John Wiley and Sons, Inc., New York, 1960.

2. Schmertmann, J. H., and J. O. Osterberg, "An Experimental Study of the Development of Cohesion and Friction with Axial Strain in Saturated Cohesive Soils," Research Conference on Shear Strength of Cohesive Soils, June, 1960.

3. Schmertmann, J. H., and J. R. Hall, "Cohesion after Non-hydrostatic Consolidation," Journal of Soil Mechanics and Foundation Division, ASCE, August, 1961.

4. Schmertmann, J. H., "Comparison of One and Two-Specimen CFS Tests," Journal of Soil Mechanics and Foundations Division, ASCE, December, 1962.

5. Overbeck, J. Th., and E. J. W. Verwey, "Theory of the Stability of the Lyophobolic Colloids," (New York: Elsevier Publishing Company), 1948.

6. Bolt, G. H., "Physico-Chemical Properties of the Electric Double Layer on Planar Surfaces," (Ph.D. Thesis, Cornell University,) 1954.

7. Glasstone, S., K. Laidler, and H. Eyring, "The Theory of Rate Processes," McGraw-Hill Book Co. Inc., New York, N. Y., 1941.

8. Mitchell, J. K., "Shearing Resistance of Soils as a Rate Process," Journal of the Soil Mechanics and Foundations Division, ASCE, Vol. 90, No. SM1, January, 1964.

9. Whitman, R. V., and K. A. Healy, "The Strength of Sands during Rapid Loadings," Journal of the Soil Mechanics and Foundation Division, ASCE, Vol. 88, No. SM2, April, 1962.

10. Hvorslev, M. J., "Physical Components of the Shear Strength of Saturated Clays," Research Conference on Shear Strength of Cohesive Soils, ASCE, June, 1960.

11. Rosenquist, I. Th., "Physico-Chemical Properties of Soils, Soil Water Systems," Journal of the Soil Mechanics and Foundations Division, ASCE, April, 1959.

12. Lambe, T. W., "Structure of Compacted Clay," Journal of Soil Mechanics and Foundations Division, Proc. of ASCE, May, 1958.

13. Seed, H. B., and C. K. Chan, "Structure and Strength Characteristics of Compacted Clays," Journal of the Soil Mechanics and Foundations Division, ASCE, April, 1960.

14. Wu, T. H., A. G. Douglas, and R. D. Goughnour, "Friction and Cohesion of Saturated Clays," Journal of the Soil Mechanics and Foundations Division, ASCE, June, 1962.

TABLE I

LOAD INCREMENTS, ANISOTROPIC CONSOLIDATION

	Group I (*20%)		Group II (*15%)		Group III (*10%)	
	Kg	KSC	Kg	KSC	Kg	KSC
1	12.47	.15	12.47	.15	12.47	.15
2	36.47	.45	36.47	.45	36.47	.45
3	84.47	1.04	84.47	1.04	84.47	1.04
4	180.47	2.28	180.47	2.28	180.47	2.28
5			372.47	4.60	372.47	4.60
6			564.47	6.96	564.47	6.96
7					746.47	9.21
8					1536.47	18.95

* Final water contents

TABLE II

SUMMARY OF SPECIMENS, ANISOTROPICALLY CONSOLIDATED

Specimen Identification	Description of Specimen
AN-H-1-1	Anisotropically consolidated, high water content, parallel to drainage.
" -2	"
" -3	"
AN-M-1-1	Anisotropically consolidated, medium water content, parallel to drainage.
" -2	"
" -3	"
AN-L-1-1	Anisotropically consolidated, low water content, parallel to drainage.
" -2	"
" -3	"
AN-H-2-1	Anisotropically consolidated, high water content, perpendicular to drainage.
" -2	"
" -3	"
AN-M-2-1	Anisotropically consolidated, medium water content, perpendicular to drainage.
" -2	"
" -3	"
AN-L-2-1	Anisotropically consolidated, low water content, perpendicular to drainage.
" -2	"
" -3	"

TABLE III

COMPUTATION SHEET FOR CFS TRIAXIAL TEST, AN-H-1-1

Strain %	1	2	3	4	5	6	7	8	9	10	11	12
σ_{d_1}	2.09	2.27	2.35	2.37	2.41	2.42	2.43	2.42	2.40	2.38	2.35	2.31
σ_{d_2}	1.82	1.93	1.99	1.99	2.02	2.00	1.99	1.96	1.93	1.90	1.86	1.80
$\Delta\sigma_d$	0.27	0.34	0.37	0.38	0.41	0.42	0.44	0.46	0.47	0.48	0.49	0.51
$2\Delta\bar{\sigma}_1 - \Delta\sigma_d$	1.73	1.67	1.64	1.62	1.59	1.58	1.56	1.54	1.53	1.52	1.51	1.49
$\frac{\Delta\sigma_d}{2\Delta\bar{\sigma}_1 - \Delta\sigma_d}$	.156	.204	.219	.234	.258	.270	.282	.299	.307	.314	.322	.342
$\phi = \sin^{-1}\frac{\Delta\sigma_d}{2\Delta\bar{\sigma}_1 - \Delta\sigma_d}$	9.96	11.50	12.51	13.58	14.50	15.68	16.39	17.40	17.88	18.30	18.80	20.0
$\Delta\bar{\sigma}_1\sigma_{d_1} - \bar{\sigma}_1(H)\Delta\sigma_d$	1.01	.91	.86	.85	.77	.725	.67	.58	.52	.46	.39	.27
$2\sqrt{\Delta\bar{\sigma}_1(\Delta\bar{\sigma}_1 - \Delta\sigma_d)}$	1.719	1.690	1.61	1.60	1.56	1.52	1.48	81.47	1.456	1.442	1.43	1.4
$C = \frac{\Delta\bar{\sigma}_1\sigma_{d_1} - \bar{\sigma}_1(H)\Delta\sigma_d}{2\sqrt{\Delta\bar{\sigma}_1(\Delta\bar{\sigma}_1 - \Delta\sigma_d}}$	.580	.537	.531	.530	.493	.476	.450	.395	.358	3.18	.274	.193

TABLE IV

SPECIMEN DATA, ANISOTROPICALLY CONSOLIDATED

		Strain rate (mm/min)	# of drains	Specimen height (in)	Water content (%)	Dry density (PSF)	Void ratio	Saturation (%)
AN-H-1	1	.00612	3	2.81	23.2	109.5	.550	100
	2	.00606	3	2.81	23.5	104.0	.625	100
	3	.00603	3	2.81	22.9	105.8	.605	100
AN-H-2	1	.00611	3	2.81	23.7	112.2	.510	100
	2	.00600	3	2.81	22.6	113.0	.500	100
	3	-	-	-	-	-	-	-
AN-M-1	1	.0061	3	2.81	16.5	125.7	.342	100
	2	.00608	3	2.81	16.2	126.5	.337	100
	3	-	-	-	-	-	-	-
AN-M-2	1	.00610	3	2.81	16.5	125.5	.344	100
	2	.00612	3	2.81	16.1	125.2	.345	100
	3	-	-	-	-	-	-	-
AN-L-2	1	.00608	2	2.81	13.6	135.8	.242	100
	2	.00605	2	2.81	13.8	132.0	.282	100
	3	.00610	2	2.81	13.5	136.2	.242	100
AN-L-2	1	.00609	2	2.81	13.3	134.0	.260	100
	2	.00608	2	2.81	12.8	135.1	.250	100
	3	.00617	0	2.81	12.6	132.8	.275	100

TABLE V

SPECIMEN DATA, ISOTROPICALLY CONSOLIDATED

		Strain rate (mm/min)	# of drains	Specimen height (in)	Water content (%)	Dry density (PSF)	Void ratio	Saturation
2S-H-1	1	.00612	3	2.81	22.6	115.5	.471	100
	2	.00602	3	2.81	21.1	116.1	.460	100
	3	.00619	0	2.81	21.3	116.4	.458	100
IS-H-2	1	.00602	3	2.79	21.4	115.2	.471	100
	2	.00605	3	2.79	22.1	116.0	.462	100
	3	.00608	3	2.79	21.8	115.8	.465	100
IS-M-1	1	.00613	3	2.81	16.8	125.2	.351	100
	2	.00602	3	2.81	16.7	123.2	.375	100
	3	-	-	-	-	-	-	-
IS-M-2	1	.00610	3	2.79	16.5	126.0	.345	100
	2	.00608	3	2.79	15.8	128.5	.320	100
	3	.00607	3	2.79	16.3	127.5	.330	100
IS-L-1	1	.0060	2	2.81	14.7	129.0	.310	100
	2	.00602	2	7.81	14.2	130.2	.300	100
	3	-	-	-	-	-	-	-
IS-L-2	1	.00605	2	2.79	13.9	128.5	.320	100
	2	.00603	2	2.79	14.4	129.1	.311	100
	3	.00609	0	2.79	14.5	129.5	.311	100

TABLE VI

SPECIMEN DATA, HARVARD MOLD-COMPACTED

		Strain rate (mm/min)	# of drains	Specimen height (in)	Water content (%)	Dry density (PSF)	Void ratio	Saturation (%)
HC-H	1	.00609	3	2.816	19.4	116.5	.455	100
	2	.00612	3	2.816	19.1	116.0	.461	100
	3	.00613	3	2.816	20.2	115.8	.465	100
HC-M	1	.00610	3	2.816	15.6	120.0	.415	100
	2	.0062	3	2.816	15.4	121.1	.399	100
	3	.00607	3	2.816	15.1	120.9	.401	100
HC-L	1	.00608	3	2.816	10.2	114.1	.480	57.8
	2	.00599	3	2.816	10.6	113.5	.495	58.8
	3	.00610	3	2.816	10.0	113.9	.490	56.0

TABLE VII

SUMMARY OF C AND ϕ AT SELECTED STRAINS, ANISOTROPICALLY CONSOLIDATED SPECIMENS

		w	dry	e	1%		5%		10%		Peak cohesion		Peak friction	
					*c	ϕ	*c	ϕ	*c	ϕ	*c	ϵ	ϕ	ϵ
AN-H-1	1	23.2	109.5	.550	.58	9.9	.49	14.5	.32	18.3	.58	1	-	-
	2	23.5	104.0	.625	.59	9.8	.46	15.2	.31	17.9	.59	1	-	-
	3[c]	22.9	105.8	.605	.56	9.9	.47	14.9	.31	18.0	.59	1	-	-
AN-H-2	1	23.7	112.2	.510	.66	7.8	.62	11.2	.53	14.0	.66	1	-	-
	2	22.6	113.0	.500	.67	7.6	.62	10.8	.52	13.9			-	-
	3	-	-	-	-	-	-	-	-	-	-	-	-	-
AN-M-1	1	16.5	125.7	.342	.53	10.5	.40	15.5	.32	16.0	.53	1	16.5	8
	2	16.2	126.5	.337	.54	9.5	.48	15.2	.36	16.1	.54	1	16.1	10
	3	-	-	-	-	-	-	-	-	-	-	-	-	-
AN-M-2	1	16.5	125.5	.344	.60	7.2	.55	13.5	.46	16.5	.60	1	-	-
	2	16.1	125.2	.345	.61	9.0	.55	13.0	.41	15.5	.61	1	-	-
	3	-	-	-	-	-	-	-	-	-	-	-	-	-
AN-L-1	1	13.6	135.8	.242	.85	4.5	.55	17.0	.12	29.0	.85	1	-	-
	2[a]	13.8	132.0	.282	.84	4.2	.62	15.9	.17	26.6	.84	1	-	-
	3[a]	13.5	136.2	.242										
AN-L-2	1	13.3	134.0	.260	.91	5.5	.66	15.3	.02	30.4	.91	1	-	-
	2	12.8	135.1	.250	.95	5.2	.62	19.1	0	31.2	.95	1	-	-
	3[b]	12.6	132.8	.275	.92	4.9	.93	10.3	6.0	17.2	1.00	3	-	-

a - 2 specimen test
b - no drainage threads
c - 3-day preconsolidation
* - in units of Kg/sq.cm.

TABLE VIII

SUMMARY OF C AND ϕ AT SELECTED STRAINS, ISOTROPICALLY CONSOLIDATED SPECIMENS

		w	dry	e	1%		5%		10%		Peak Cohesion		Peak Friction
					*c	ϕ	*c	ϕ	*c	ϕ	*c	ϵ	
IS-H-1	1	22.6	115.5	.471	.49	5.5	.57	11.4	.45	14.0	.57	2	- -
	2	21.1	116.1	.460	.51	6.0	.57	9.0	.49	13.5	.60	2	- -
	3[b]	21.3	116.4	.458	.51	6.2	.64	9.9	.55	13.9	.55	5	- -
IS-H-2	1	21.4	115.2	.471	.48	5.5	.50	10.5	.45	13.0	.50	2	- -
	2[a]	22.1	116.0	.462									
	3[a]	21.8	115.8	.465	.40	5.3	.55	11.2	.50	12.5	.55	5	- -
IS-M-1	1	16.8	125.2	.351	.62	5.3	.49	13.8	.43	15.2	.62	1	- -
	2	16.7	123.2	.375	.62	4.0	.55	12.5	.48	15.5	.62	1	- -
	3	-	-	-	-	-	-	-	-	-	-	-	- -
IS-M-2	1	16.5	126.0	.345	.63	7.5	.53	13.6	.45	16.0	.64	1.5	- -
	2	15.8	128.5	.32	.67	5.8	.60	12.8	.50	15.0	.67	1	- -
	3[c]	16.3	127.5	.330	-	-	-	-	-	-	-	-	- -
IS-L-1	1	14.7	129.0	.312	.60	6.0	.58	13.0	.43	15.1	.69	2	- -
	2	14.2	130.2	.300	.65	6.2	.59	13.9	.45	17.8	.66	2	- -
	3	-	-	-	-	-	-	-	-	-	-	-	- -
IS-L-2	1	13.9	128.5	.32	.67	5.8	.60	12.8	.50	15.0	.67	1	- -
	2	14.4	129.1	.311	.62	7.5	.59	13.0	.40	18.0	.62	1	- -
	3[b]	14.5	129.5	.310	.84	3.0	.82	11.7	.76	11.9	.85	2	- -

a - 2 specimen test
b - no drainage threads
b^1 - no drainage threads, no filter paper
c - zero pore pressure
* - in units of Kg/sq.cm.

TABLE IX

SUMMARY OF C AND ϕ AT SELECTED STRAINS, HARVARD MOLD-COMPACTED SPECIMENS

		W	dry	e	1%		5%		10%		Peak Cohesion		Peak Friction
					*c	ϕ	*c	ϕ	*c	ϕ	*c	ϕ	
HC-H	1	19.4	116.5	.455	.42	2.8	.40	11.2	.22	16.5	.46	2	- -
	2	19.1	116.0	.461	.42	3.2	.34	12.8	.26	15.1	.44	2	- -
	3	20.2	115.8	.465	.46	2.1	.39	11.5	.25	15.2	.46	1	- -
HC-M	1	15.6	120.0	.415	.56	6.0	.56	13.1	.41	17.2	.62	2	- -
	2	15.4	121.1	.399	.52	6.1	.61	11.0	.40	14.2	.65	3	- -
	3	15.1	120.9	.401	.61	6.1	.62	13.0	.46	17.4	.65	2	- -
HC-L	1	10.2	114.1	.480	.62	4.5	.52	11.0	.42	18.1	.62	1	- -
	2	10.6	113.5	.495	.56	3.5	.48	12.1	.42	17.0	.58	2	- -
	3	10.0	113.9	.490	.58	3.6	.60	12.0	.47	16.3	.62	2	- -

* - in units of Kg/sq.cm.

TABLE X

COHESION-FRICTION-STRAIN TRIAXIAL TEST

Sample & Test No. AN-H-1-1 Sheet No. 1

σ_3 5 $\bar{\sigma}_1$ (H) 4 $\bar{\sigma}_1$ (L) 3 Strain Rate 0.00612 mm/min

Date 1964	Time	$\bar{\sigma}_1$ Kg/sq.cm.	Strain dial (in)	Load dial (in) (10^2)	Deviator stress Kg/sq.cm.	Strain (%)	Pore pressure Kg/sq.cm.
4-12	1504	Set up for consolidation under hydrostatic pressure of 5.0 Kg/sq.cm.					
		Back pressure of 0.5 Kg/sq.cm. applied, σ_3 then equal to 5 - 0.5 = 4.5 Kg/sq.cm.					
	2304	Back pressure removed					
4-13	1410	Set up for CFS test					
		Pore pressure 1 Kg/sq/cm applied					
	1526	4	0	0	0	0	1.00
	1533	"	.0012	.45	.20	.0428	1.20
	1550	"	.0042	1.15	.52	.150	1.52
	1603	"	.0063	1.80	.825	.225	1.825
	1622	"	.0100	2.77	1.268	.357	2.268
	1630	"	.0117	3.18	1.455	.427	2.455
	1652	"	.0162	3.90	1.78	.591	2.78
	1654						3.78
	1706	3	.0199	3.90	1.779	.711	3.779
	1730	"	.0250	3.96	1.80	.893	3.80
	1745	"	.0286	4.01	1.822	1.02	3.822
	1755	"	.0310	4.05	1.840	1.105	3.84
	1756						2.84
	1904	4	.0470	.50	2.252	1.68	3.252
	1933	"	.0540	.503	2.262	1.93	3.262
	1951	"	.0580	.510	2.295	2.07	3.295
	2012	"	.0652	.513	2.320	2.26	3.320
	2016						4.32
	2033	3	.0685	.429	1.928	2.44	3.928
	2049	"	.0725	.434	1.944	2.59	3.944
	2108	"	.0772	.436	1.95	2.76	3.95
	2126						2.95
	2144	4	.0856	.447	1.992	3.06	2.992
	2202	"	.0904	.483	2.17	3.23	3.17
	2226	"	.0961	.517	2.298	3.43	3.298
	2314	"	.1080	.538	2.375	3.86	3.375
	2342	"	.1149	.539	2.38	4.10	3.38
	2345						4.38

TABLE X (Cont.)

COHESION-FRICTION-STRAIN TRIAXIAL TEST

Sample & Test No. 1 Sheet No. 2

σ_3 5 $\bar{\sigma}_1$ (H) 4 $\bar{\sigma}_1$ (L) 3 Strain Rate 0.00612 mm/min

Date 1964	Time	$\bar{\sigma}_1$ Kg/sq.cm	Strain dial (in)	Load dial (in) (10^2)	Deviator stress Kg/sq.cm.	Strain (%)	Pore pressure Kg/sq.cm.
4-15	0001	3	.1190	4.40	1.94	4.25	3.94
	0018	"	.1235	4.50	1.982	4.41	3.982
	0105	"	.1359	4.57	2.02	4.82	4.020
	0139	"	.1448	4.580	2.02	5.15	4.020
	0756	4	.2365	5.85	2.469	8.45	3.469
	0814	"	.2408	5.60	2.352	8.60	3.352
	0843	"	.2475	5.70	2.39	8.85	3.390
	0921	"	.2561	5.72	2.39	9.15	3.39
	0953	"	.2636	5.75	2.396	9.40	3.396
	0954						4.396
	1008	3	.2672	4.70	1.96	9.50	3.96
	1020	"	.2700	4.68	1.95	9.63	3.95
	1052	"	.2771	4.56	1.892	9.89	3.892
	1118	"	.2835	4.60	1.902	10.11	3.902
	1235	"	.3015	4.49	1.842	10.78	3.842
	1237						2.842
	1303	4	.3080	4.79	1.968	11.00	2.968
	1319	"	.3120	5.14	2.10	11.14	3.10
	1330	"	.3141	5.30	2.165	11.21	3.165
	1353	"	.3200	5.50	2.20	11.41	3.20
	1425	"	.3272	5.61	2.282	11.68	3.282
	1447	"	.3322	5.65	2.30	11.88	3.30
	1501	"	.3359	5.70	2.309	11.99	3.309
	1514	"	.3390	5.70	2.30	12.10	3.30
	1526	3	.3420	4.78	1.93	12.21	3.93
	1547	"	.3445	4.68	1.89	12.30	3.89

PLATE I
Anisotropic Consolidation Apparatus

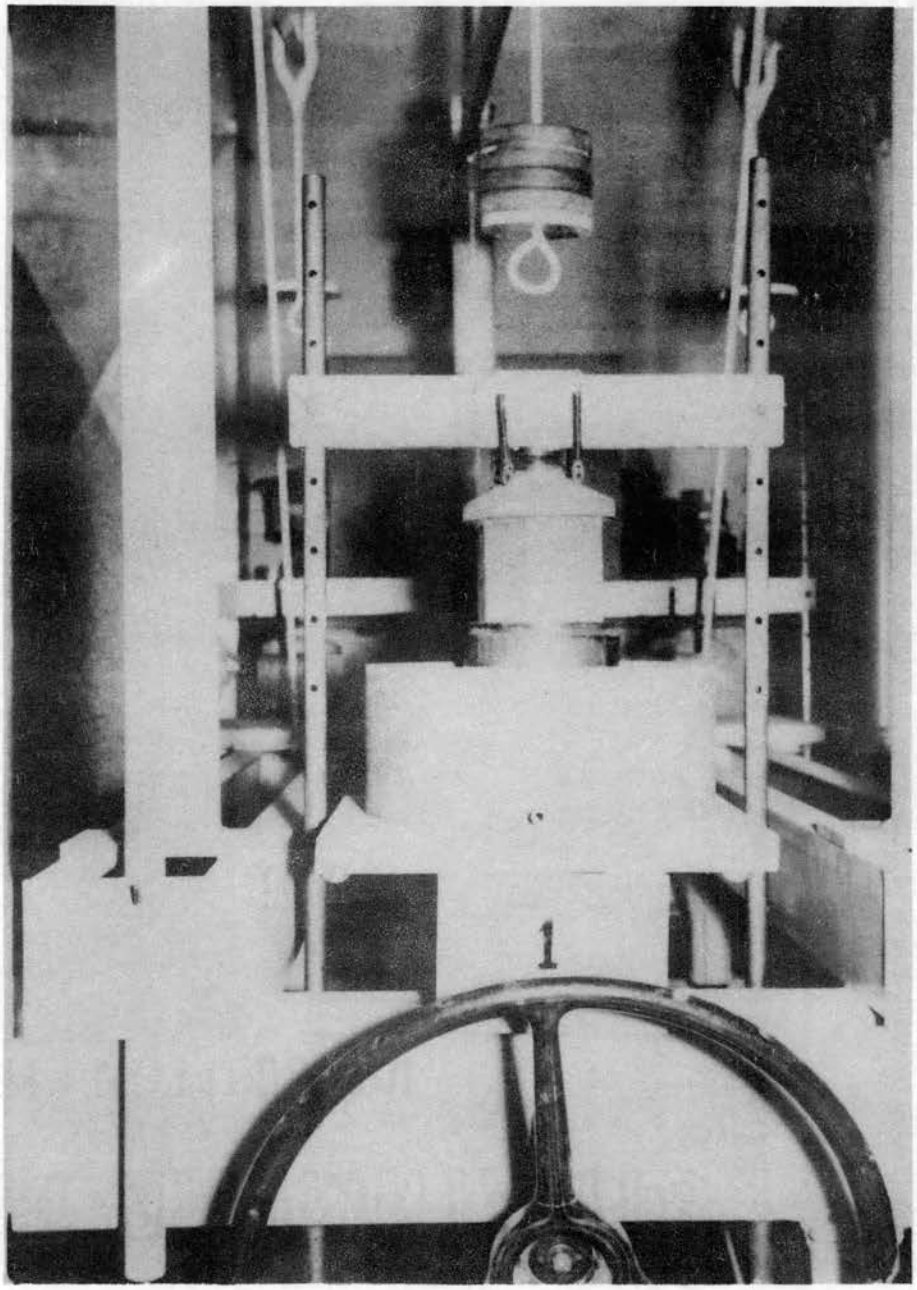

PLATE II
Isotropic Consolidation Apparatus

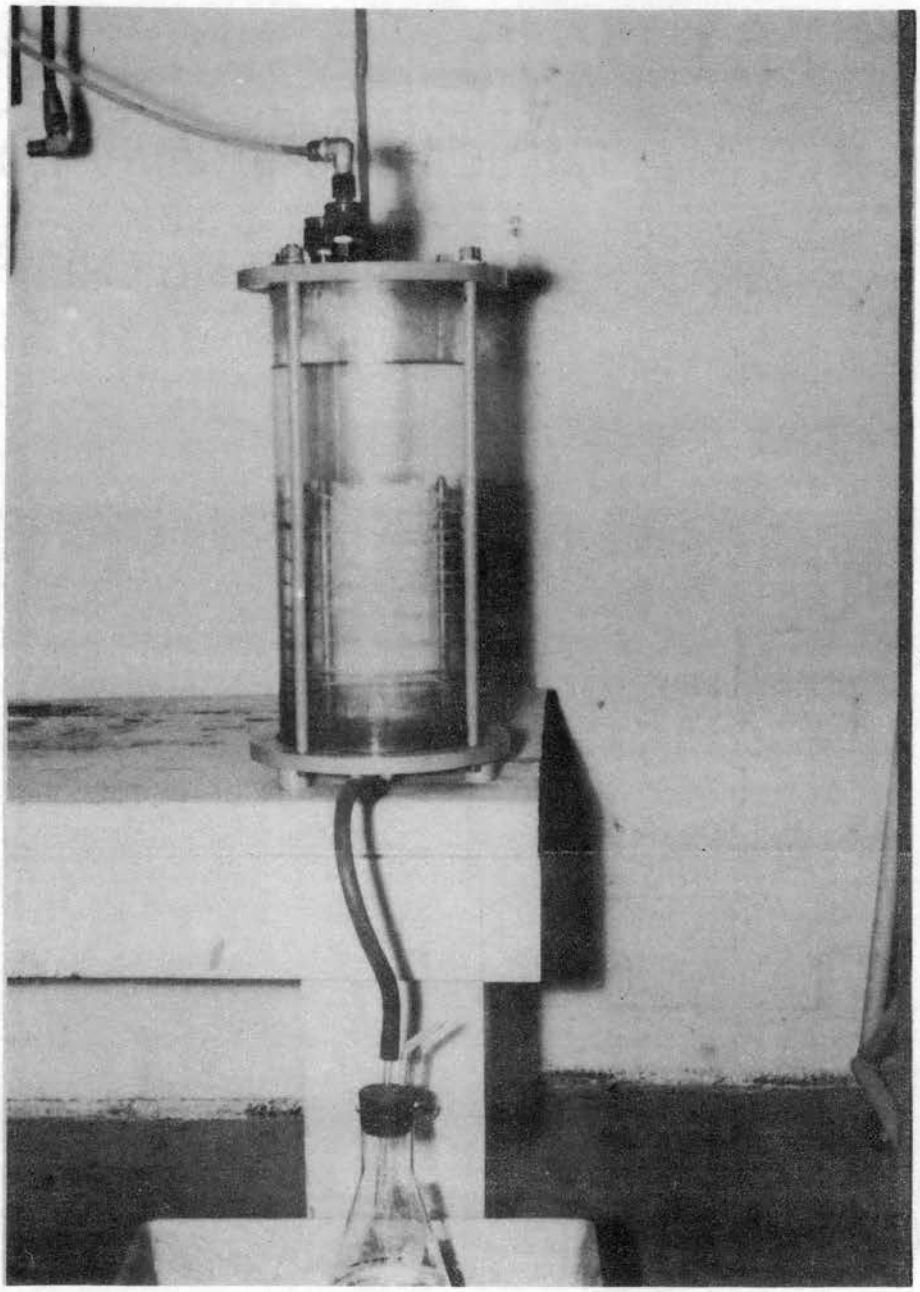

PLATE III
Modified CFS Test Equipment

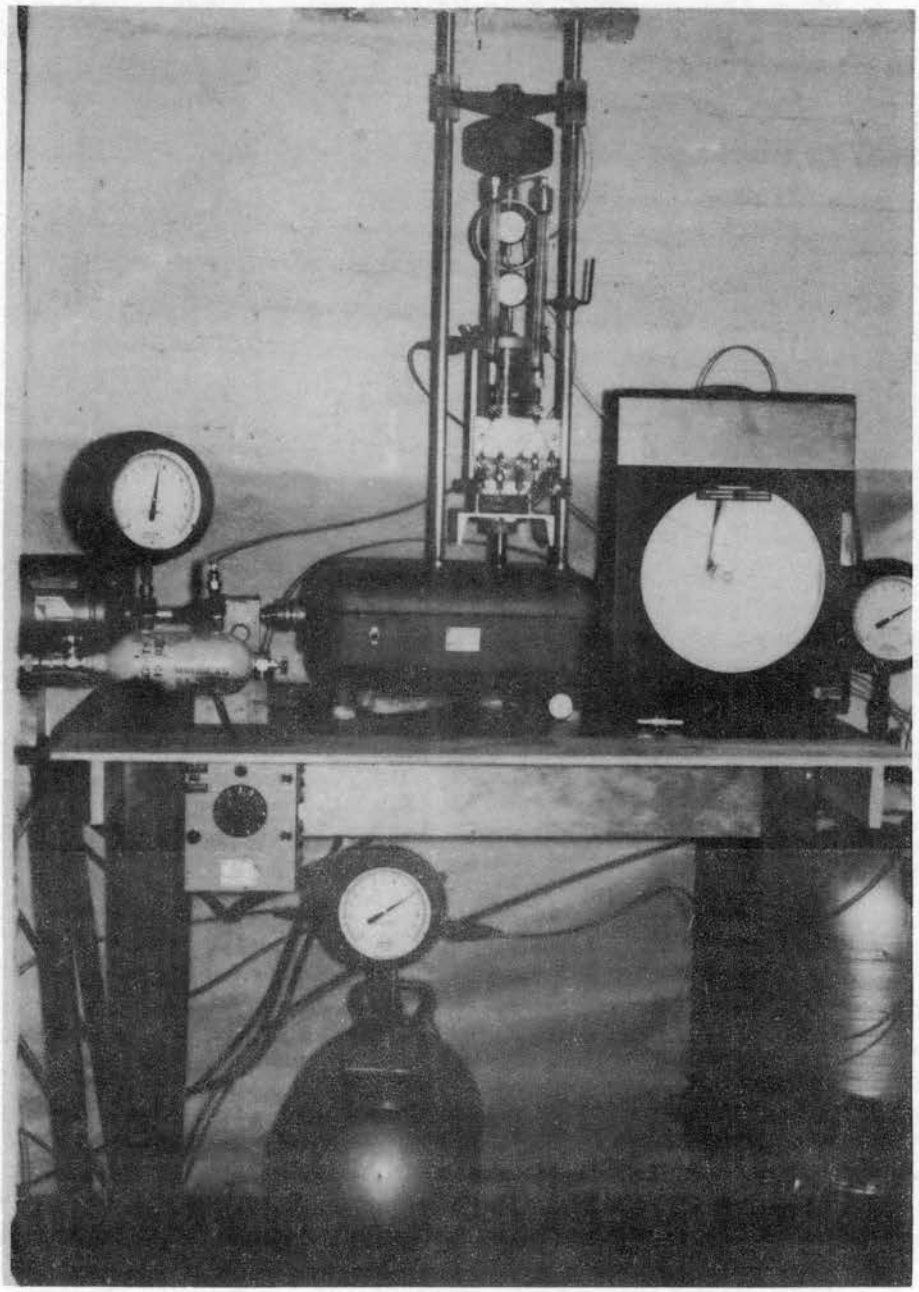

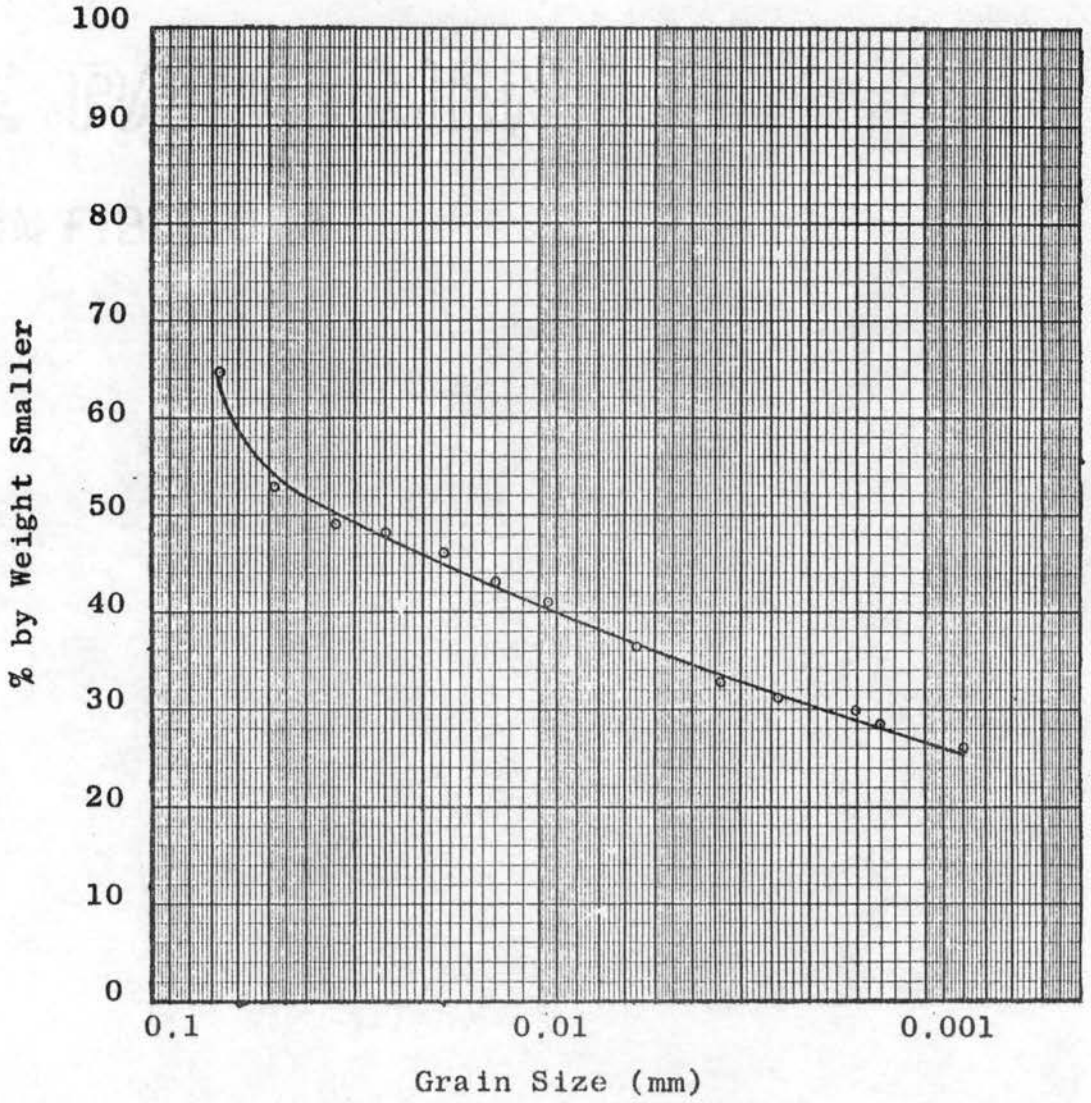

Fig. 3 - GRAIN SIZE DISTRIBUTION CURVE FOR PERMIAN RED CLAY

1. Soil Specimen
2. Porous Stone
3. Burette
4. Capillary Tube
5. Pore Pressure Gauge
6. Lateral Pressure Gauge
7. Regulator
8. Gear Train

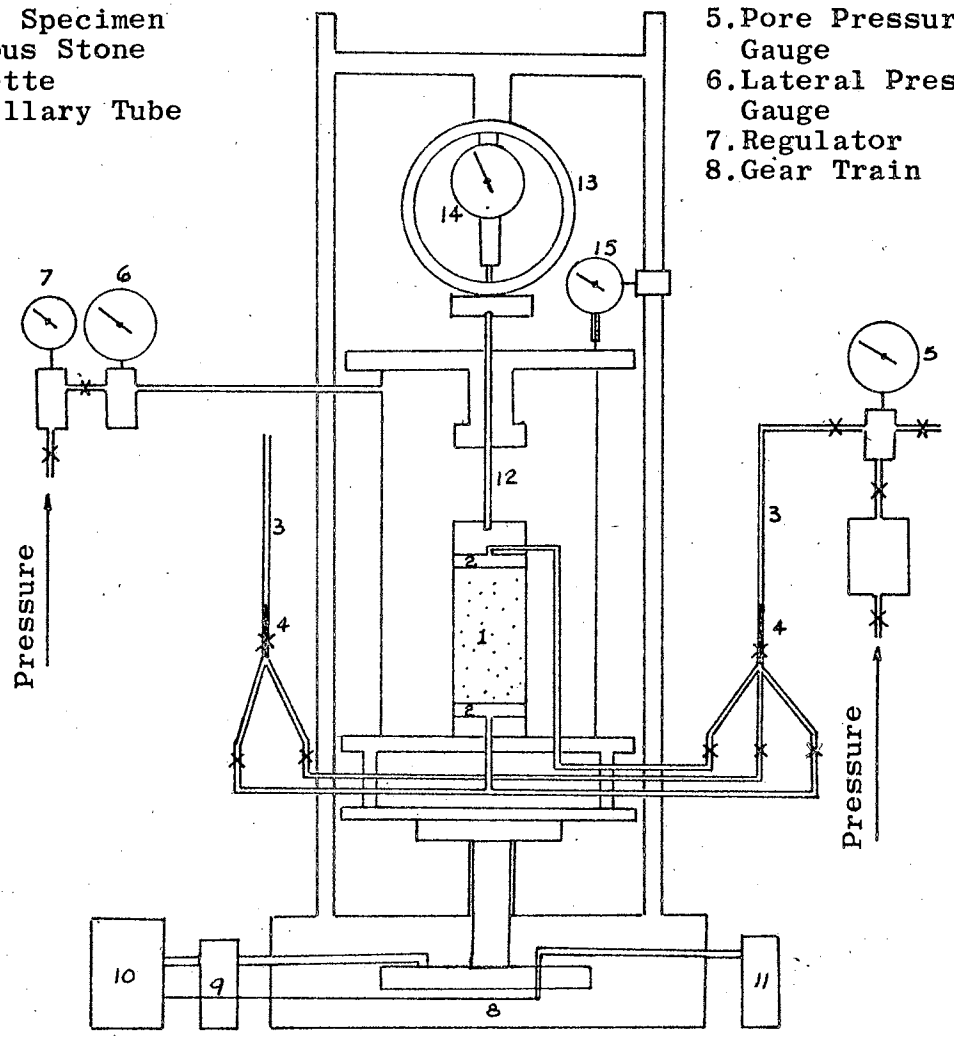

9. Gear Reductor
10. Motor
11. Speed Control
12. Piston Rod
13. Proving Ring
14. Proving Ring Dial
15. Strain Gauge

Fig. 4 - MODIFIED CFS TEST EQUIPMENT, Schematic Diagram

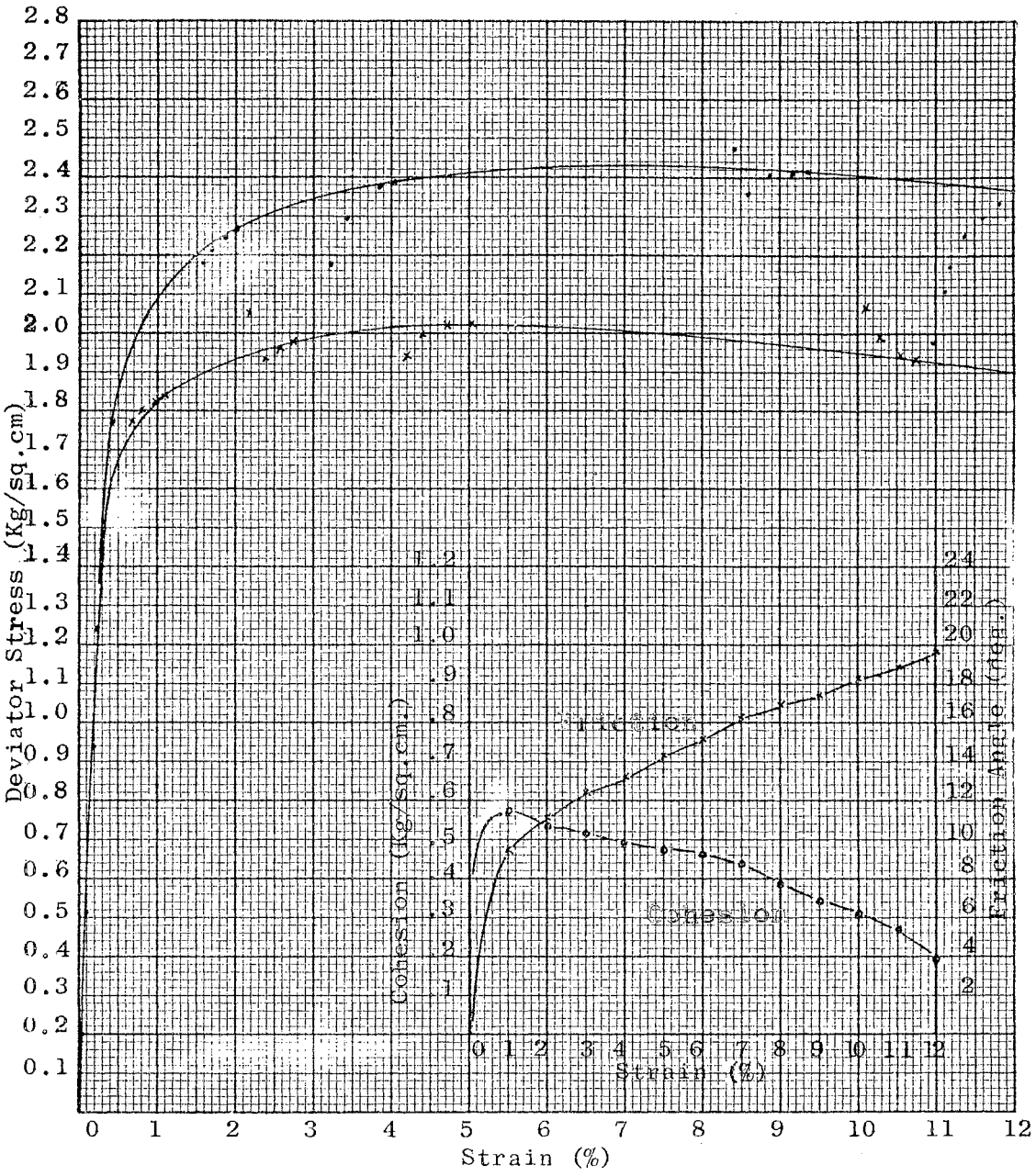

Fig. 5 - STRESS-STRAIN, CFS TEST, AN-H-1-1

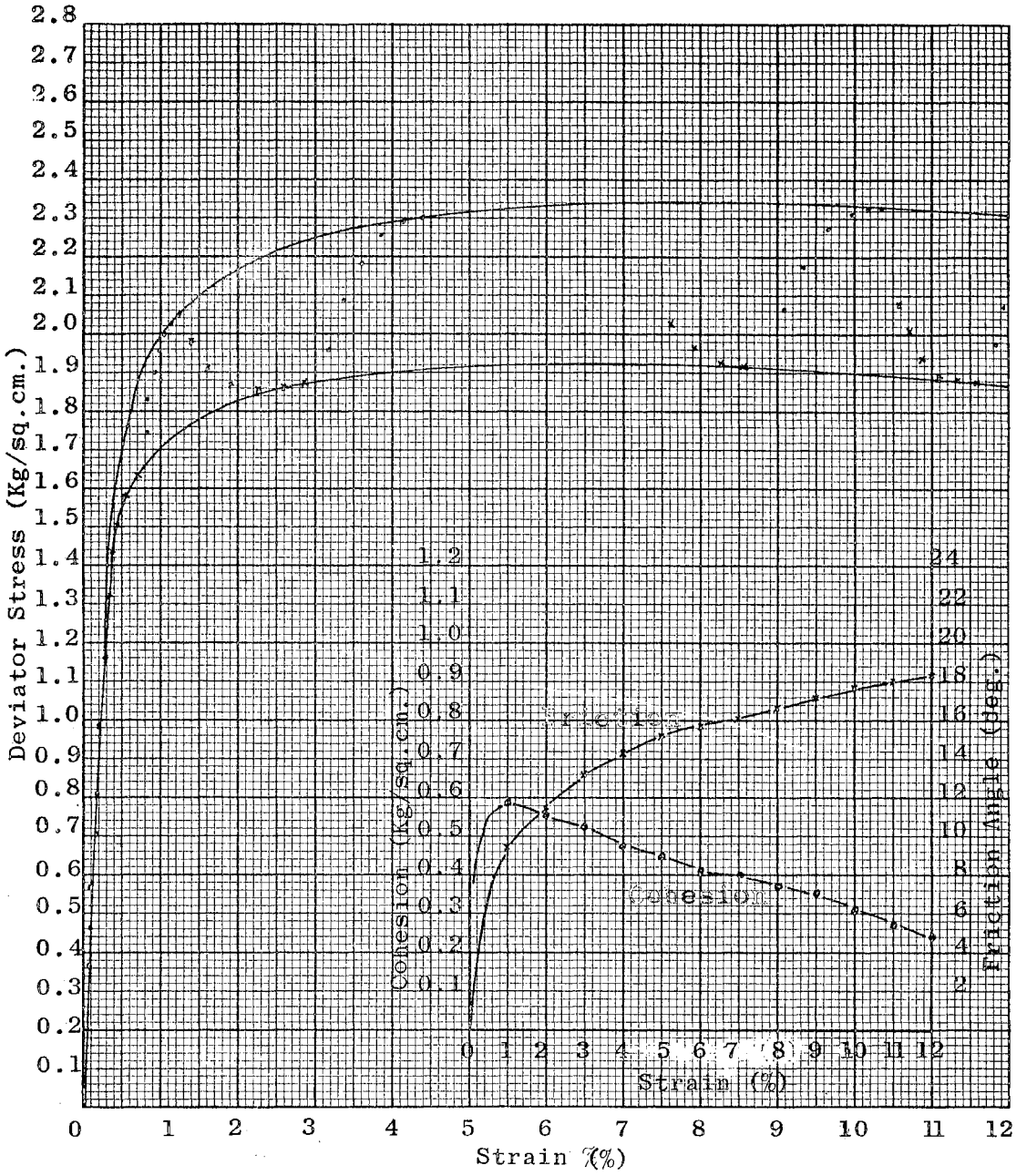

Fig. 6 - STRESS-STRAIN, CFS TEST, AN-H-1-2

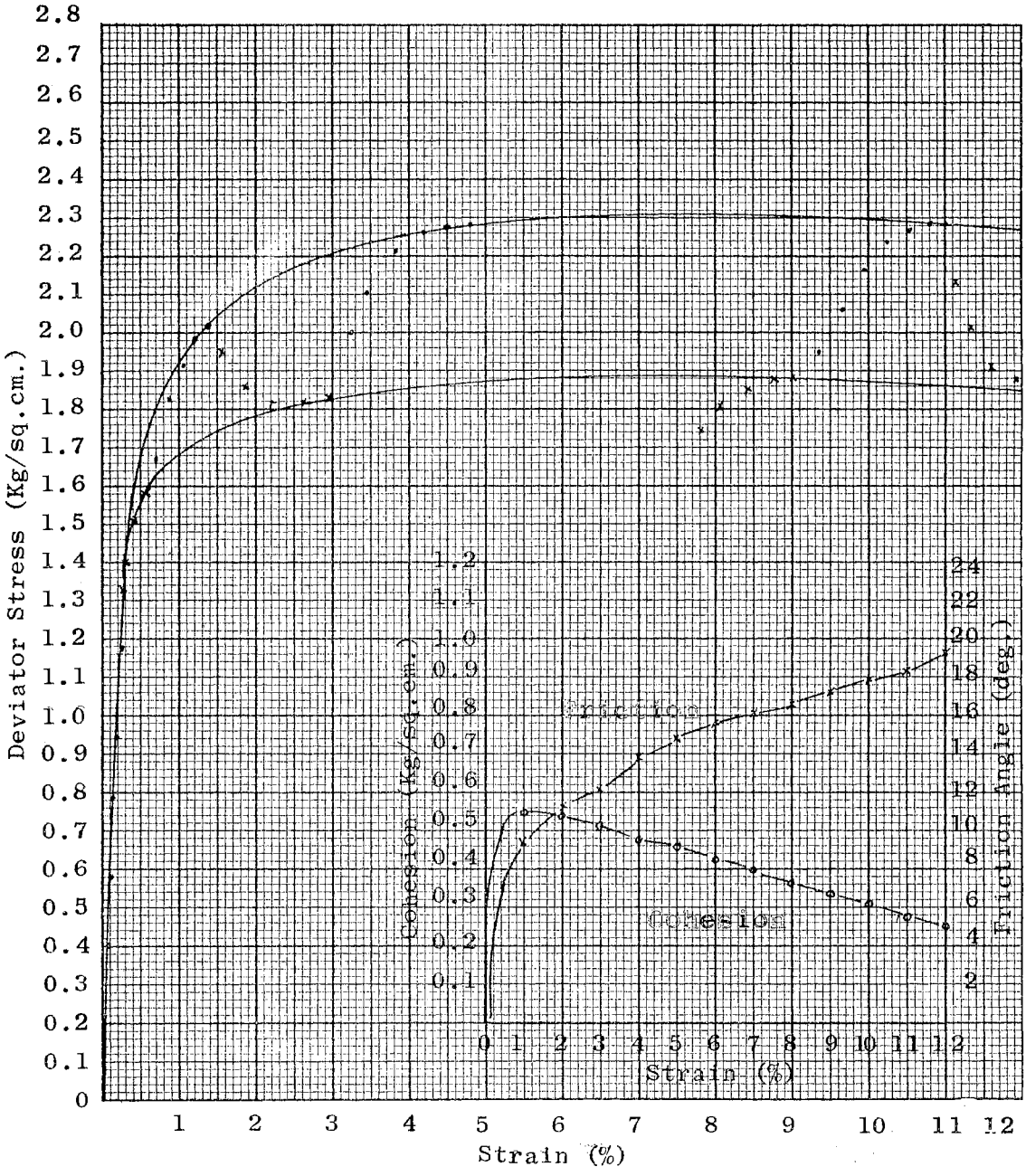

Fig. 7 - STRESS-STRAIN, CFS TEST, AN-H-1-3

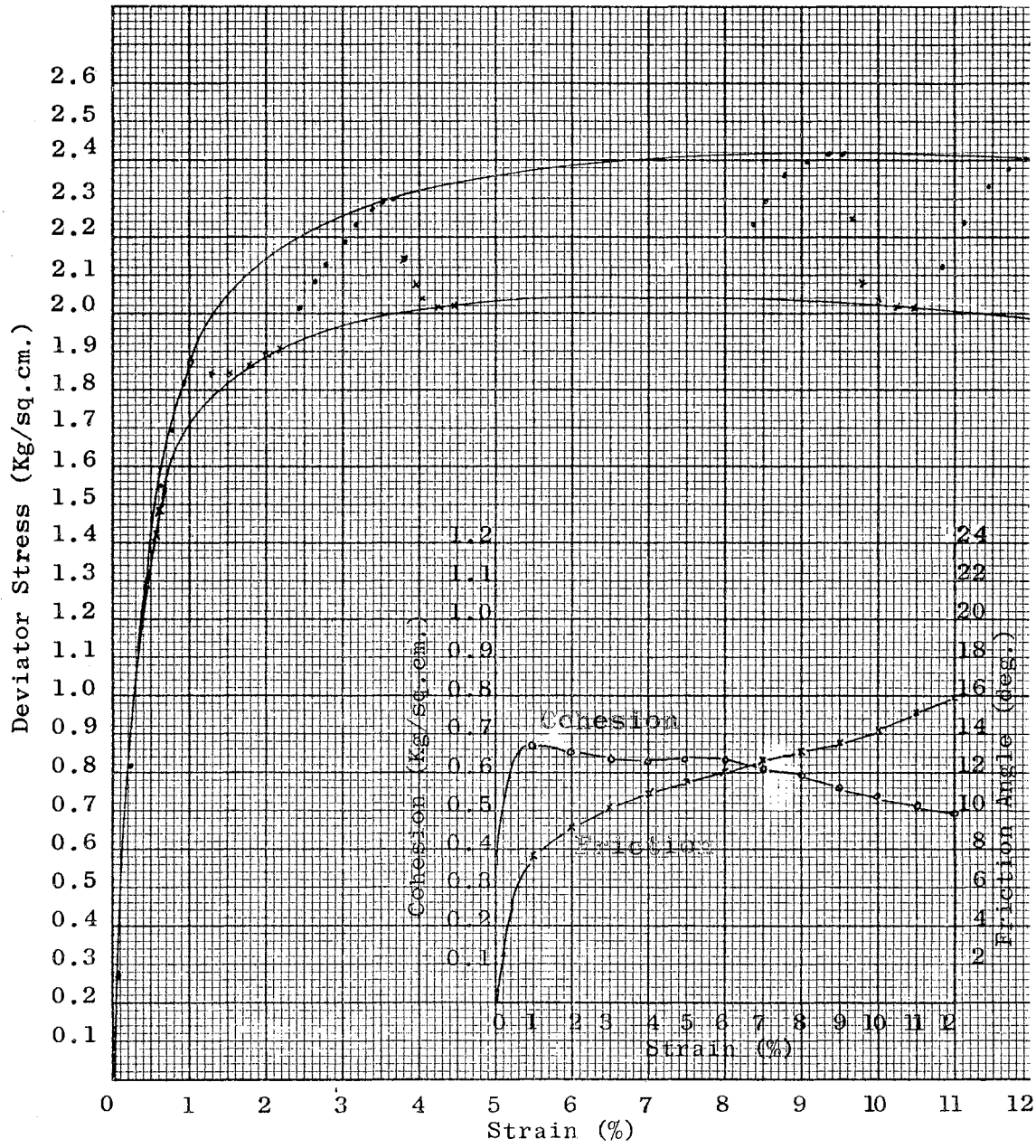

Fig. 8 - STRESS_STRAIN, CFS TEST, AN-H-2-1

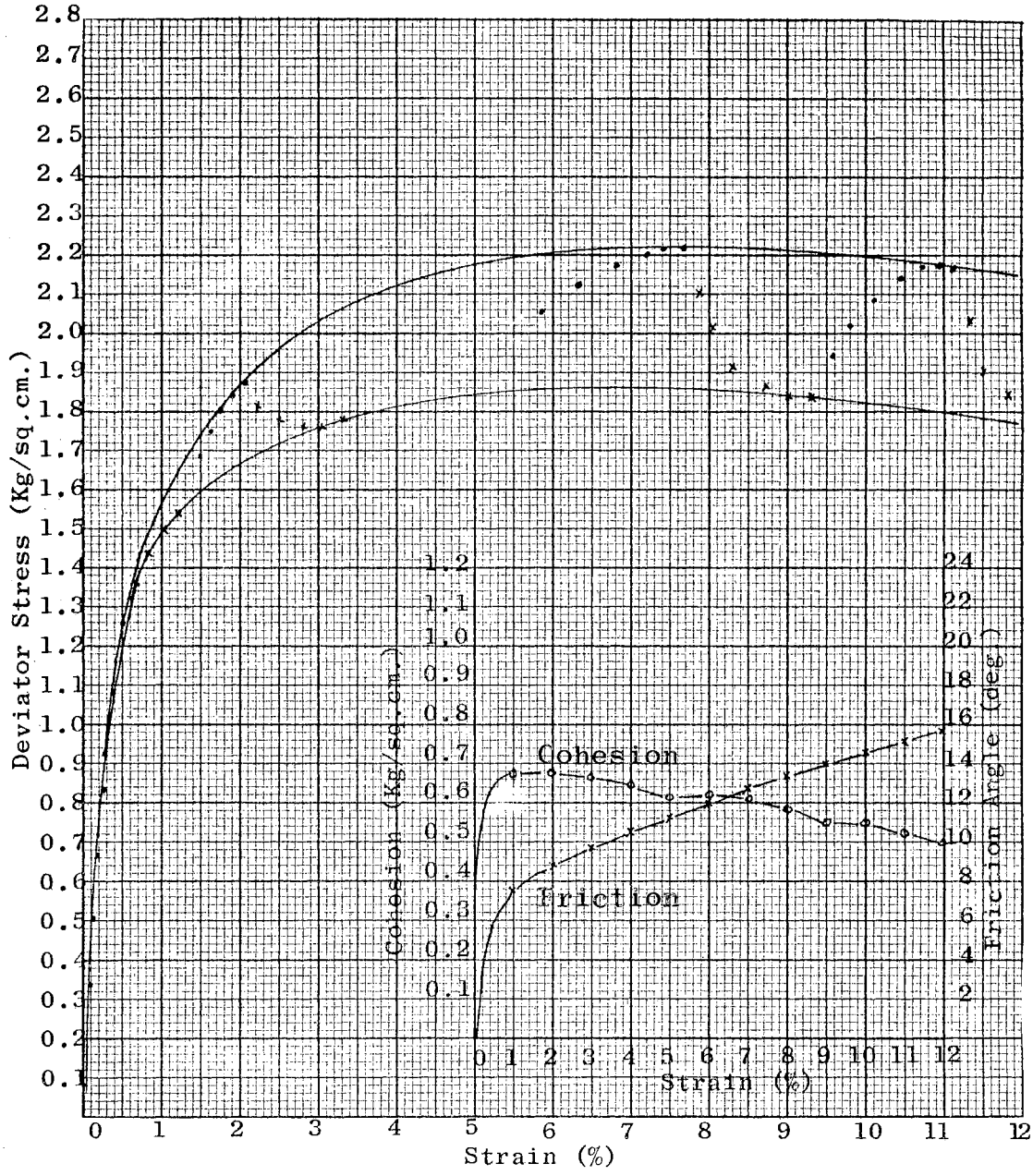

Fig. 9 - STRESS-STRAIN, CFS TEST, AN-H-2-2

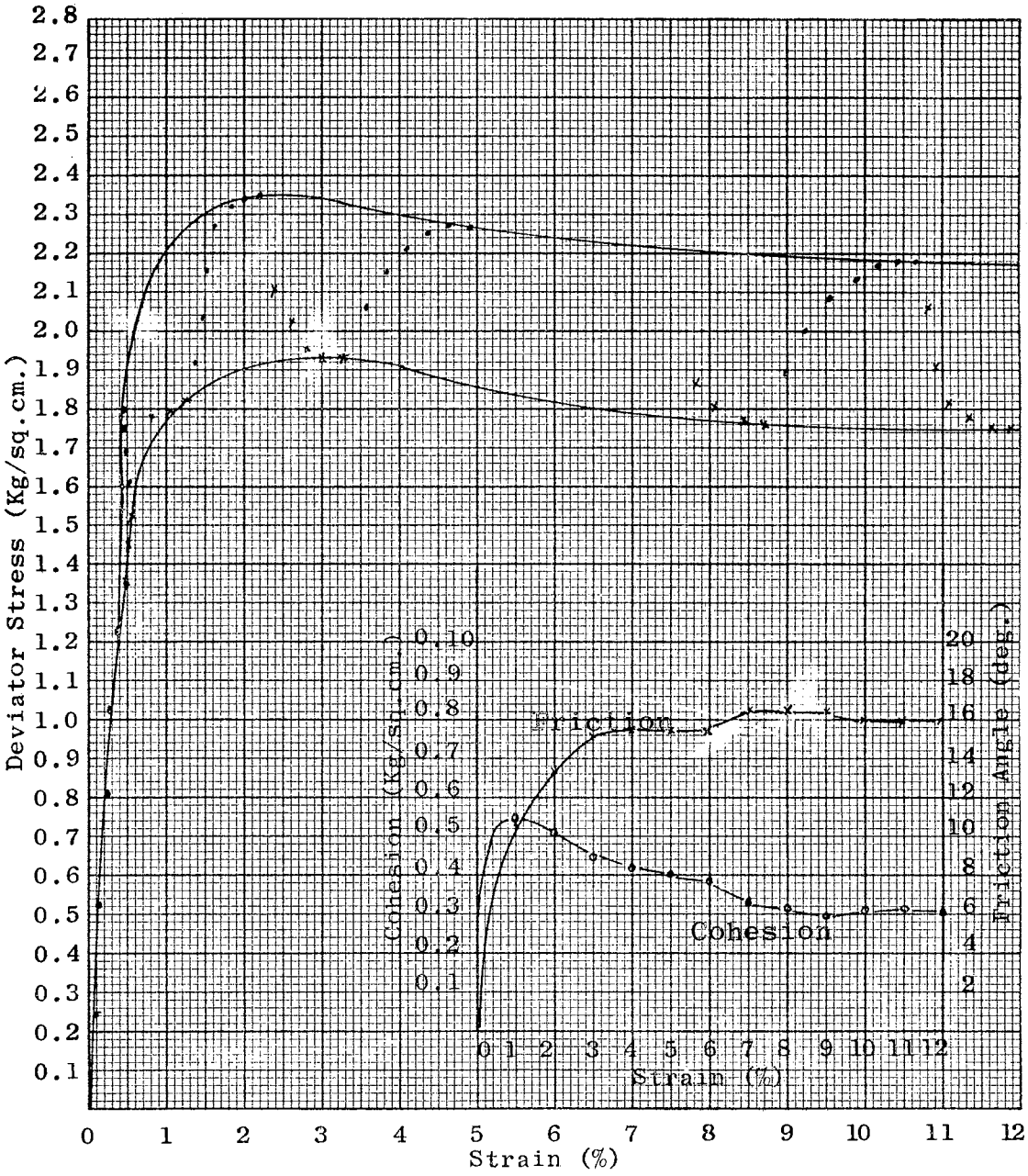

Fig. 10 - STRESS-STRAIN, CFS TEST, AN-M-1-1

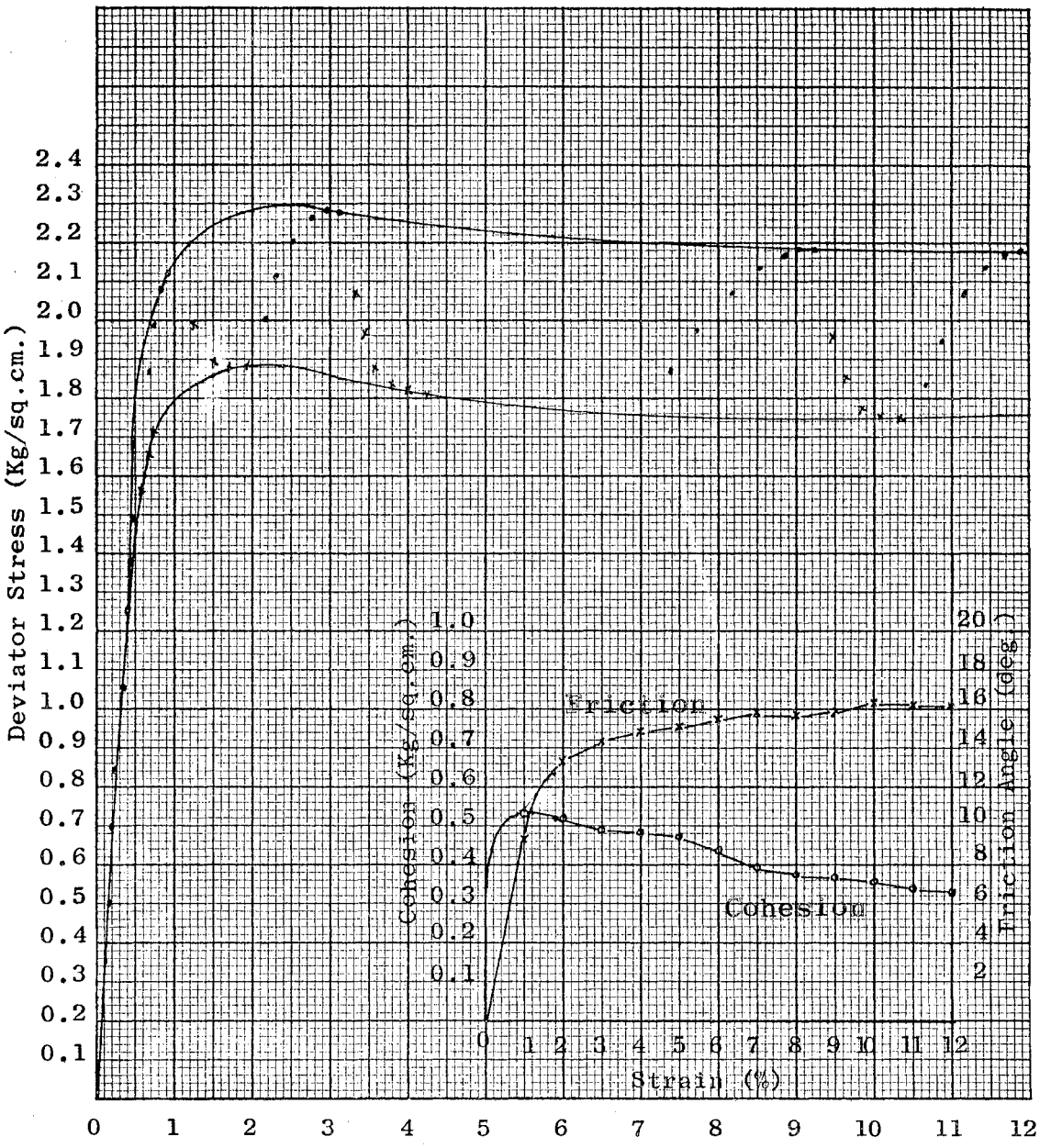

Fig. 11 - STRESS-STRAIN, CFS TEST, AN-M-1-2

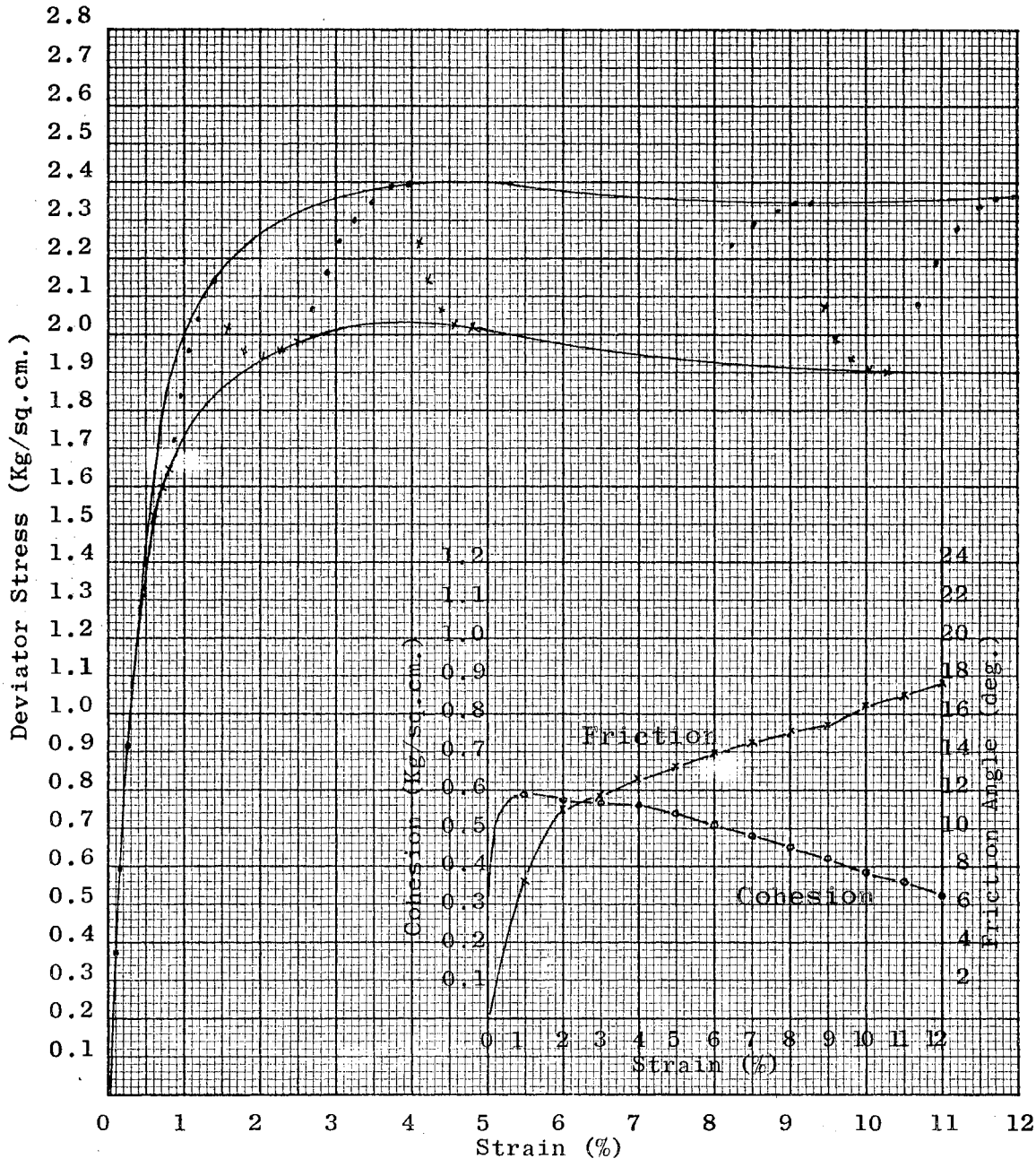

Fig. 12 - STRESS-STRAIN, CFS TEST, AN-M-2-1

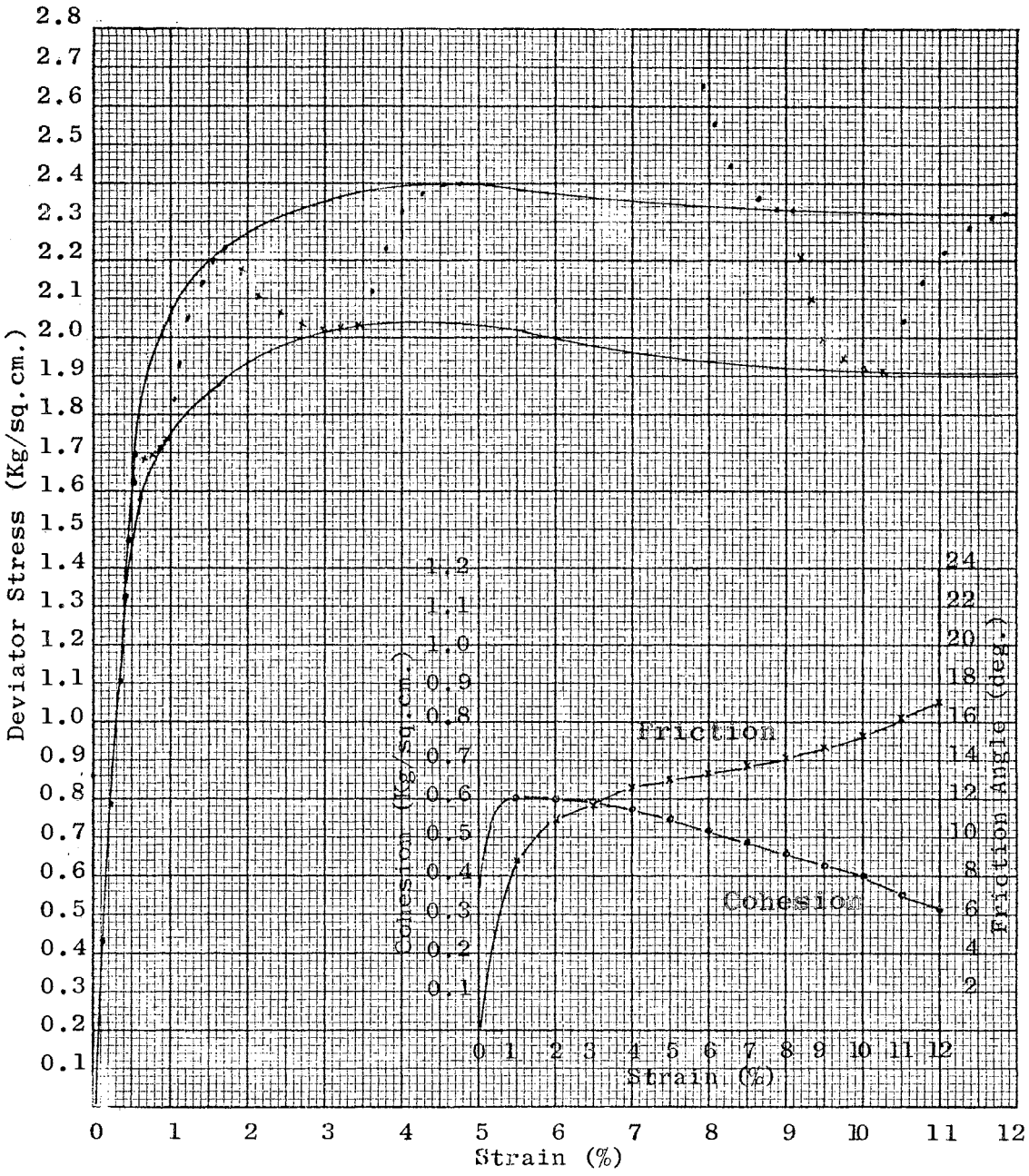

Fig. 13 - STRESS-STRAIN, CFS TEST, AN-M-2-2

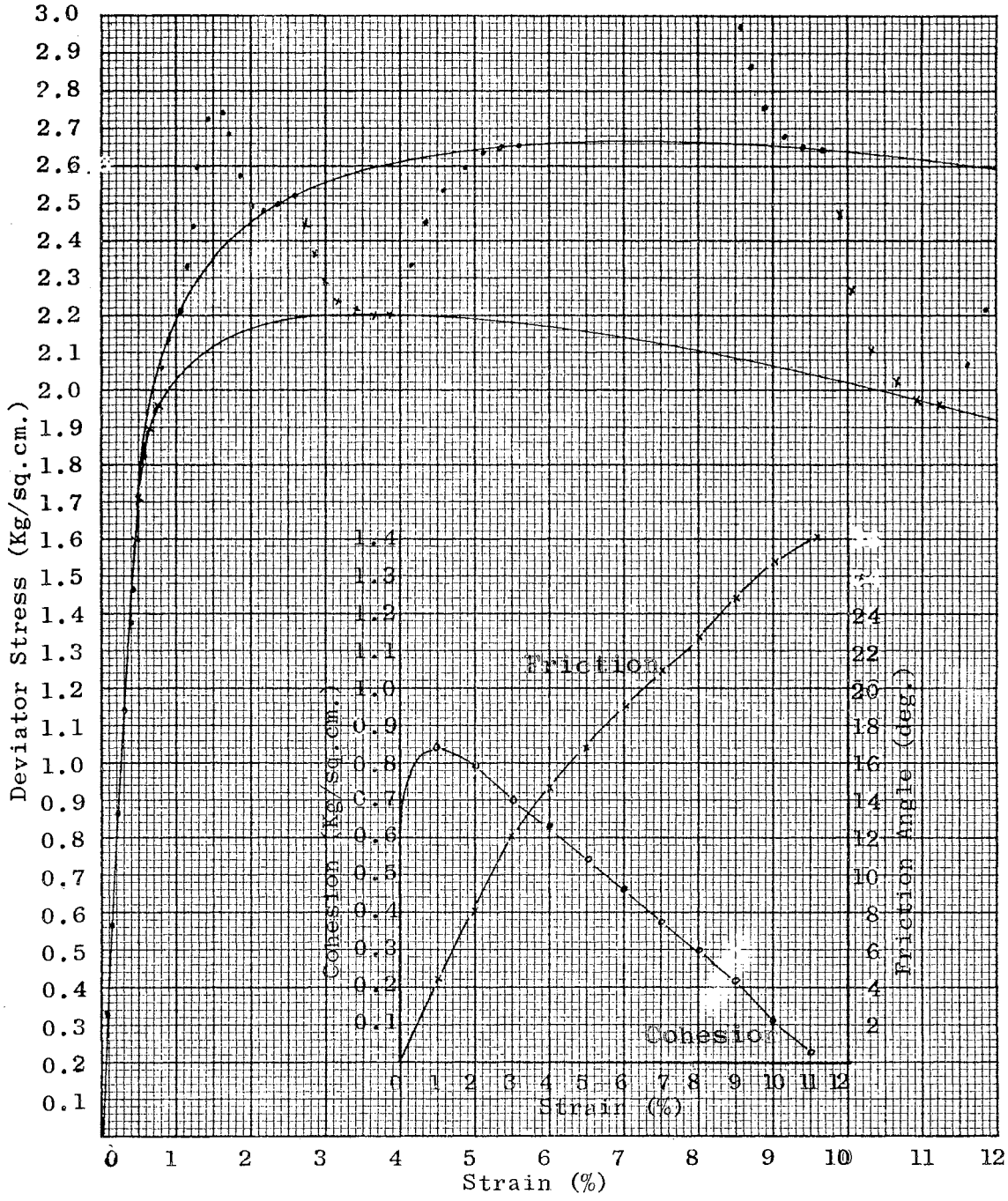

Fig. 14 - STRESS-STRAIN, CFS TEST, AN-L-1-1

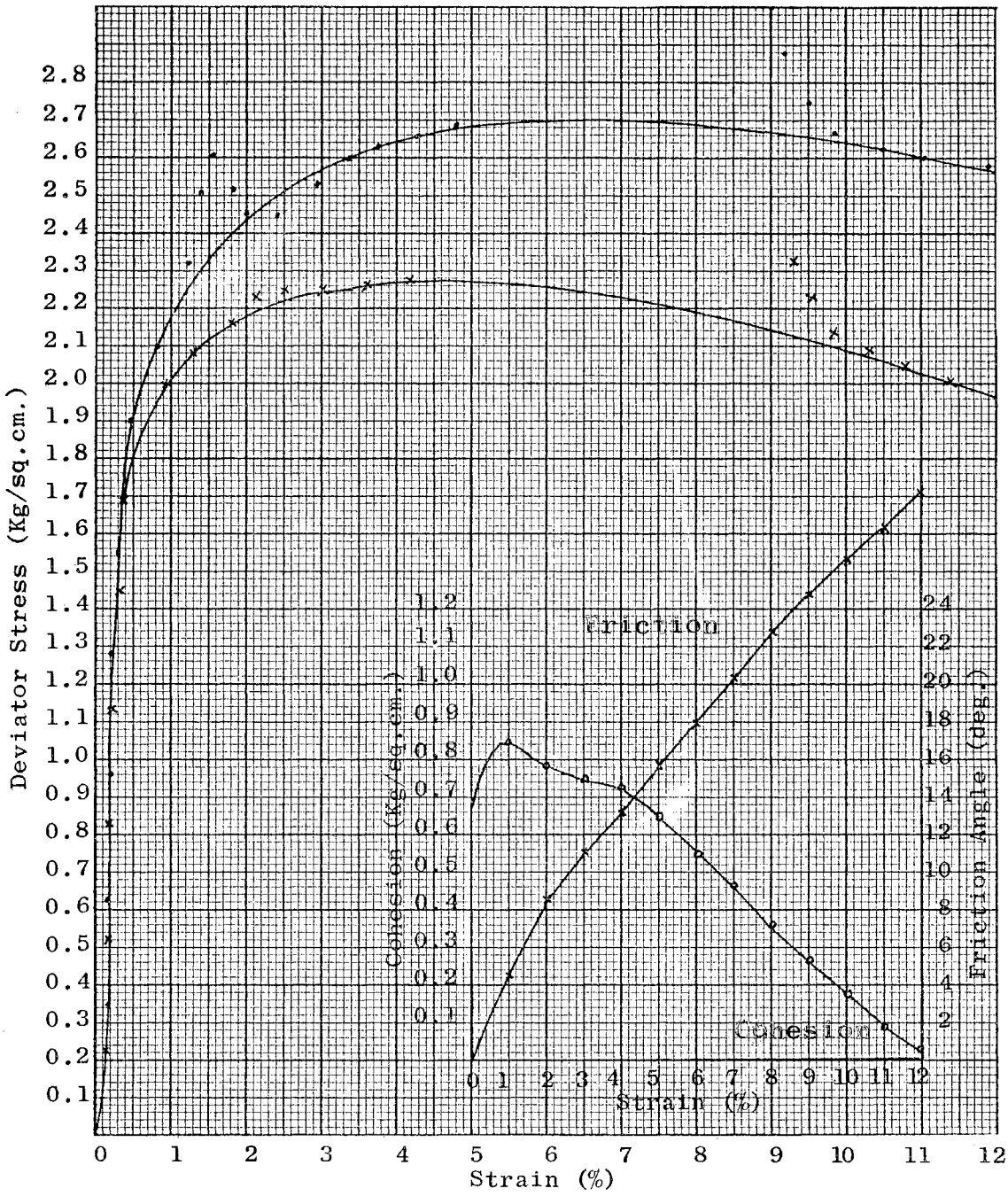

Fig. 15 - STRESS-STRAIN, CFS TEST, AN-L-1-2,3, 2 Specimen Test

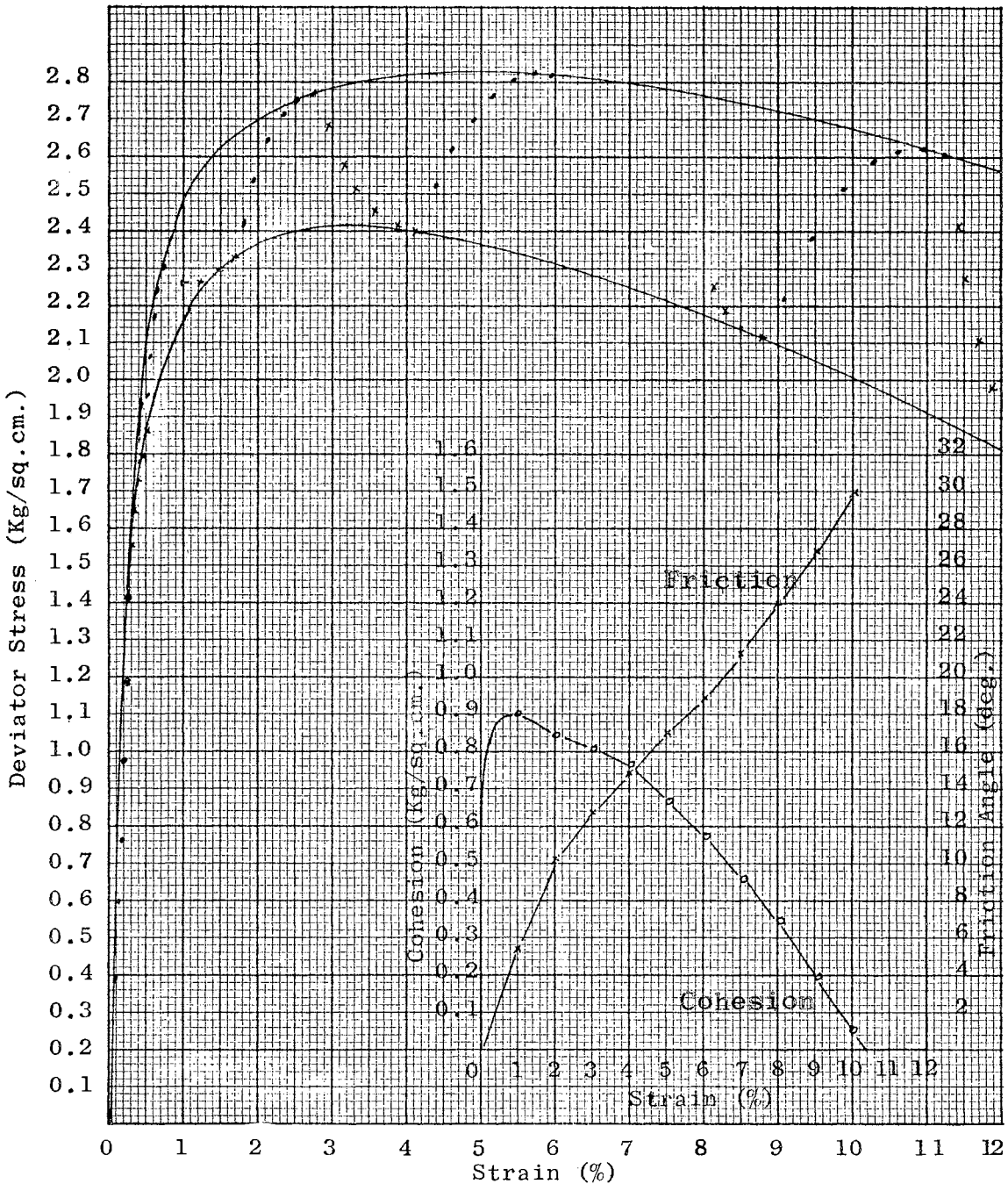

Fig. 16 - STRESS-STRAIN, CFS TEST, AN-L-2-1

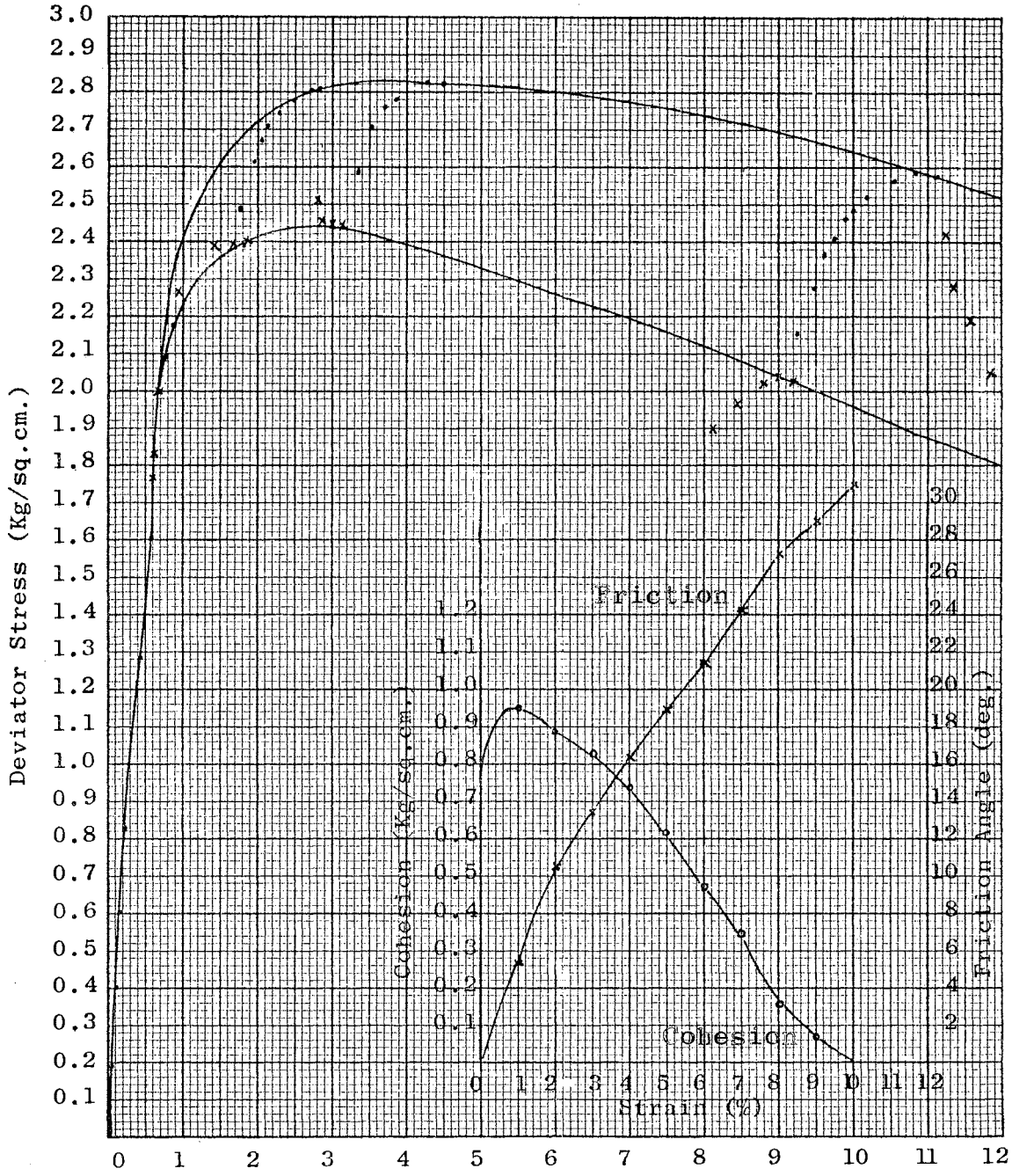

Fig. 17 - STRESS-STRAIN, CFS TEST, AN-L-2-2

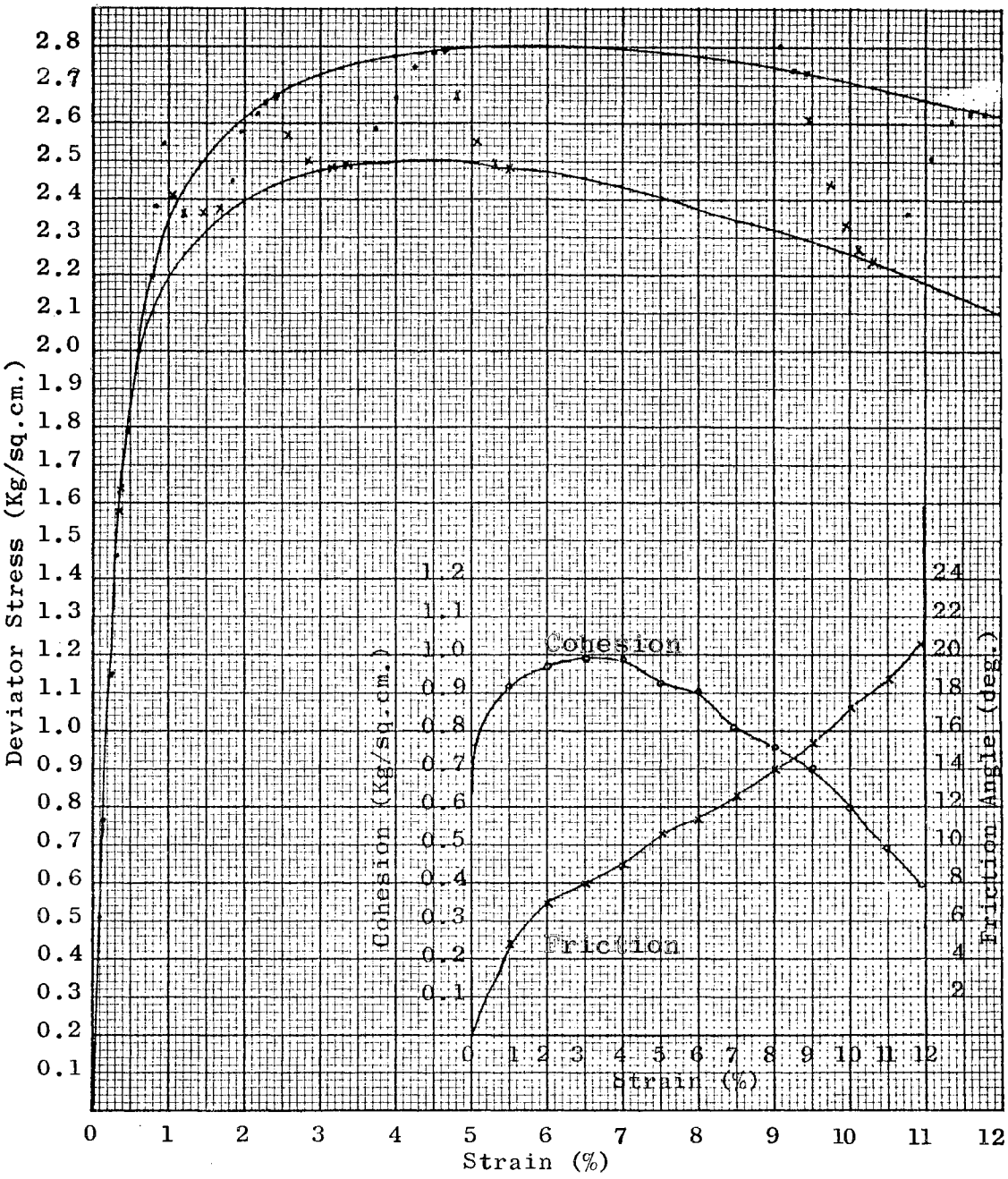

Fig. 18 - STRESS-STRAIN, CFS TEST, AN-L-2-3, No Drainage Threads

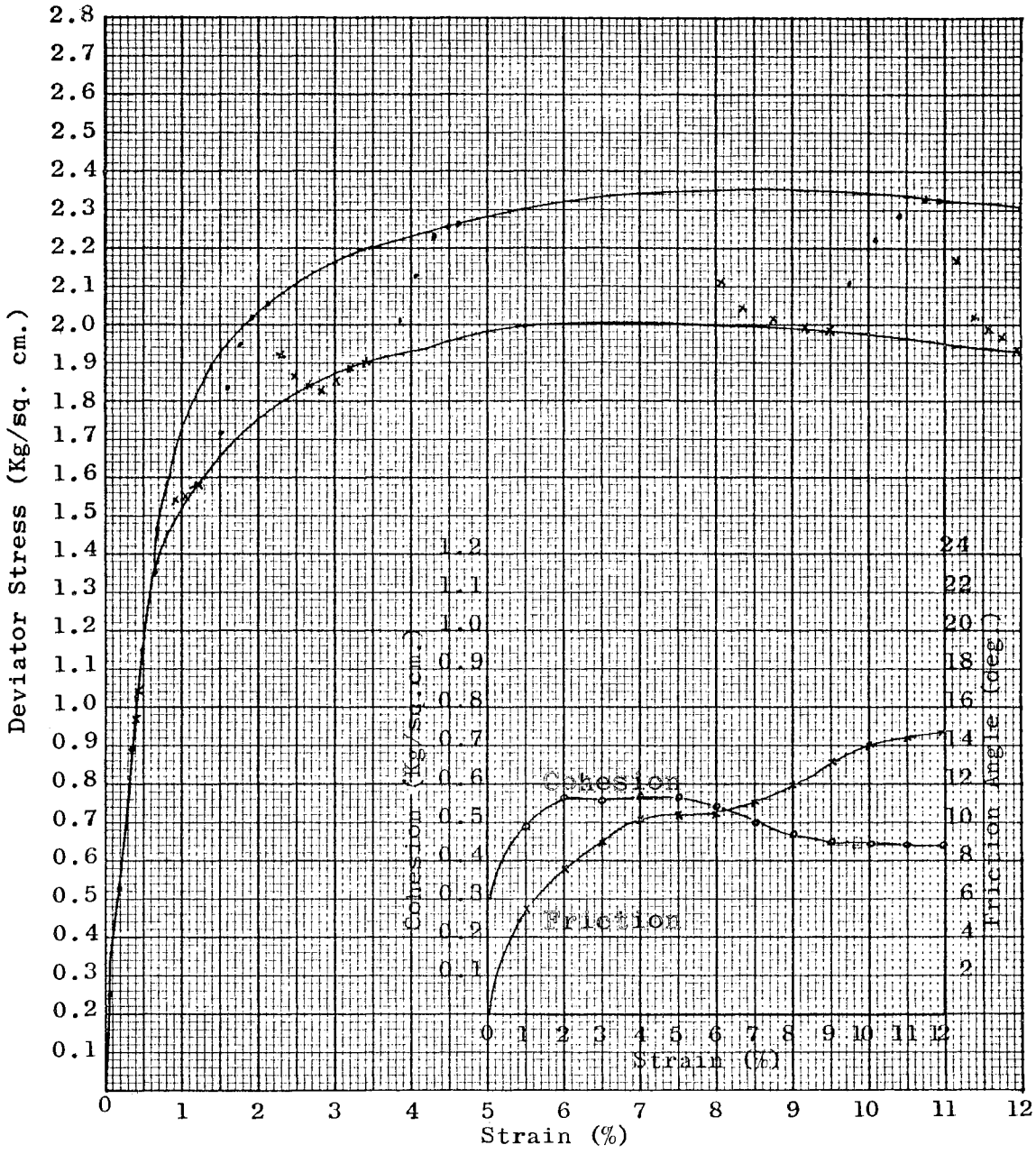

Fig. 19 - STRESS-STRAIN, CFS TEST, IS-H-1-1

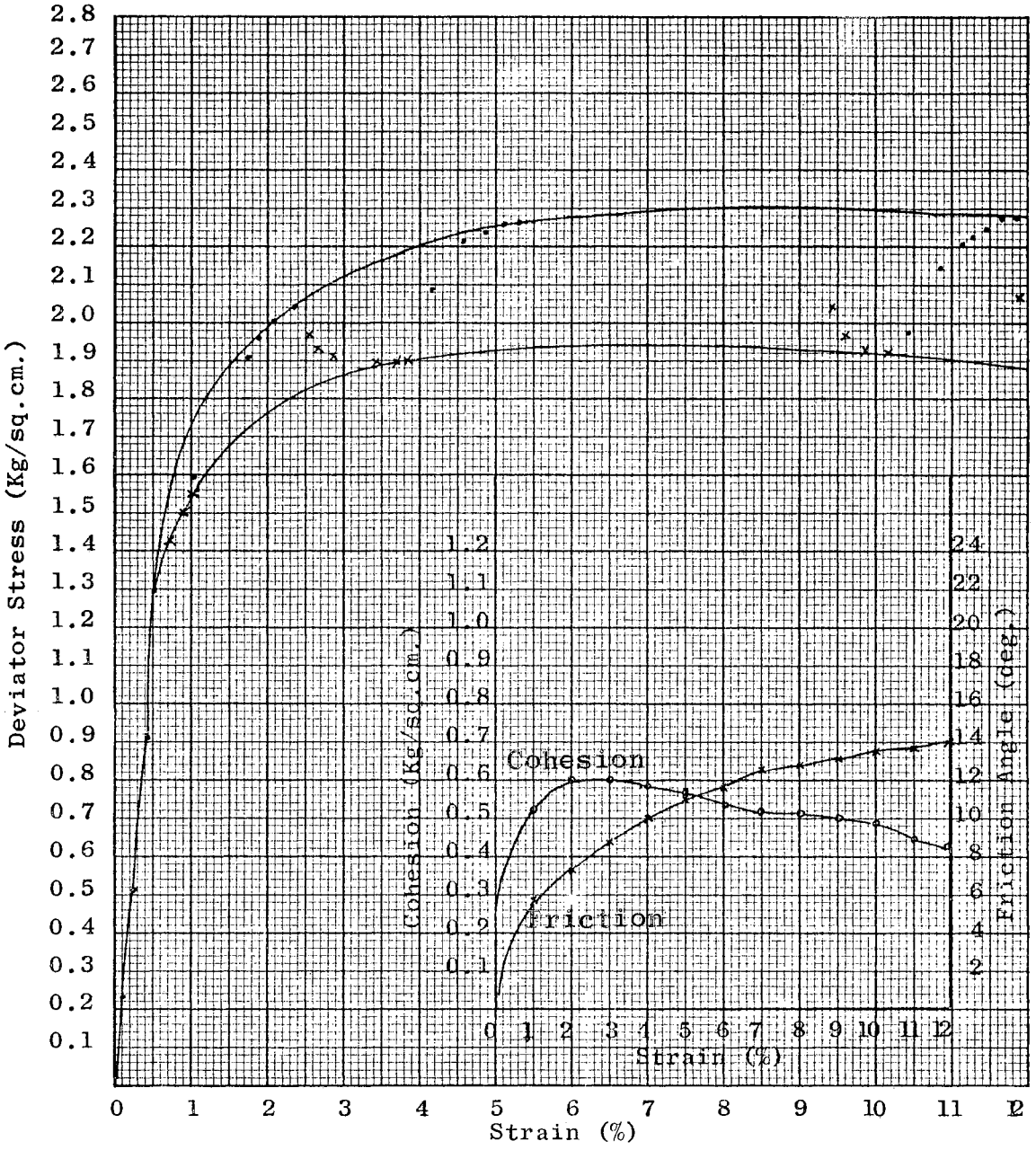

Fig. 20 - STRESS-STRAIN, CFS TEST, IS-H-1-2

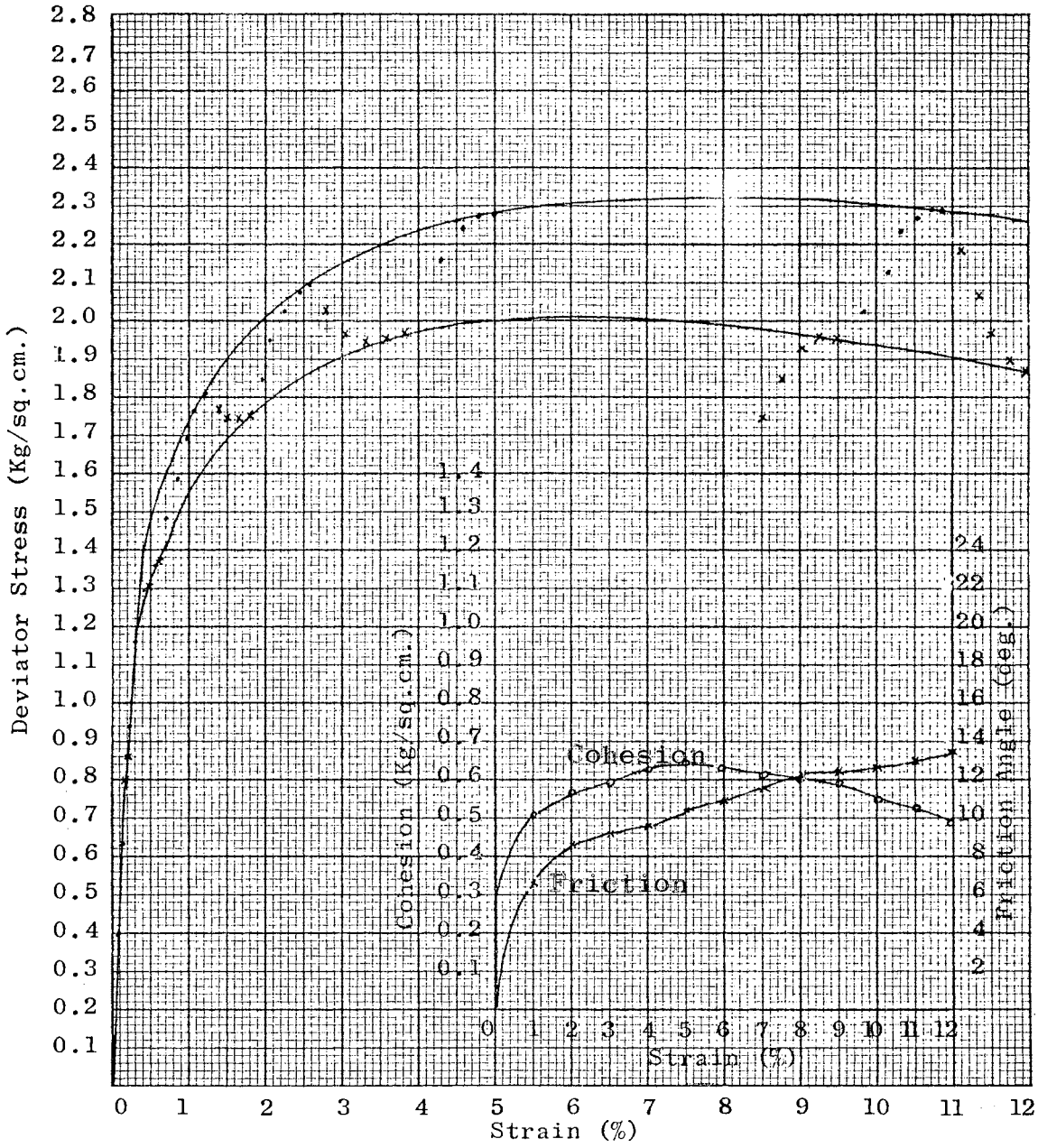

Fig. 21 - STRESS-STRAIN, CFS TEST, IS-H-1-3, No Drainage Threads, No Filter Paper

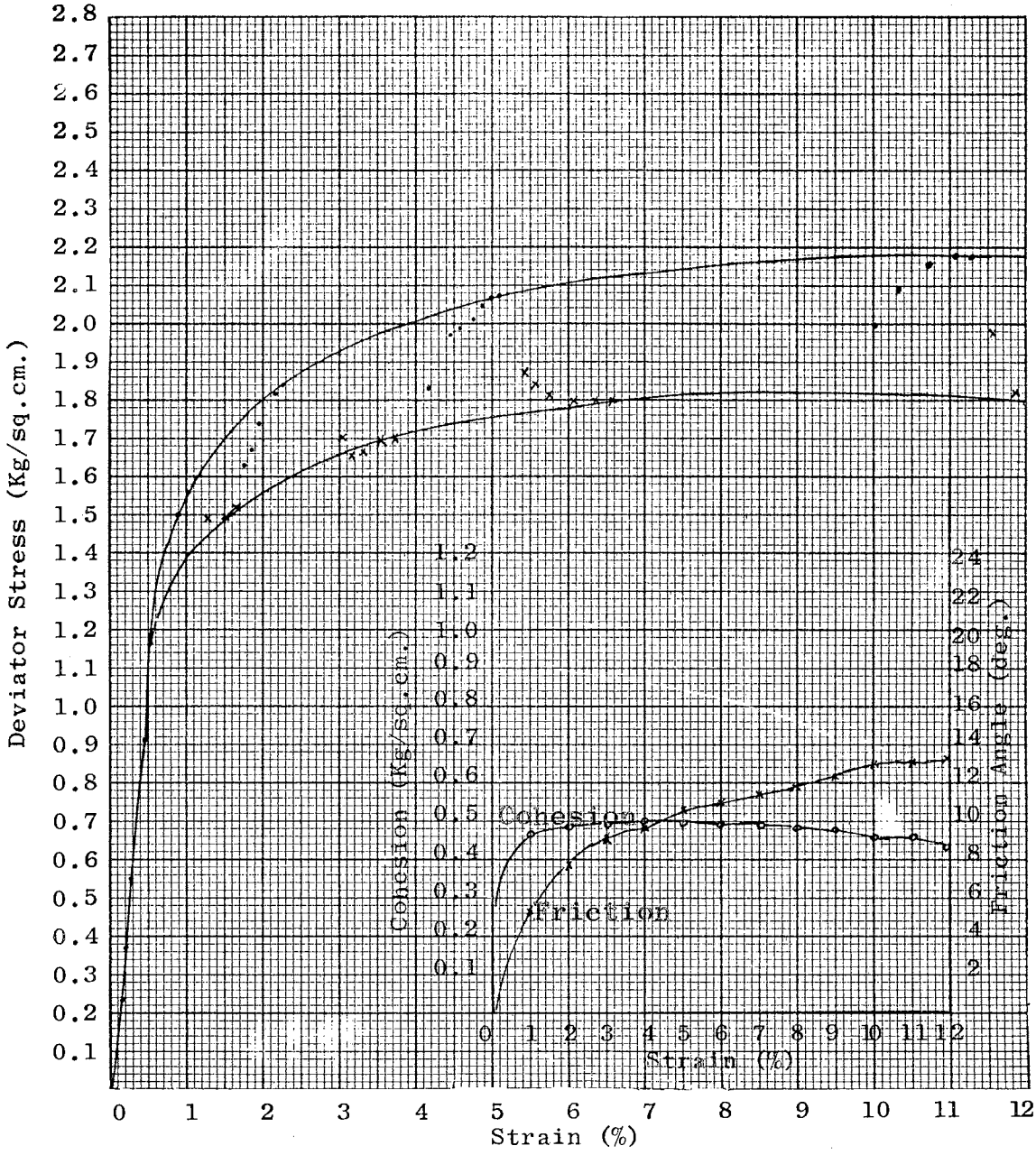

Fig. 22 - STRESS-STRAIN, CFS TEST, IS-H-2-1

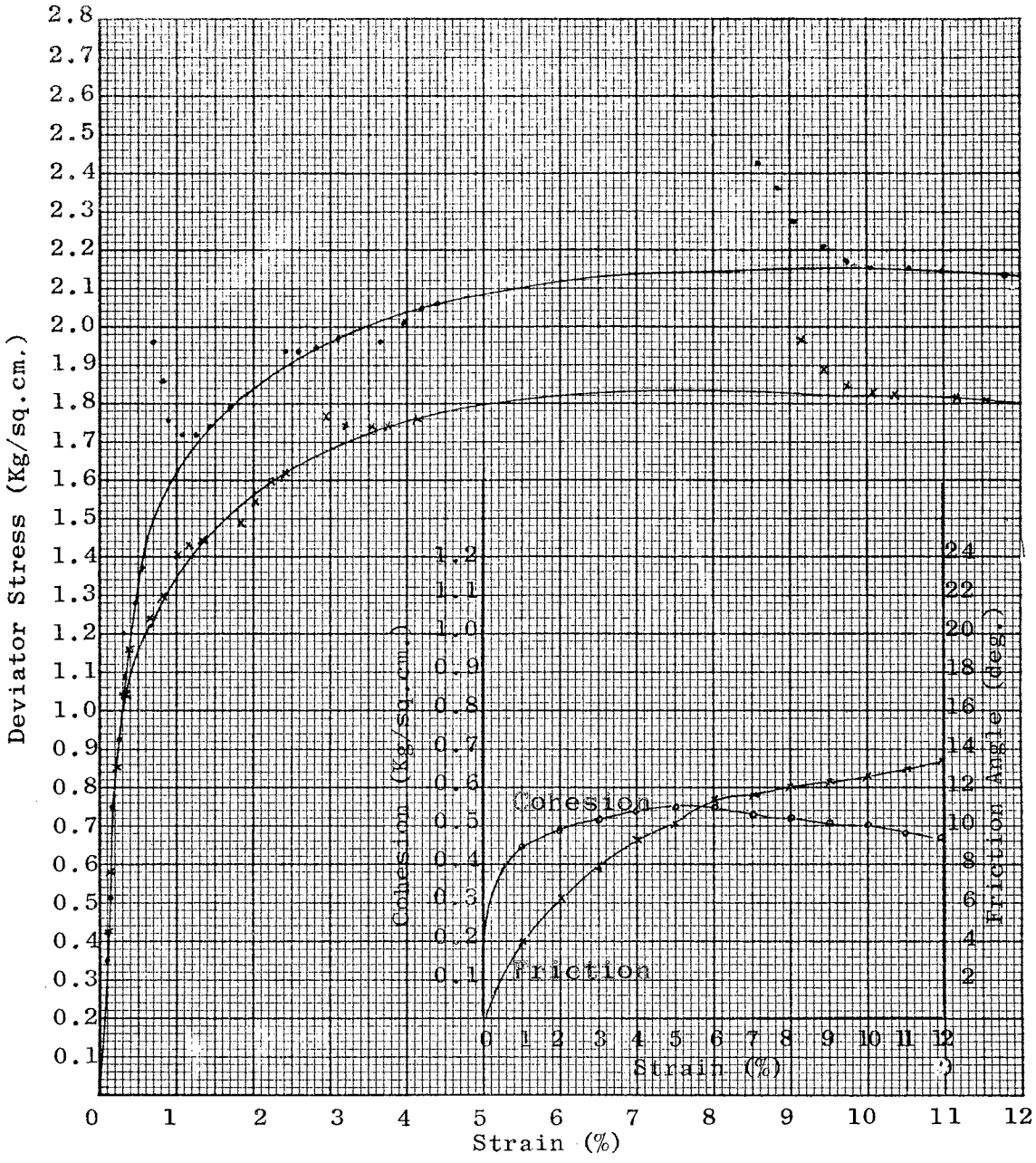

Fig. 23 - STRESS-STRAIN, CFS TEST, IS-H-2-2, 3, 2 Specimen Test

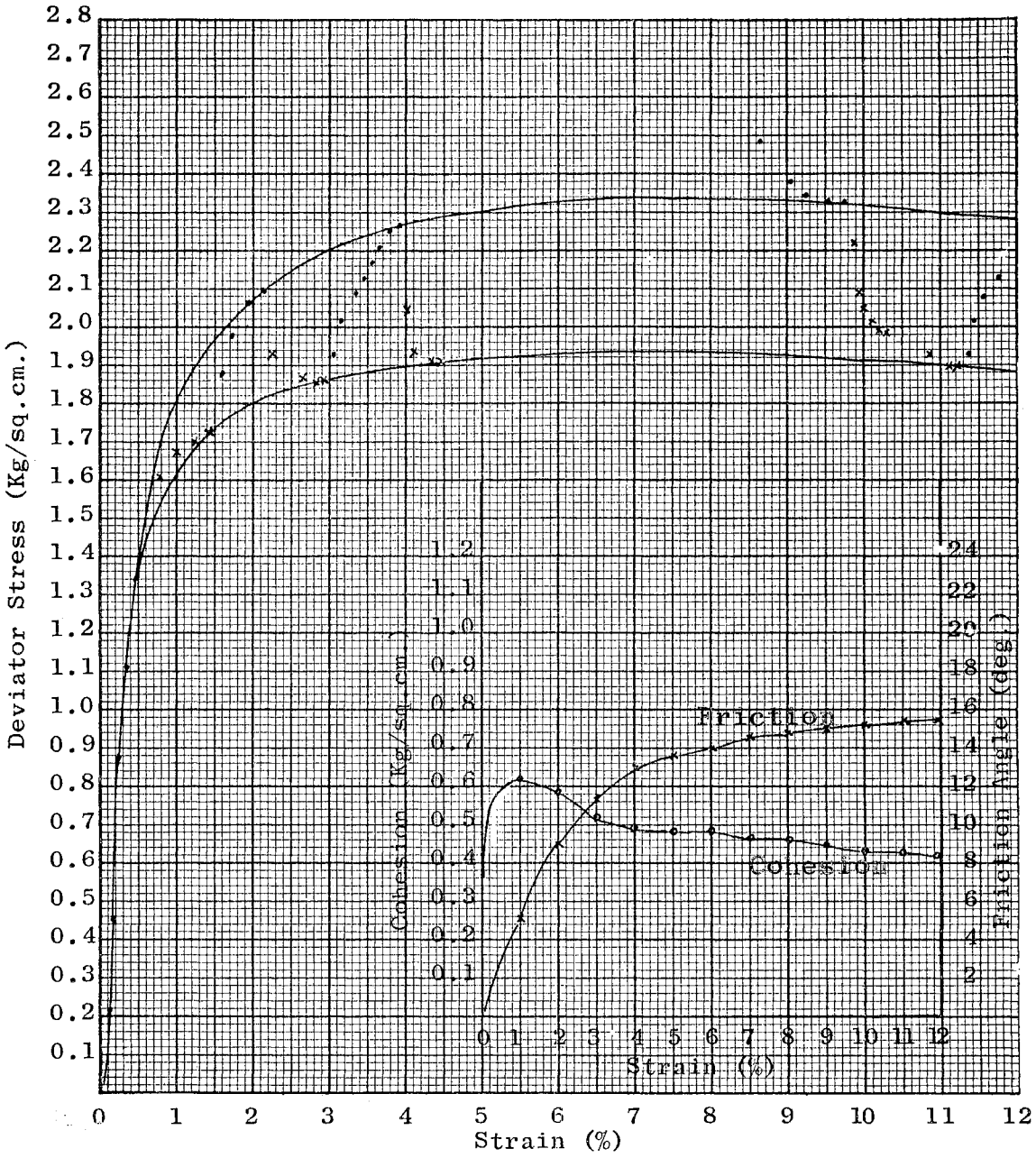

Fig. 24 - STRESS-STRAIN, CFS TEST, IS-M-1-1

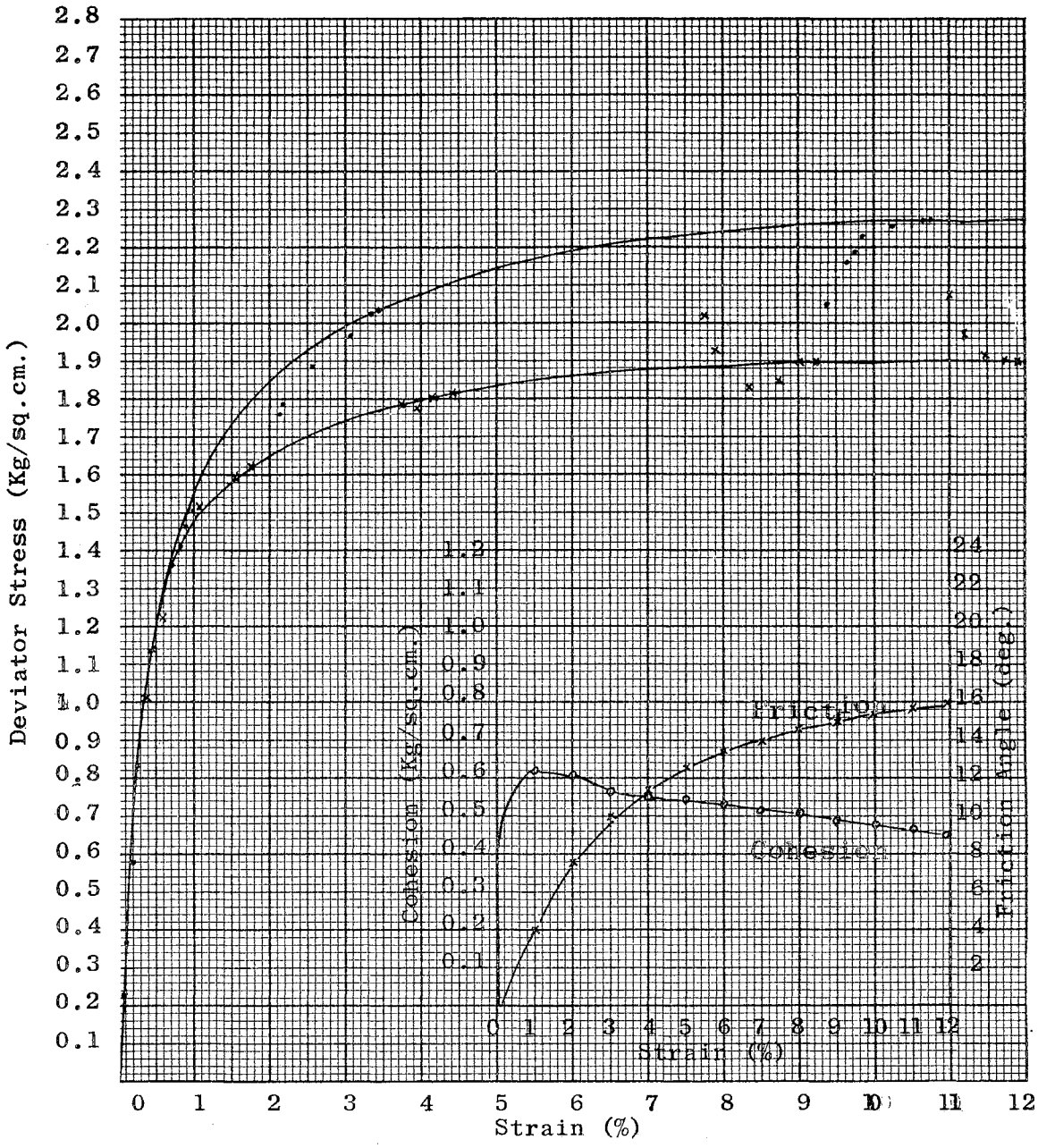

Fig. 25 - STRESS-STRAIN, CFS TEST, IS-M-1-2

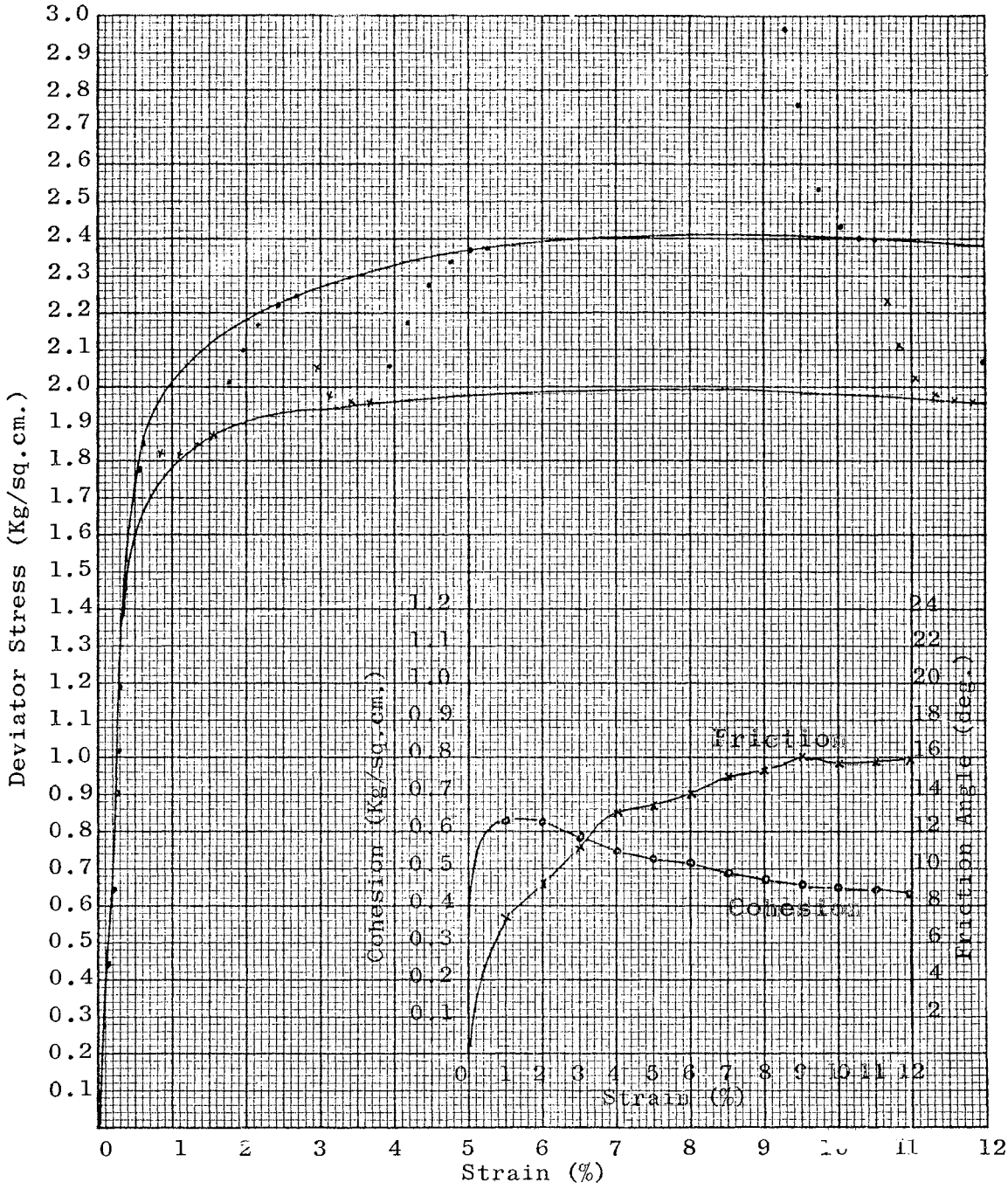

Fig. 26 - STRESS-STRAIN, CFS TEST, IS-M-2-1

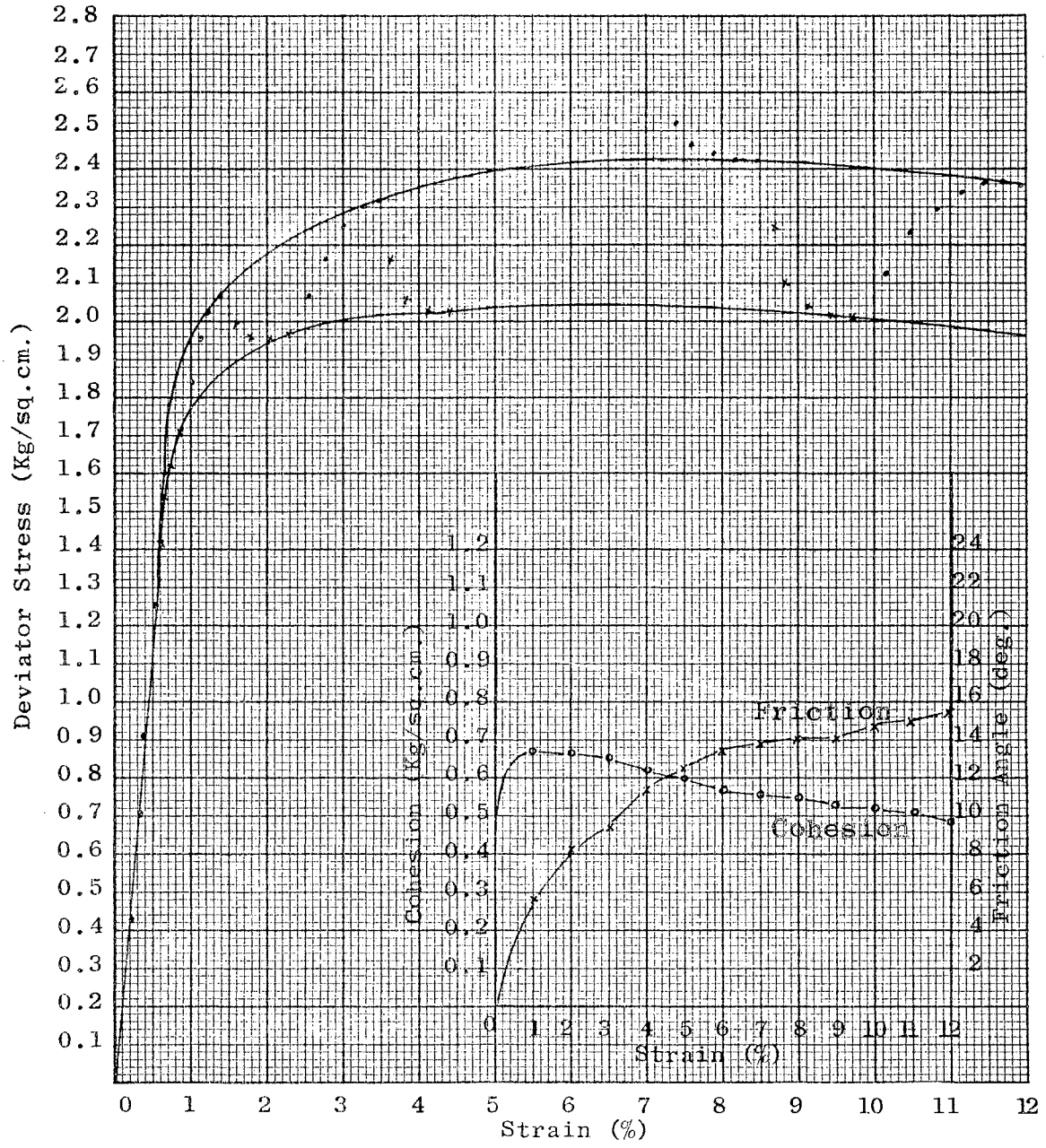

Fig. 27 - STRESS-STRAIN, CFS TEST, IS-M-2-2

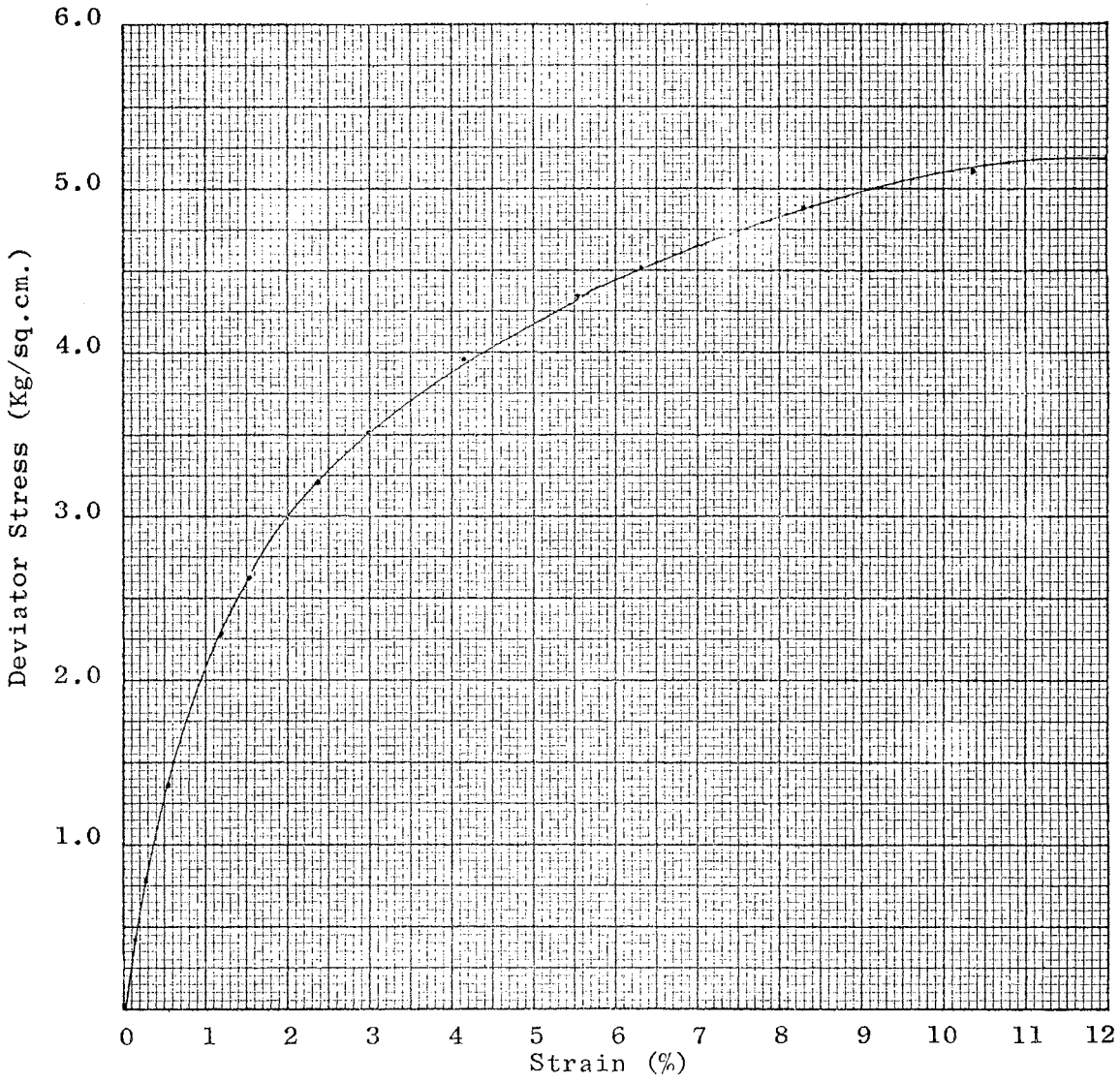

Fig. 28 - STRESS-STRAIN, CFS TEST, IS-M-2-3, Zero Pore Pressure

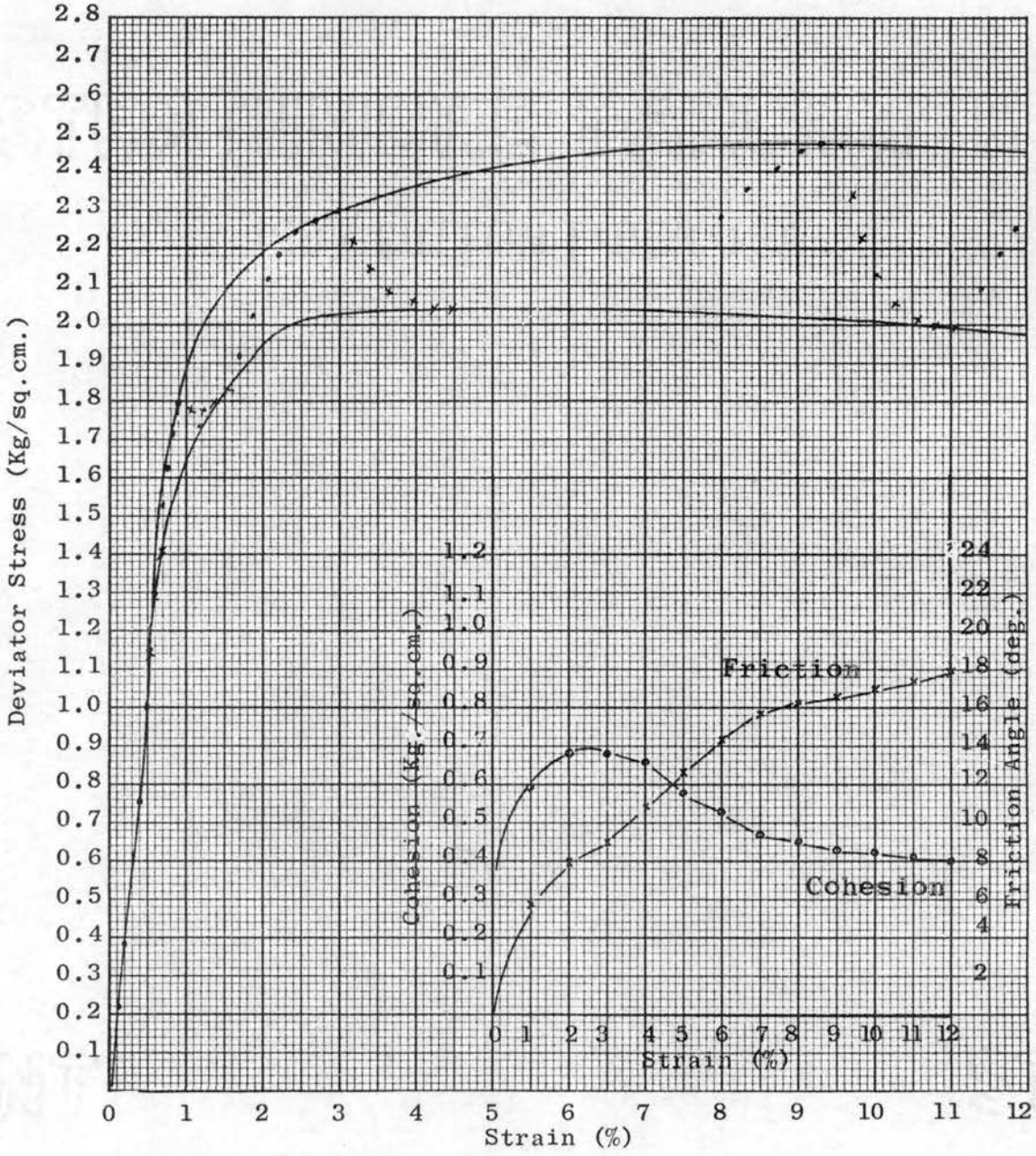

Fig. 29 - STRESS-STRAIN, CFS TEST, IS-L-1-1

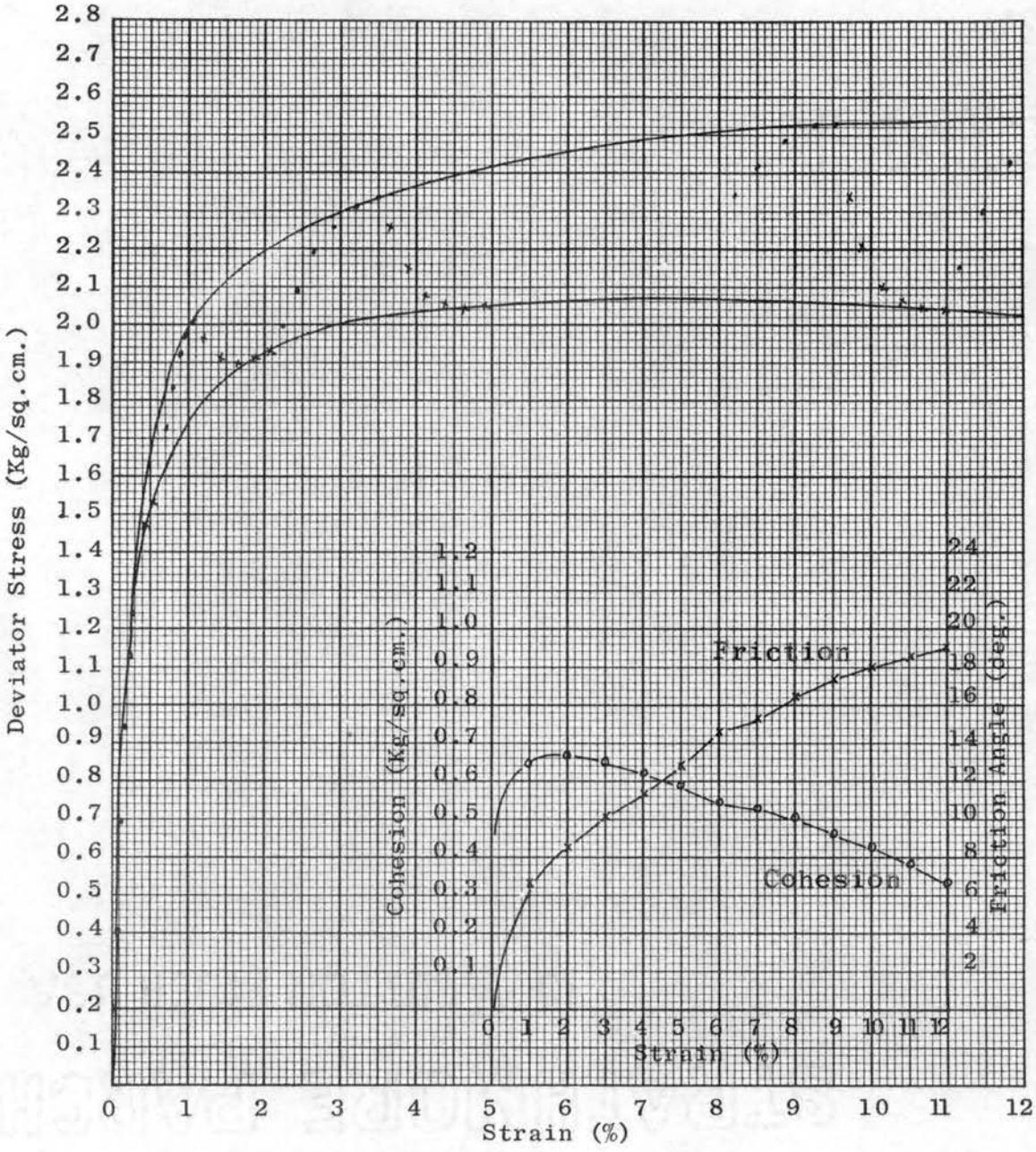

Fig. 30 - STRESS-STRAIN, CFS TEST, IS-L-1-2

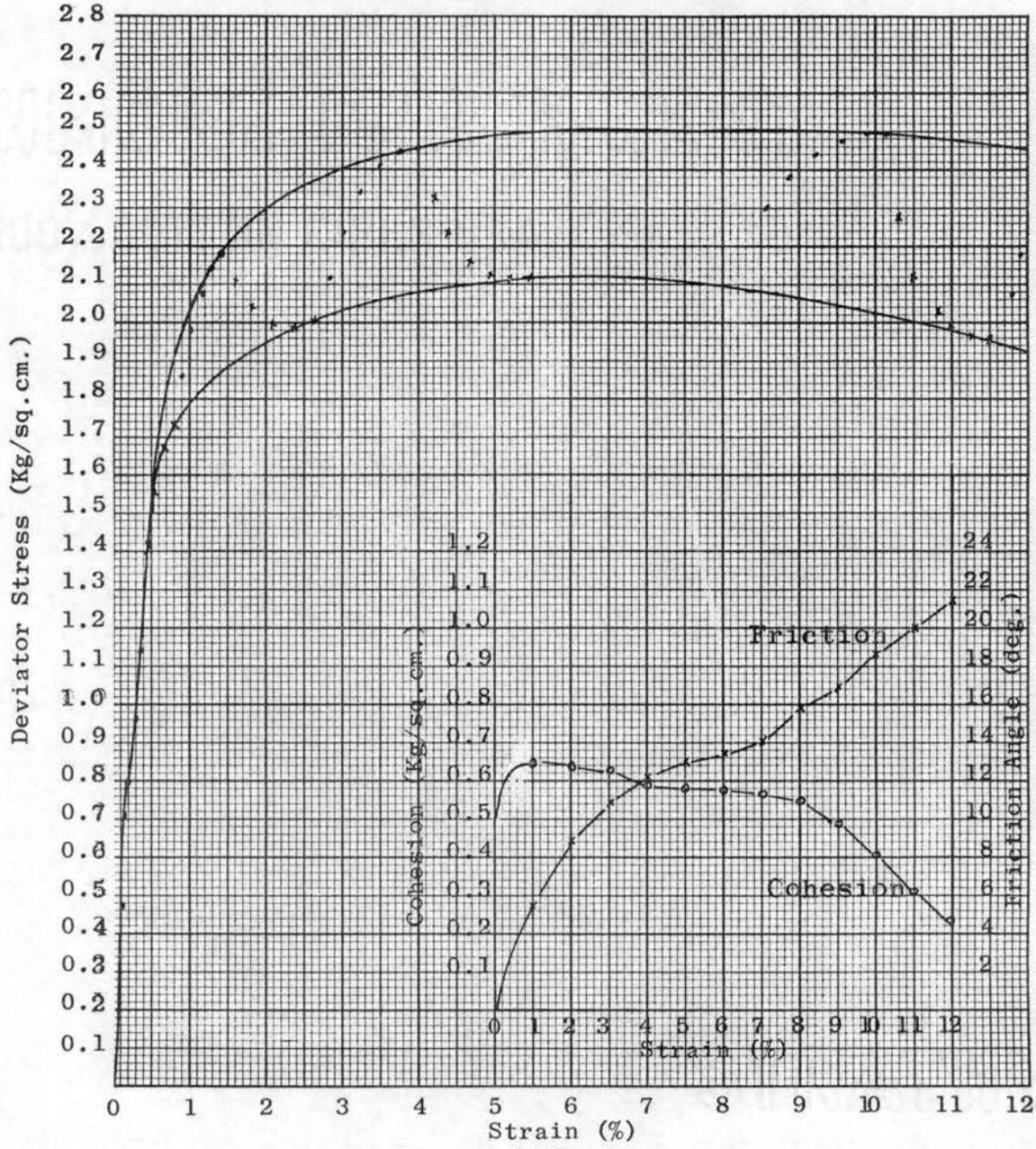

Fig. 31 - STRESS-STRAIN, CFS TEST, IS-L-2-1

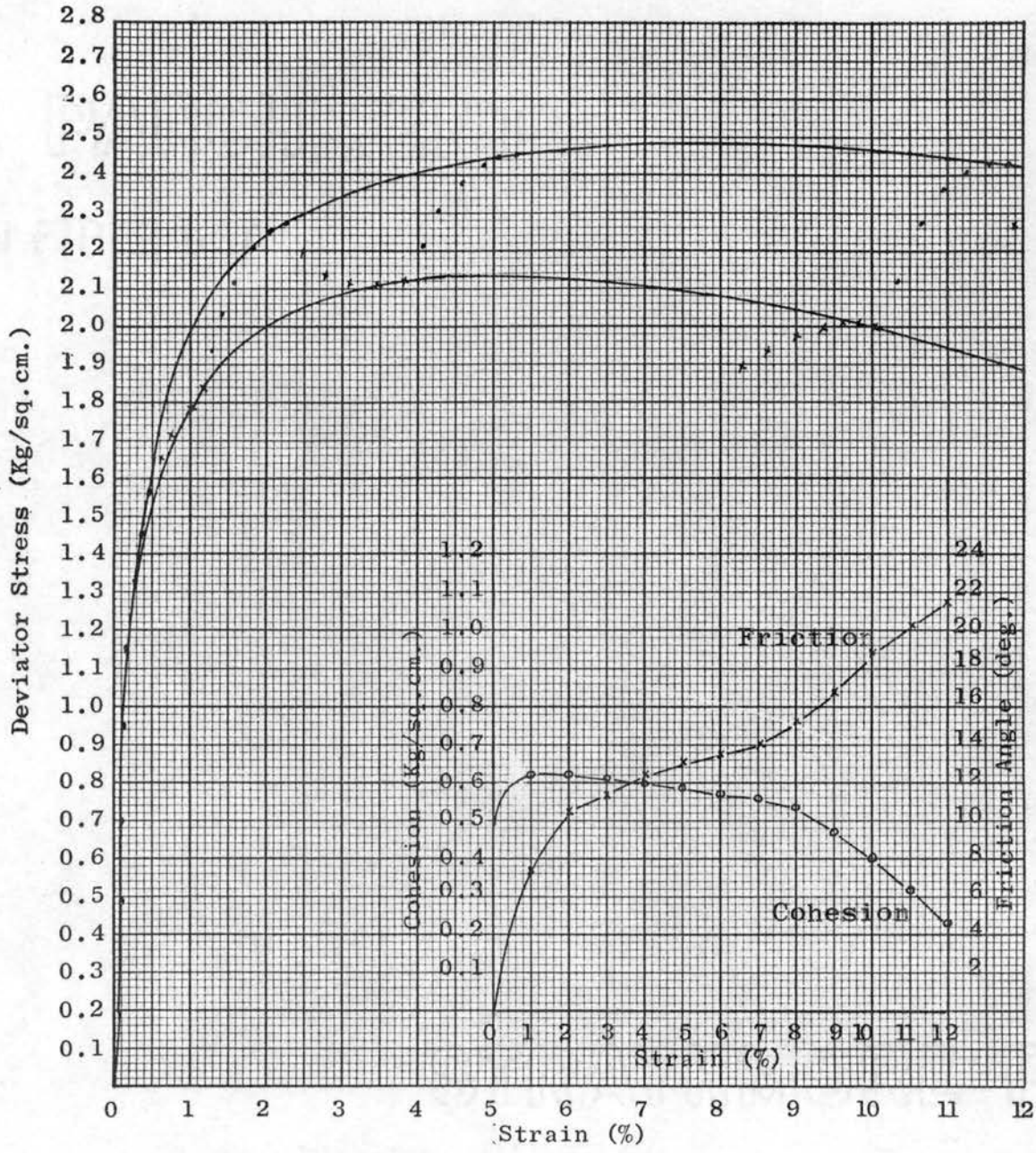

Fig. 32 - STRESS-STRAIN, CFS TEST, IS-L-2-2

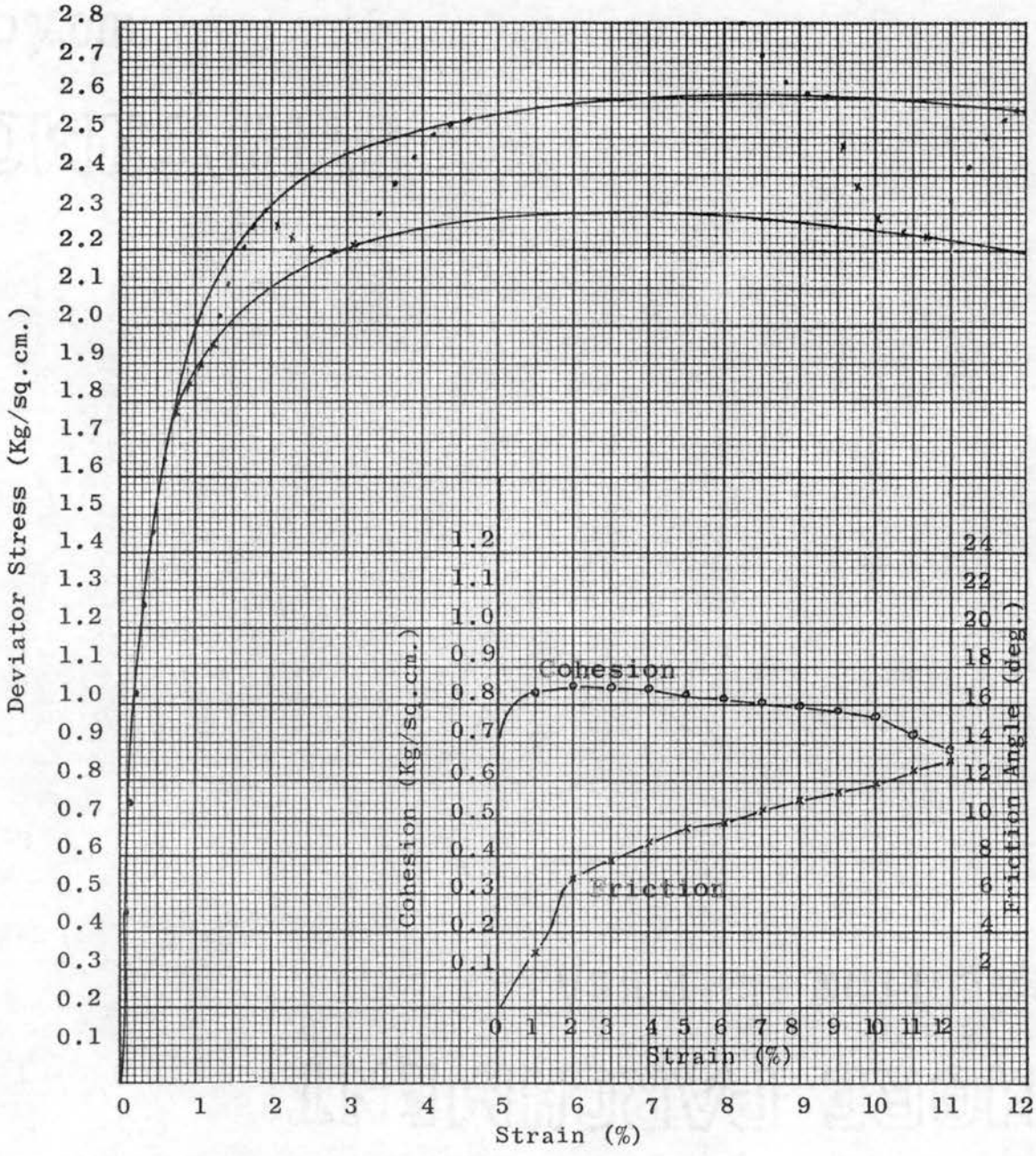

Fig. 33 - STRESS-STRAIN, CFS TEST, IS-L-2-3, No Drainage Threads

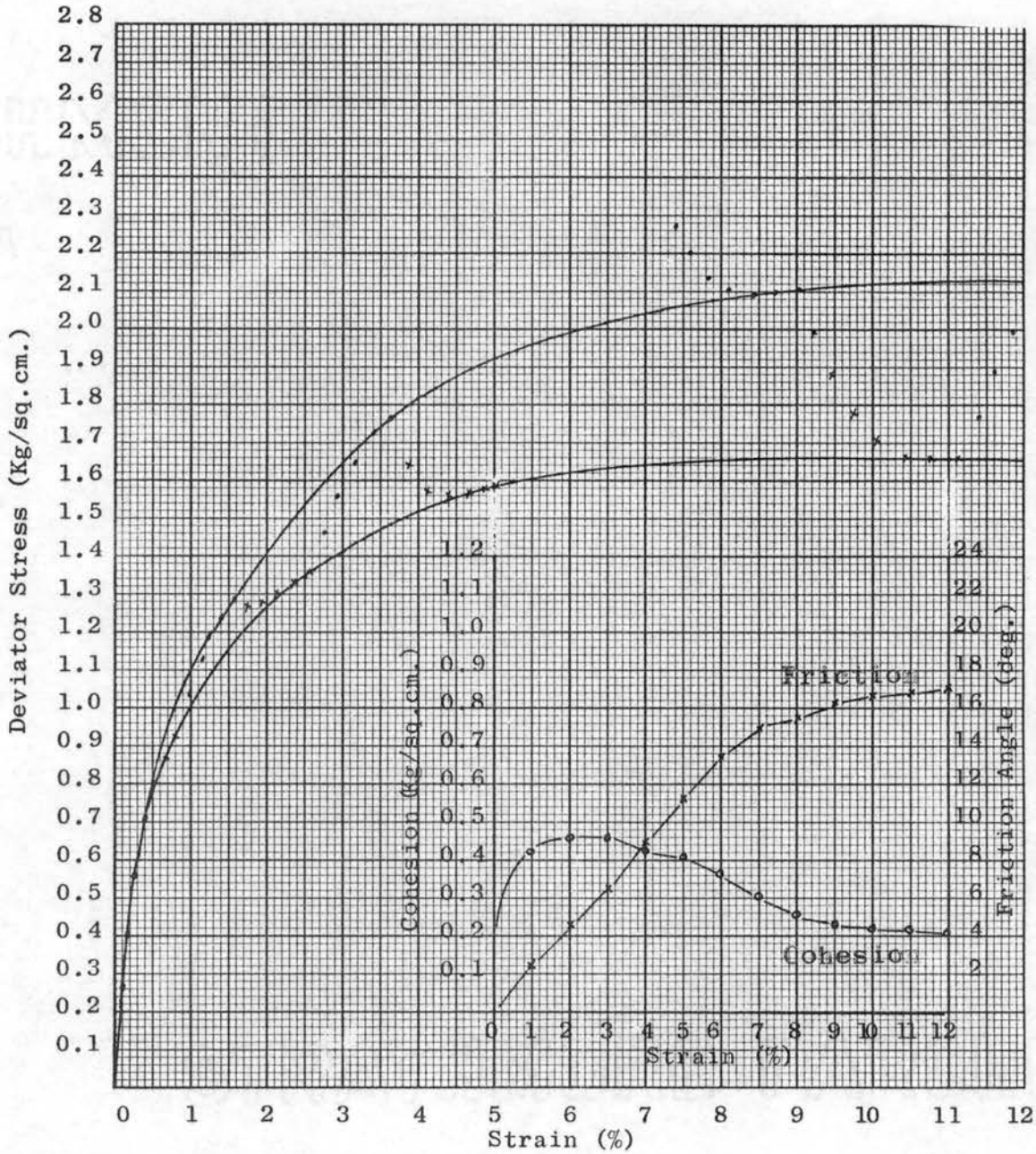

Fig. 34 - STRESS-STRAIN, CFS TEST, HC-H-1

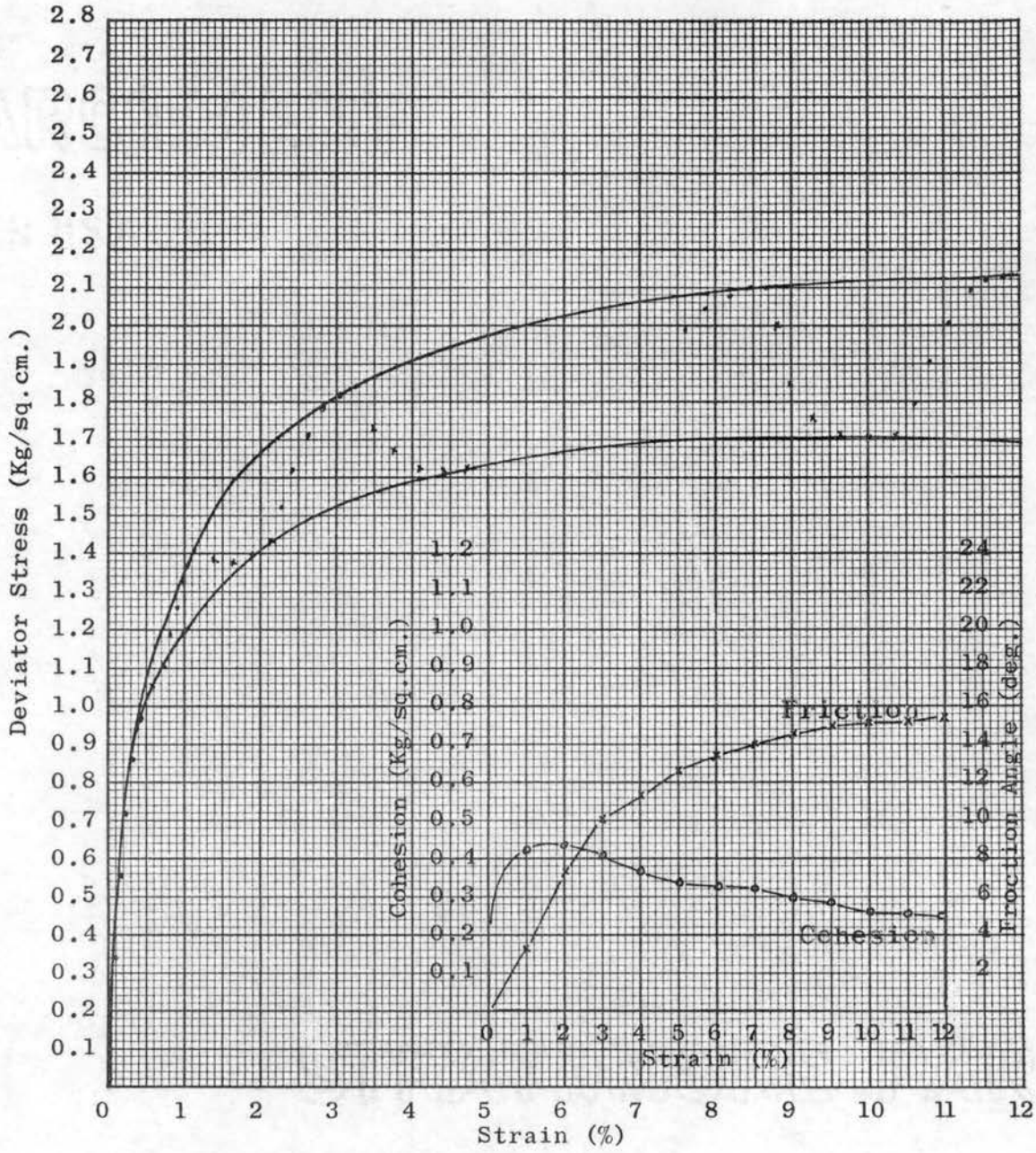

Fig. 35 - STRESS-STRAIN, CFS TEST, HC-H-2

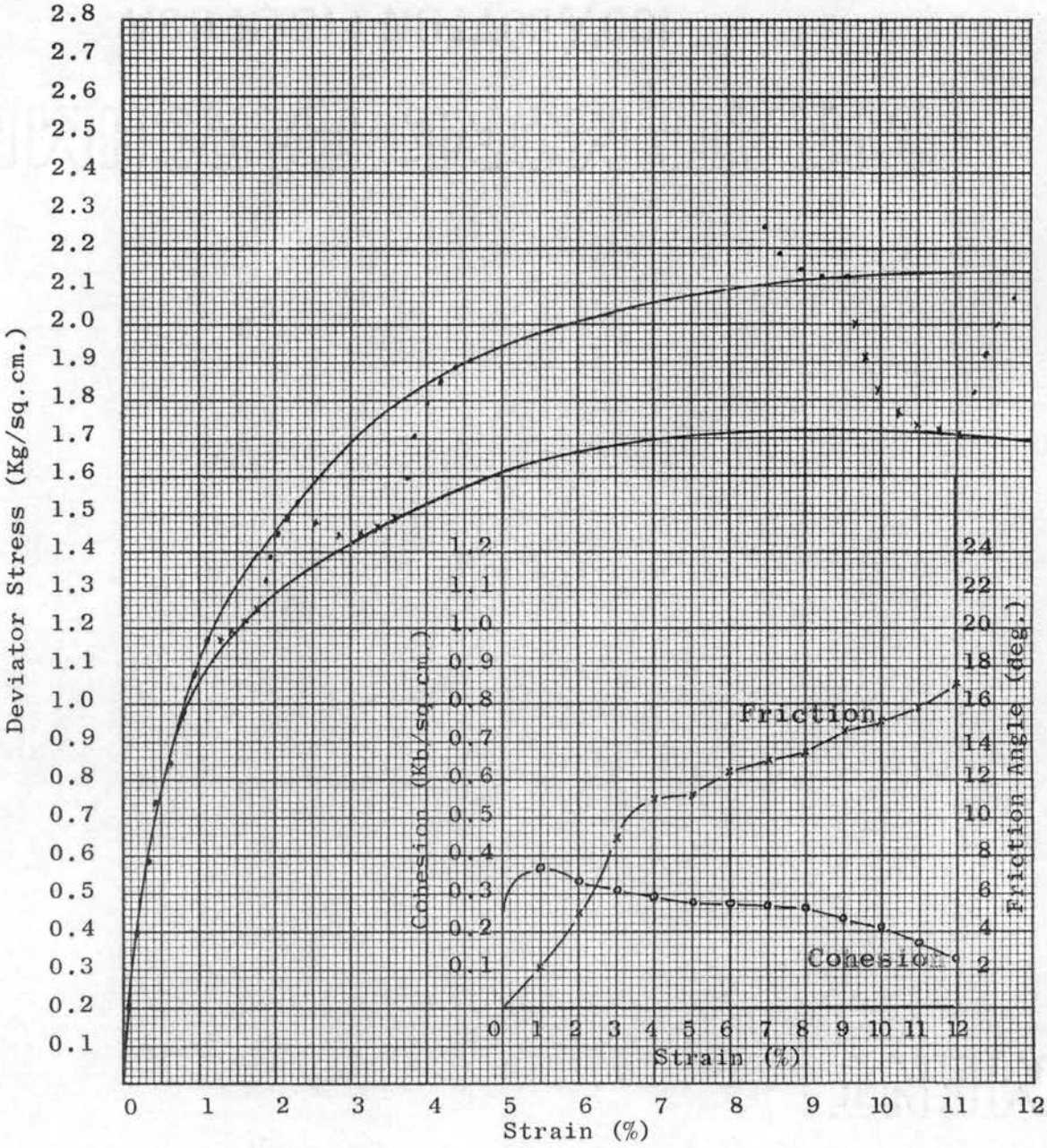

Fig. 36 - STRESS-STRAIN, CFS TEST, HC-H-3

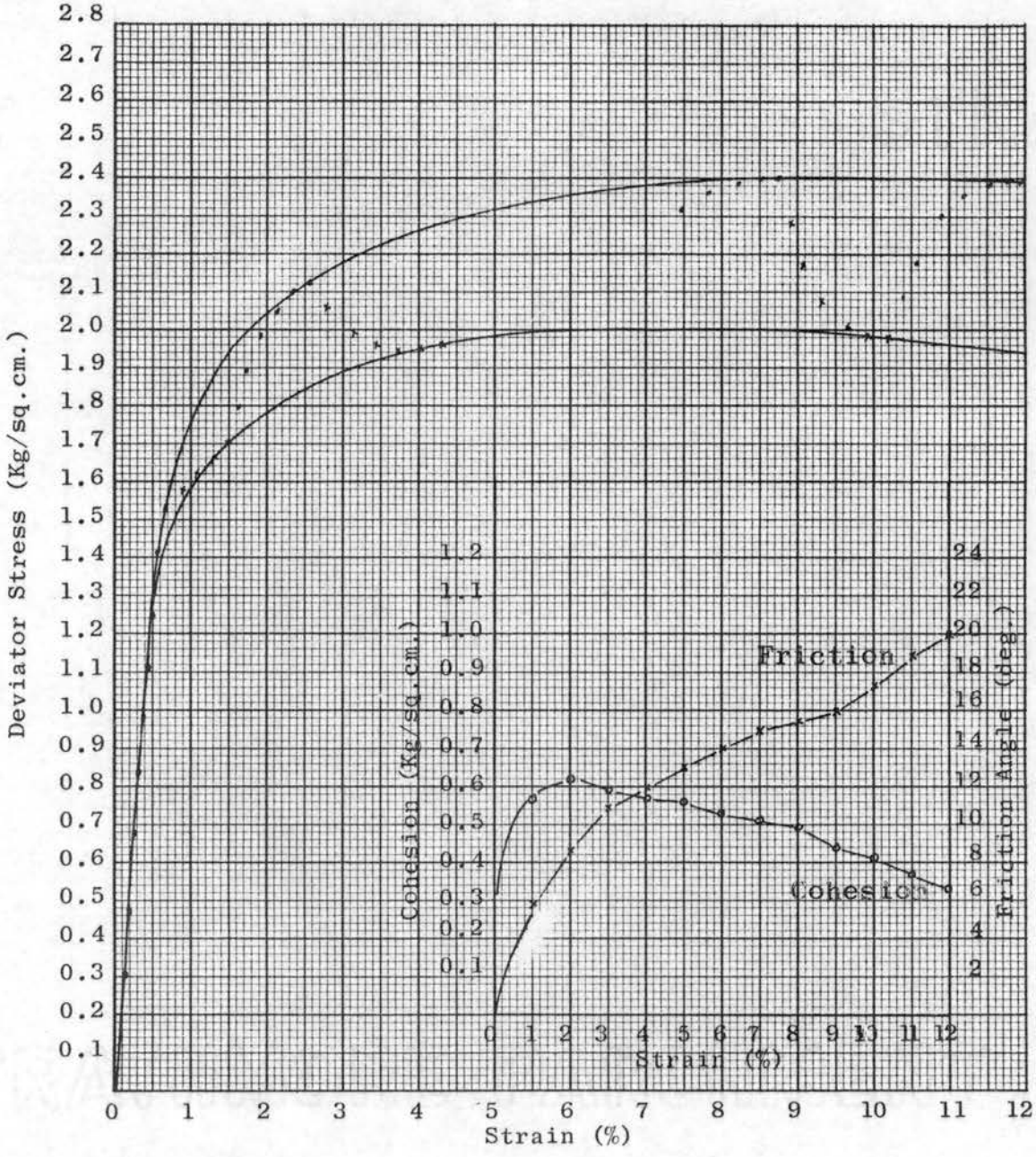

Fig. 37 - STRESS-STRAIN, CFS TEST, HC-M-1

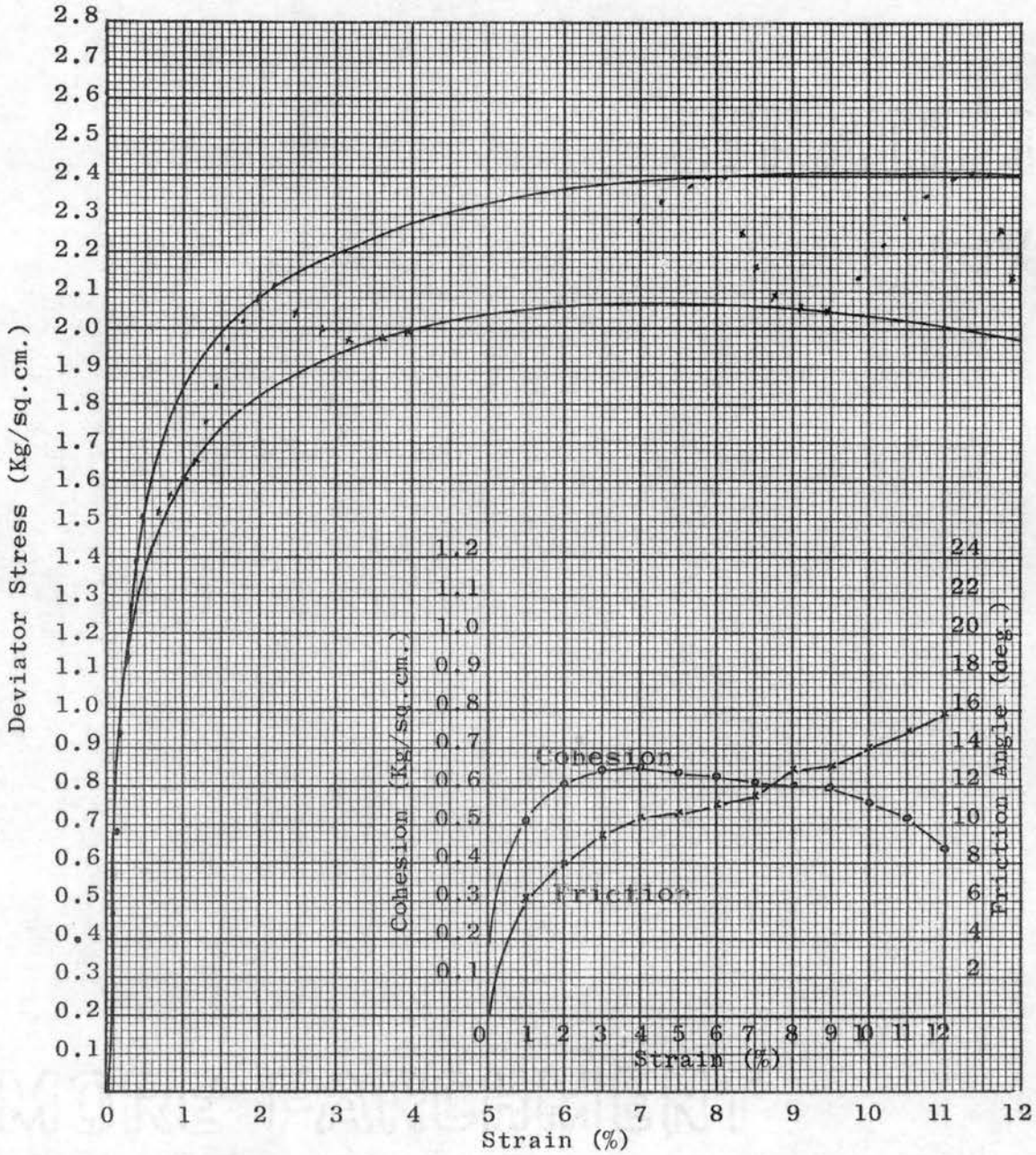

Fig. 38 - STRESS-STRAIN, CFS TEST, HC-M-2

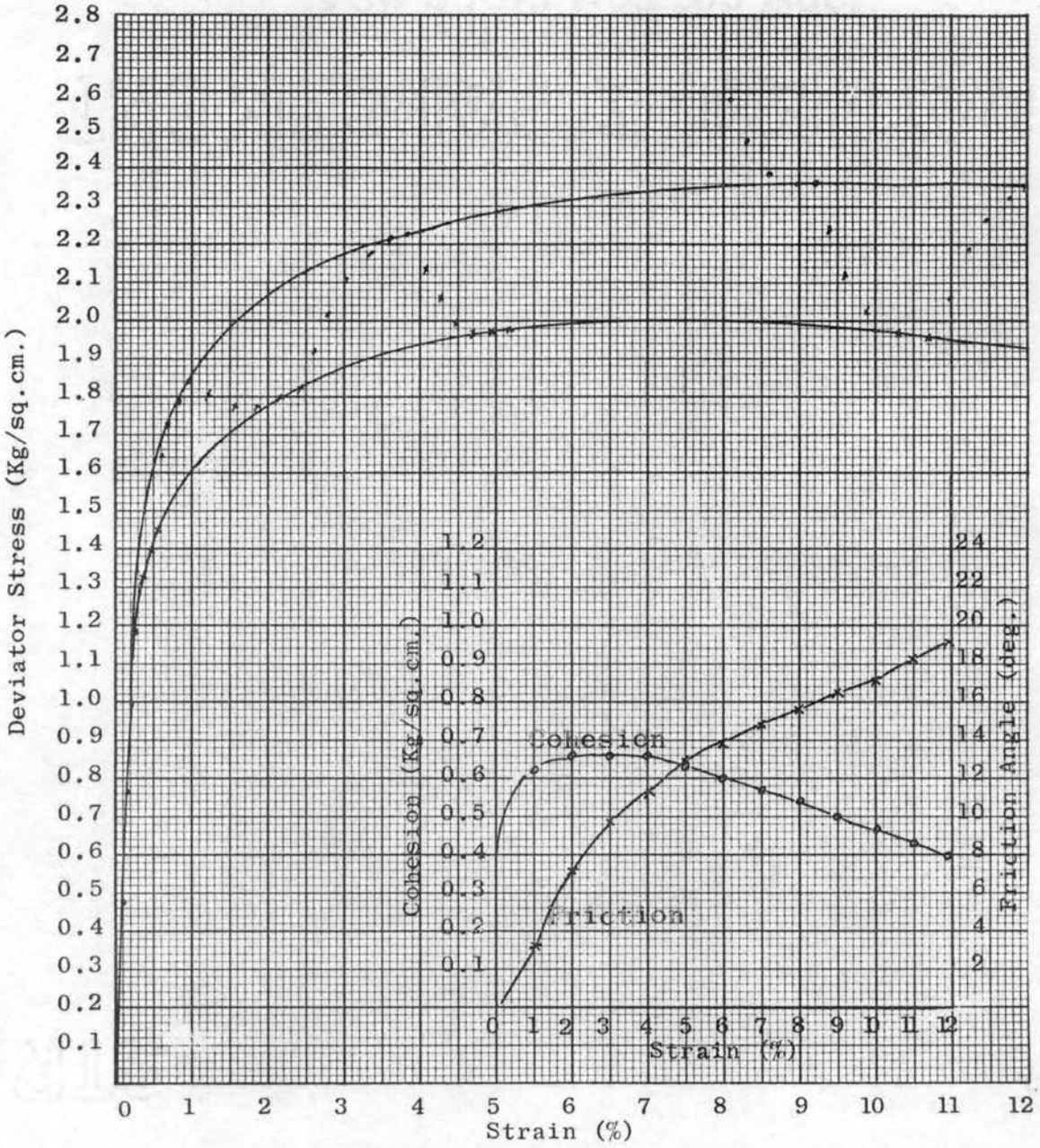

Fig. 39 - STRESS-STRAIN, CFS TEST, HC-M-3

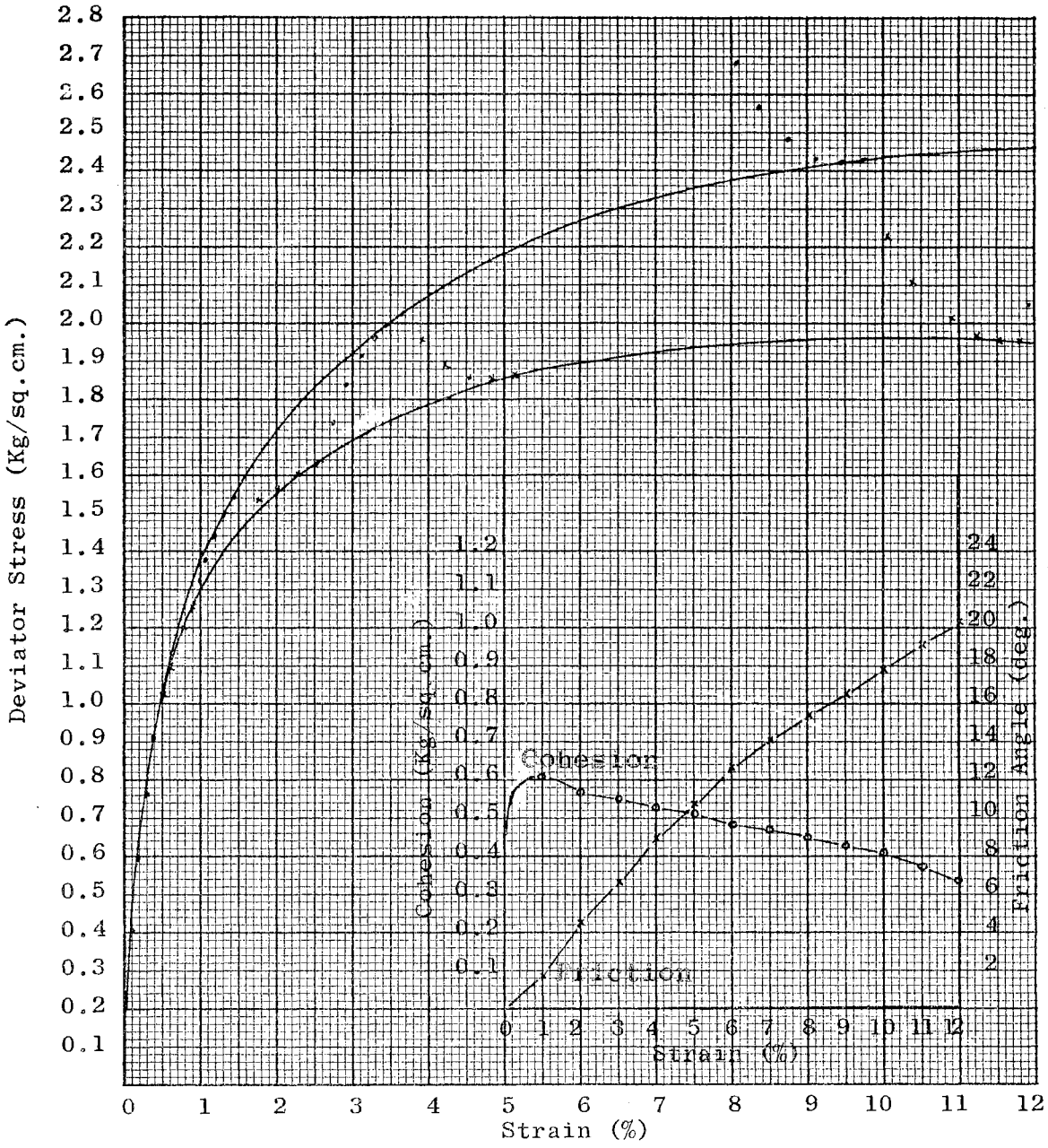

Fig. 40 - STRESS-STRAIN, CFS TEST, HC-L-1

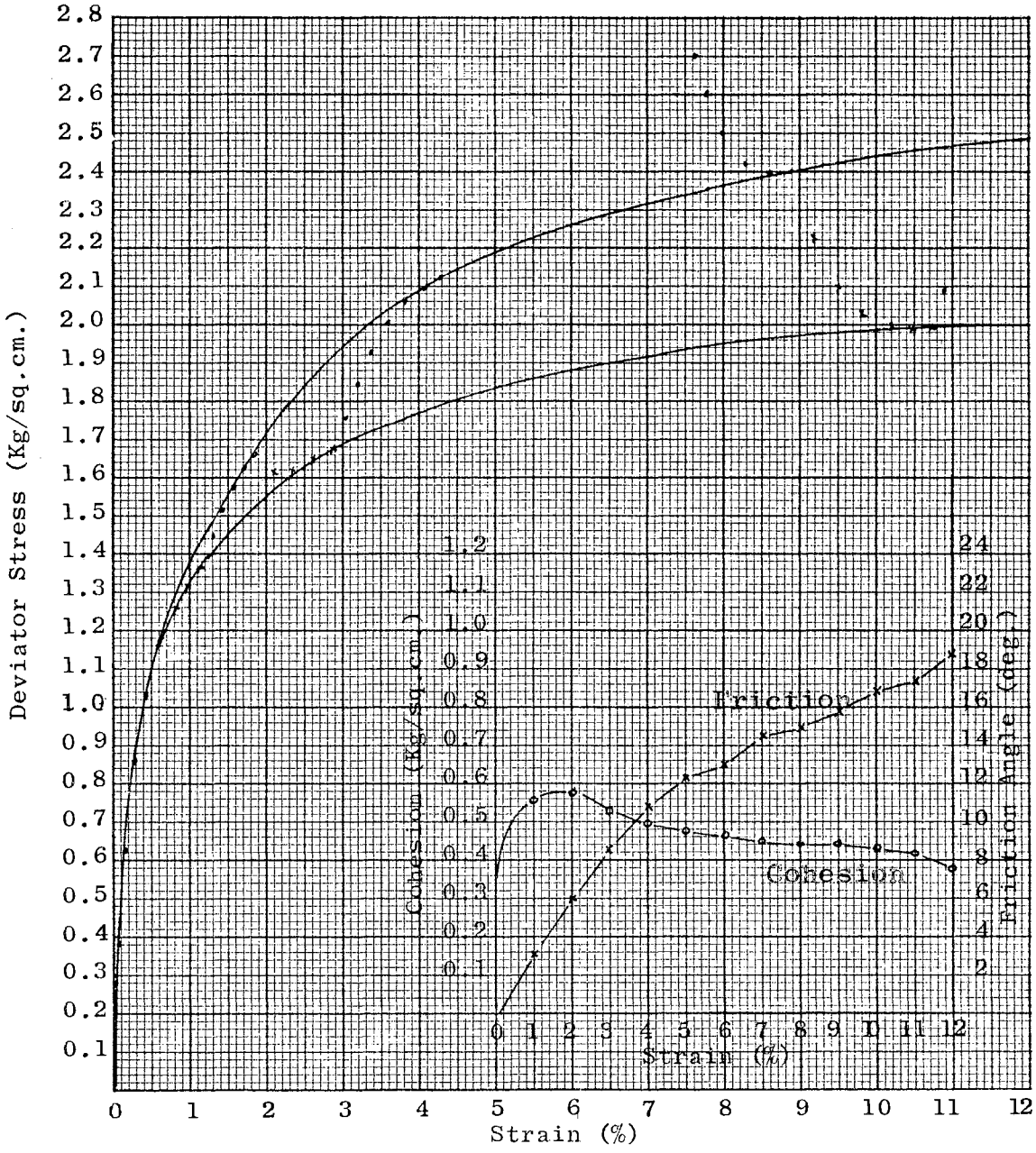

Fig. 41 - STRESS-STRAIN, CFS TEST, HC-L-2

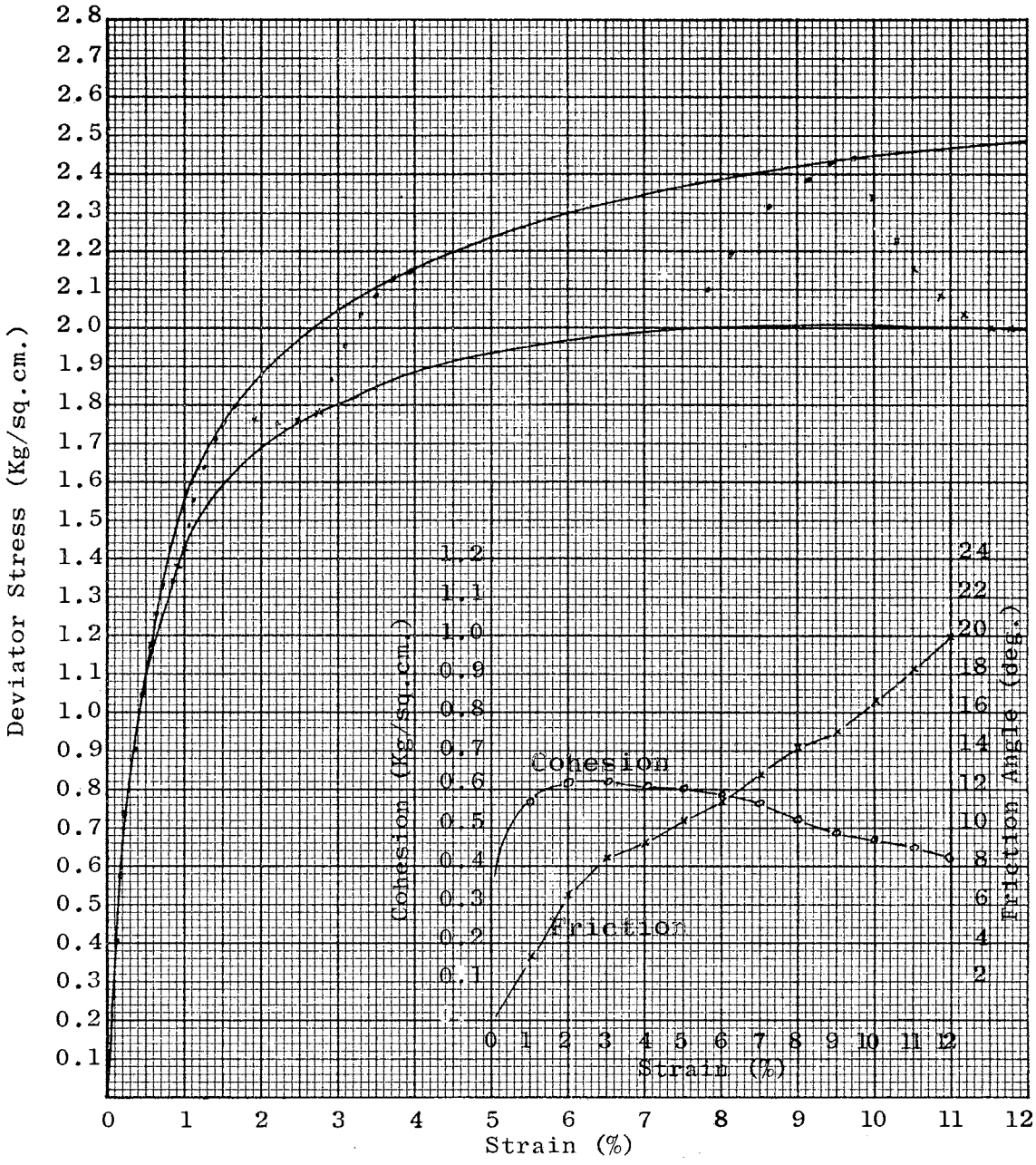

Fig. 42 - STRESS-STRAIN, CFS TEST, HC-L-3

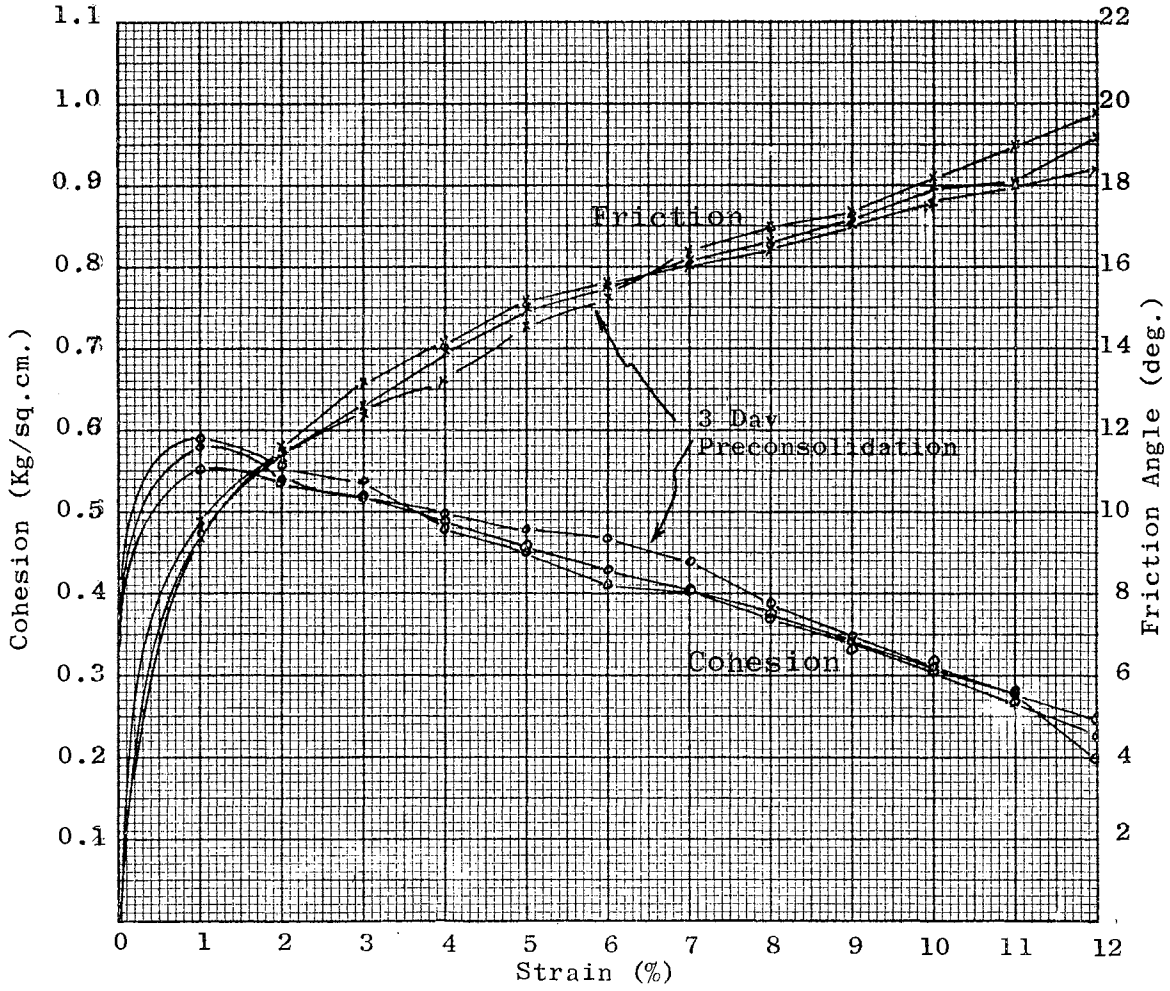

Fig. 43 - C AND ϕ VERSUS STRAIN - AN-H-1

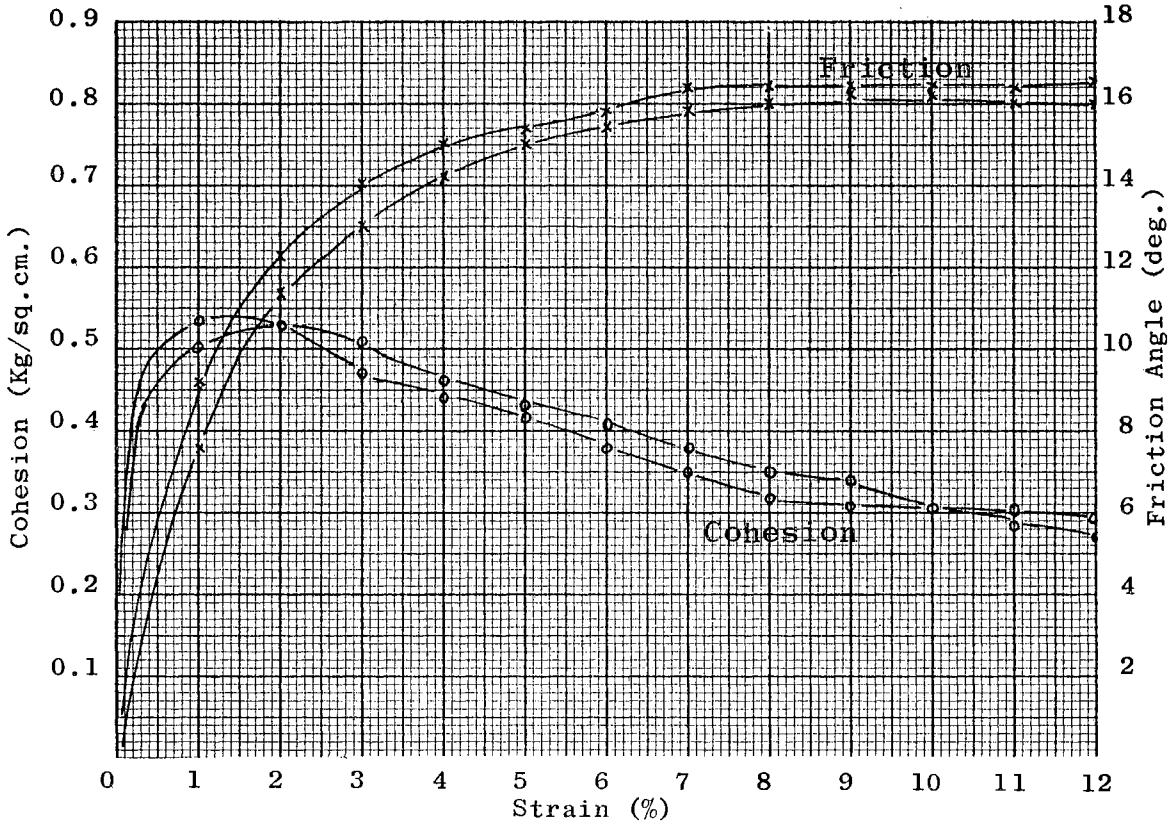

Fig. 44 - C AND ϕ VERSUS STRAIN - AN-M-1

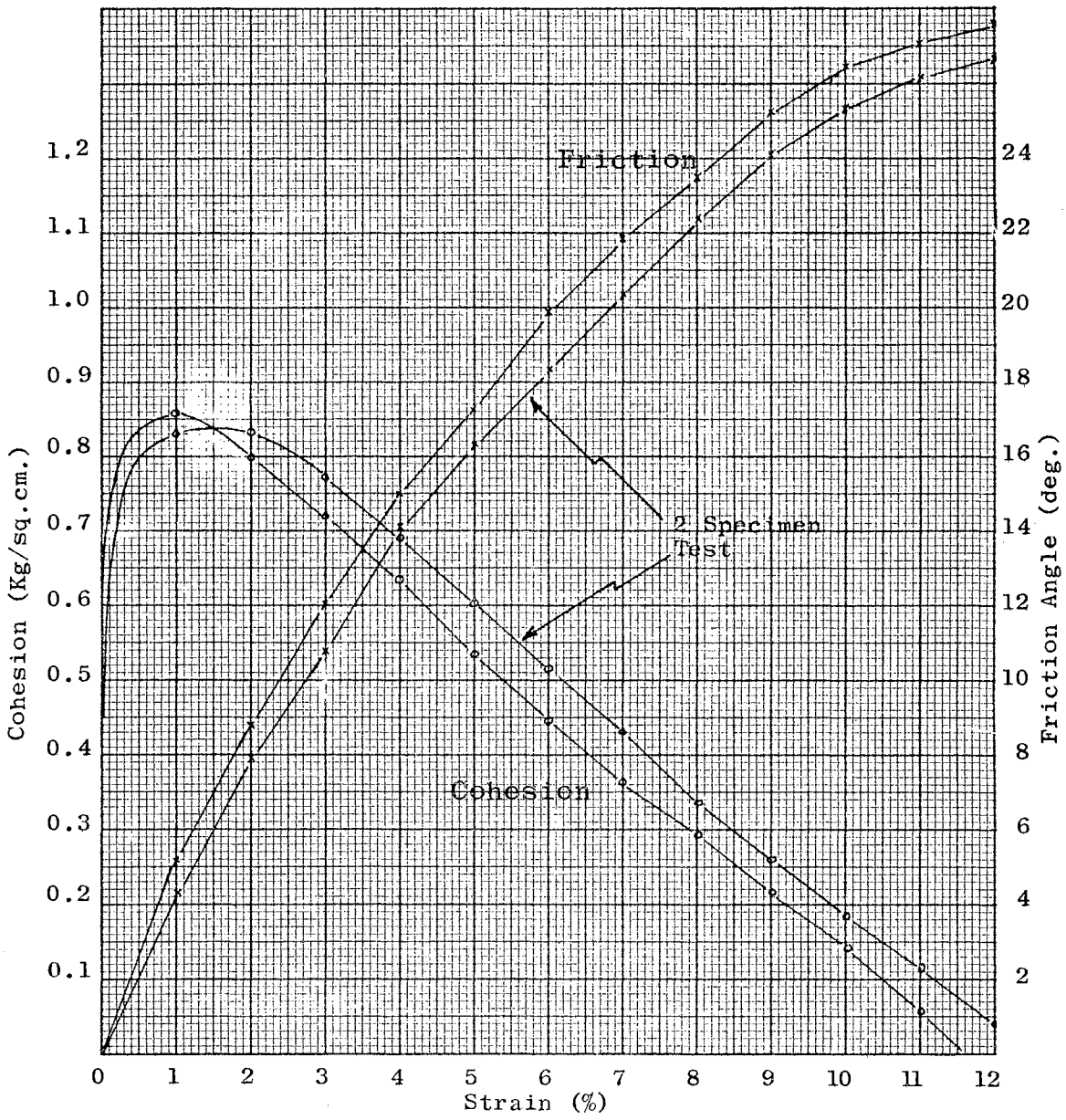

Fig. 45 - C AND ϕ VERSUS STRAIN - AN-L-1

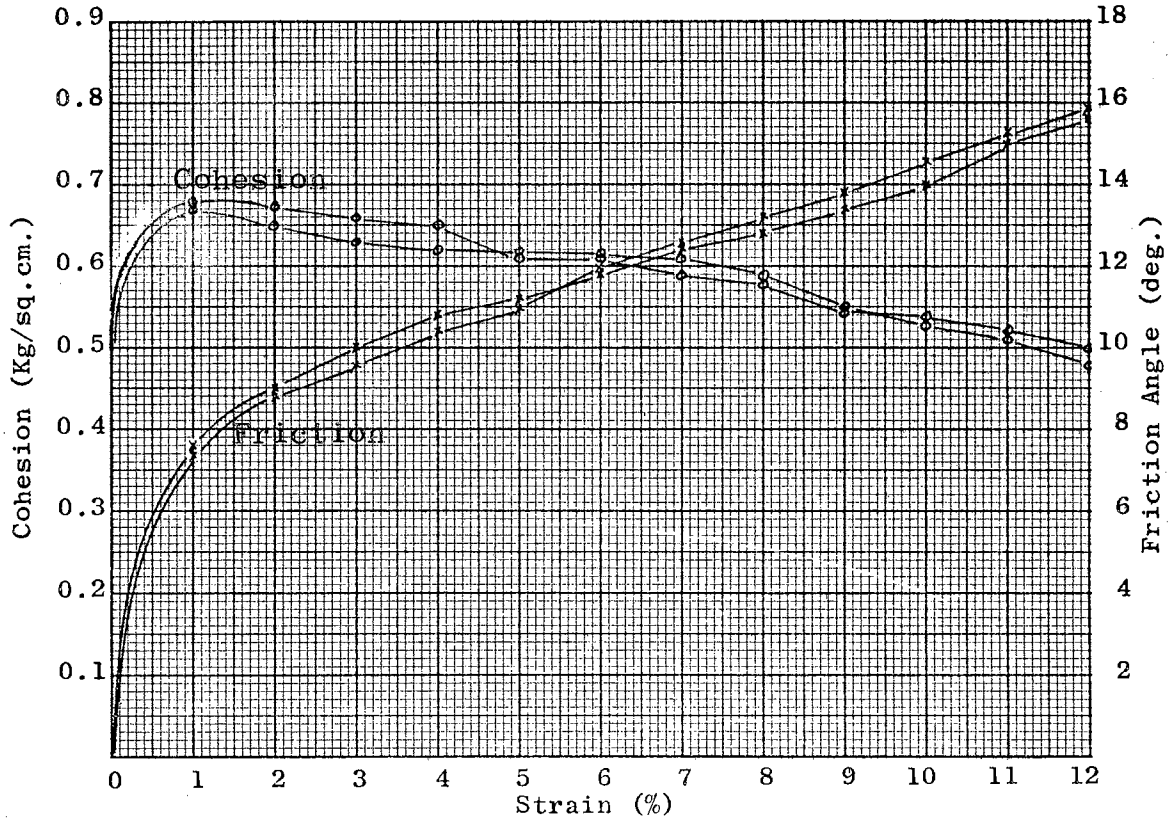

Fig. 46 - C AND Φ VERSUS STRAIN - AN-H-2

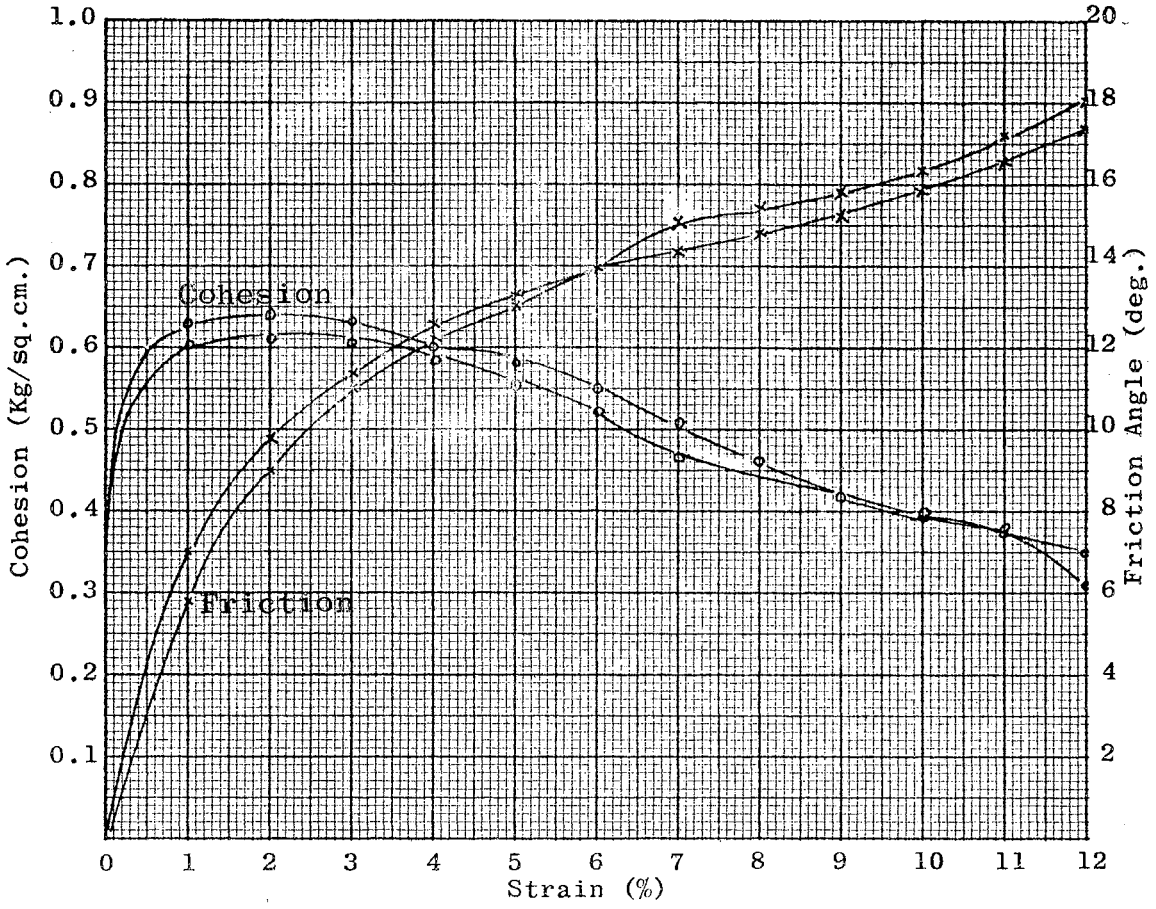

Fig. 47 - C AND ϕ VERSUS STRAIN - AN-M-2

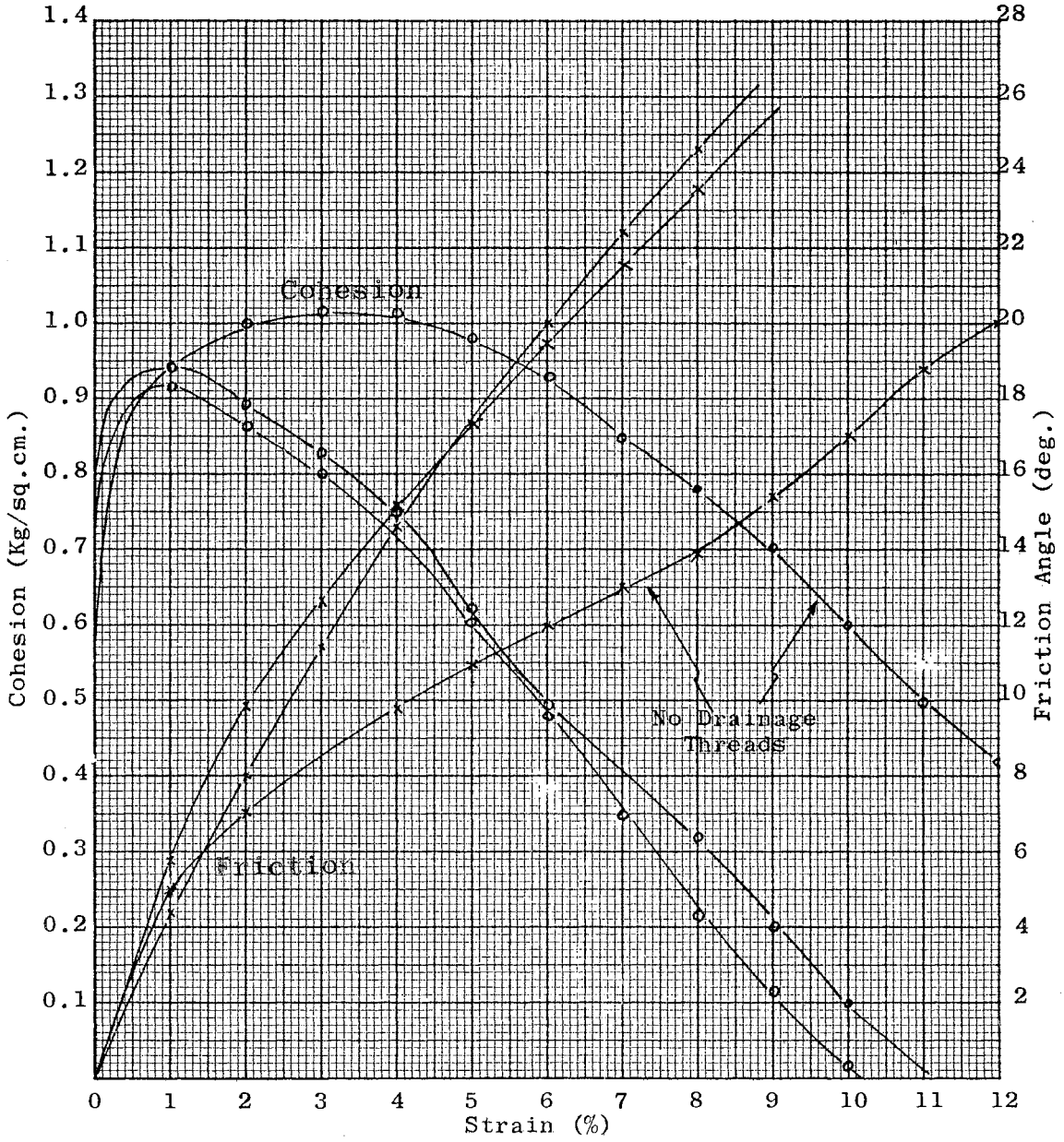

Fig. 48 - C AND Φ VERSUS STRAIN - AN-L-2

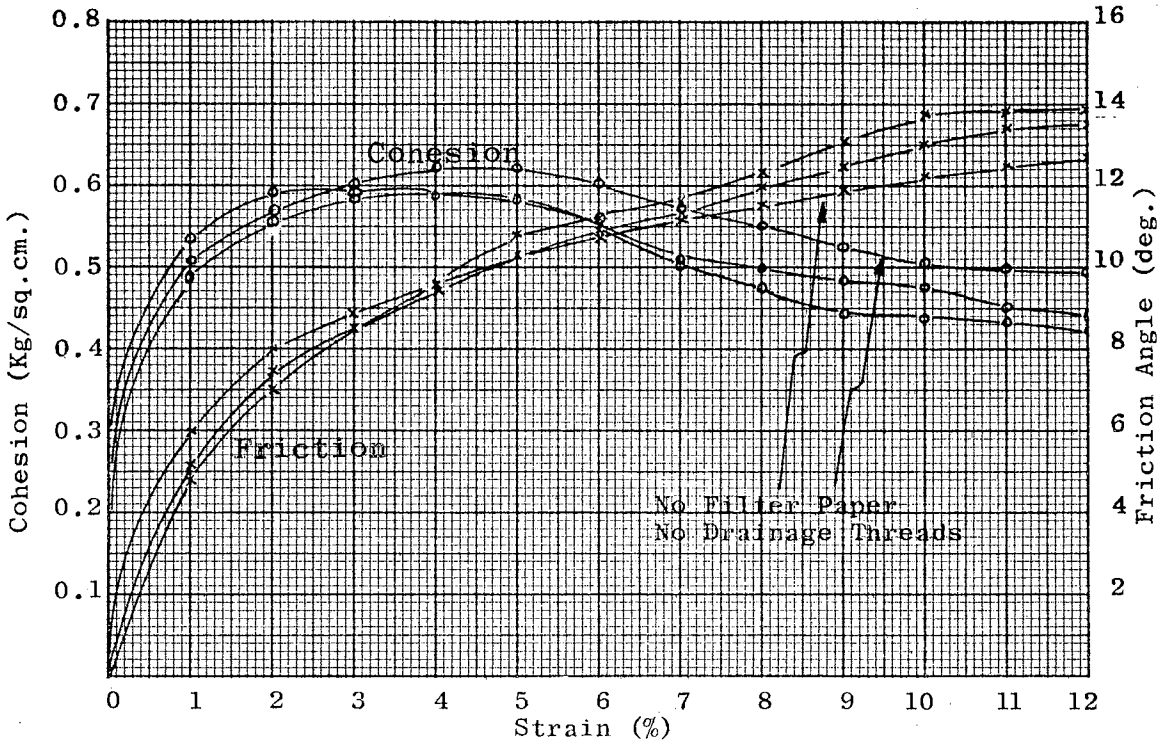

Fig. 49 - C AND ϕ VERSUS STRAIN - IS-H-1

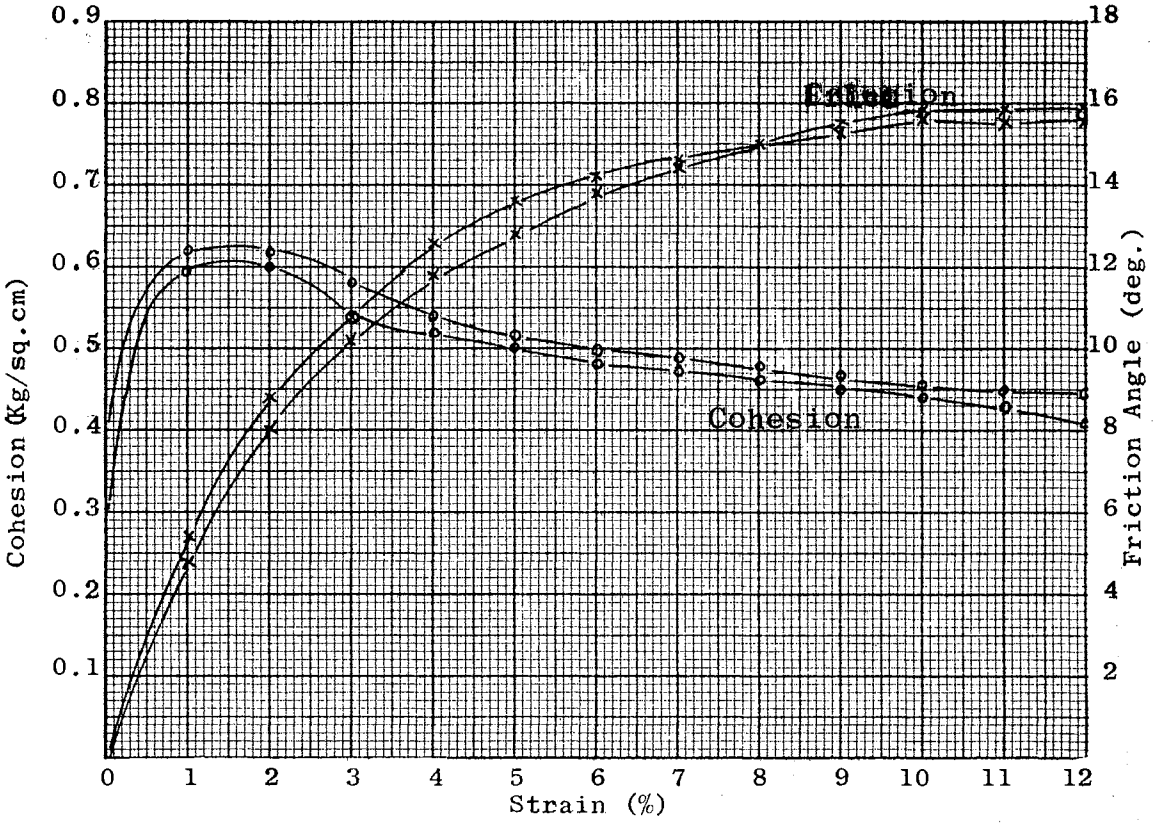

Fig. 50 - C AND ϕ VERSUS STRAIN - IS-M-1

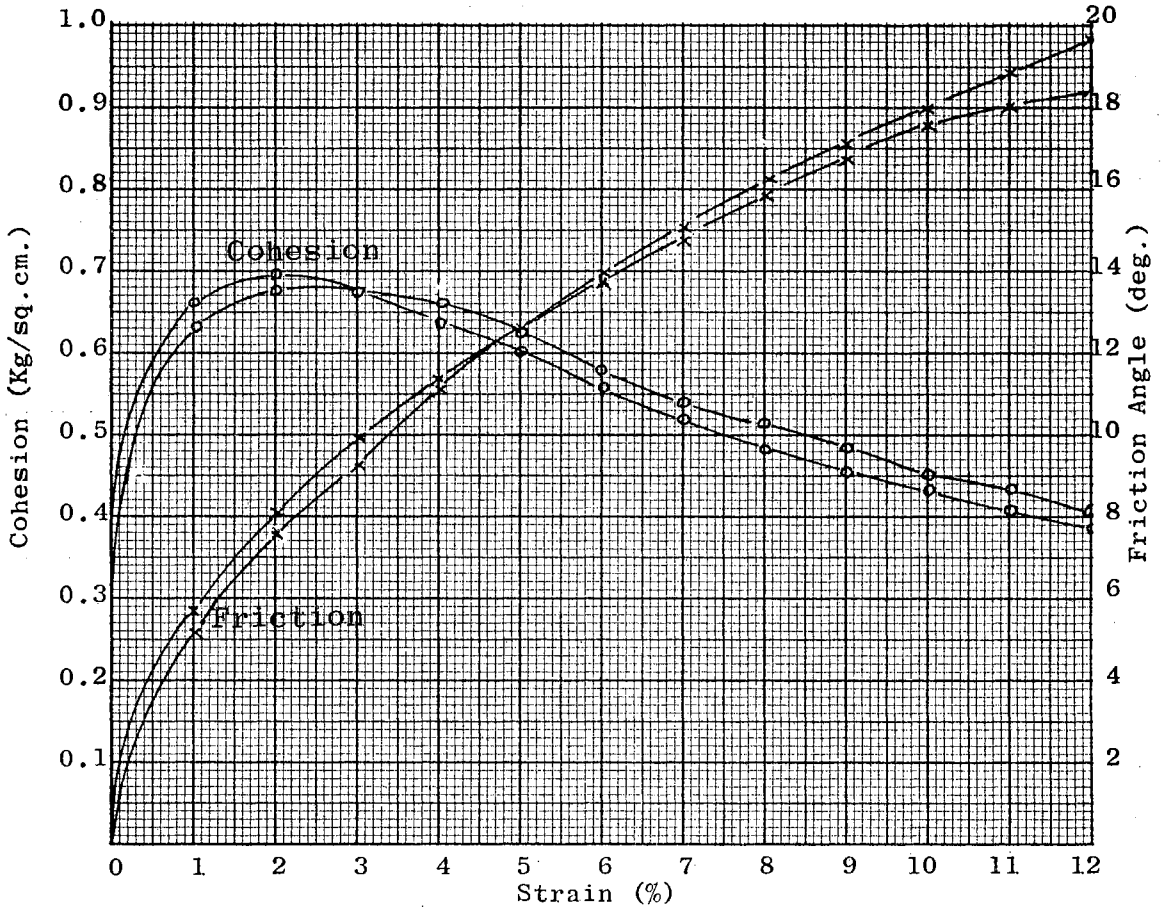

Fig. 51 - C AND ϕ VERSUS STRAIN - IS-L-1

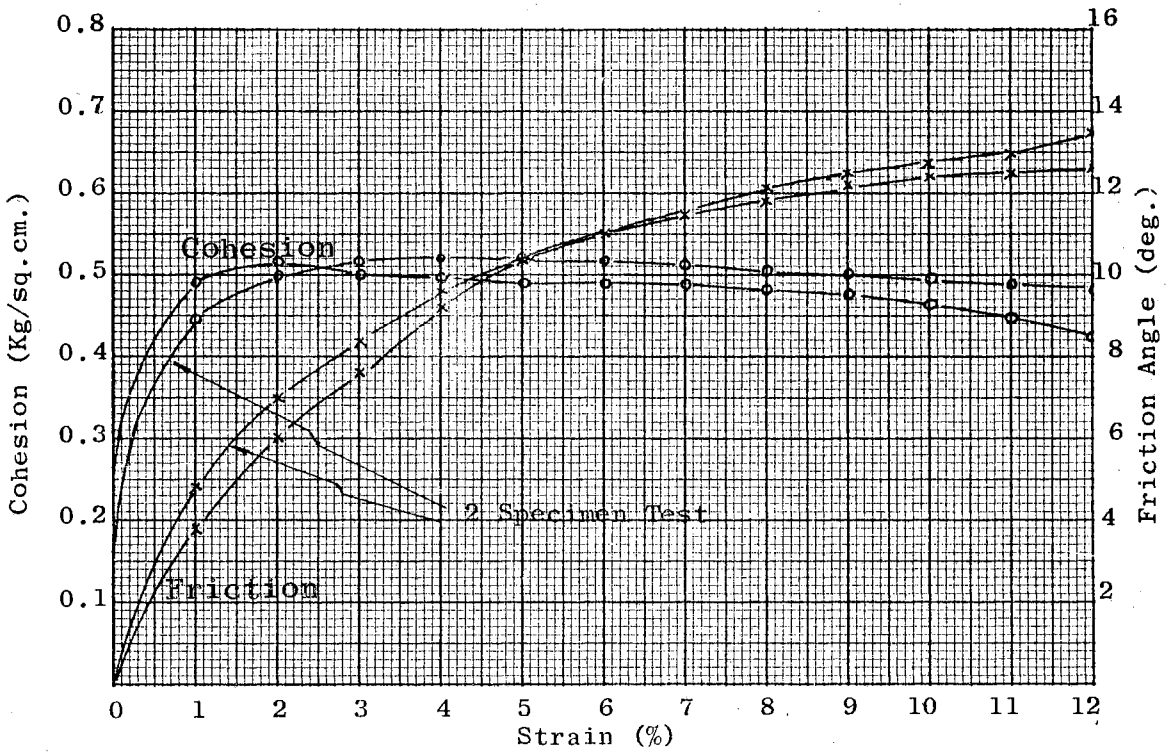

Fig. 52 - C AND ϕ VERSUS STRAIN - IS-H-2

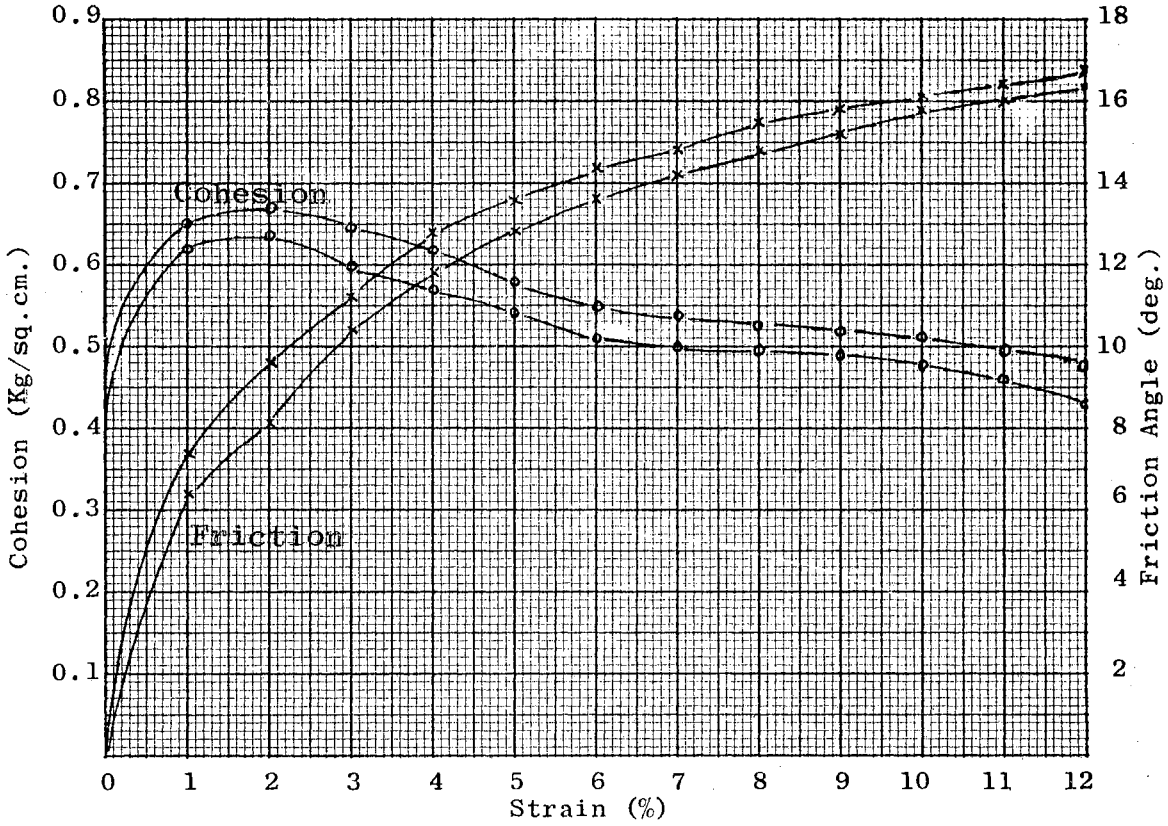

Fig. 53 - C AND ϕ VERSUS STRAIN - IS-M-2

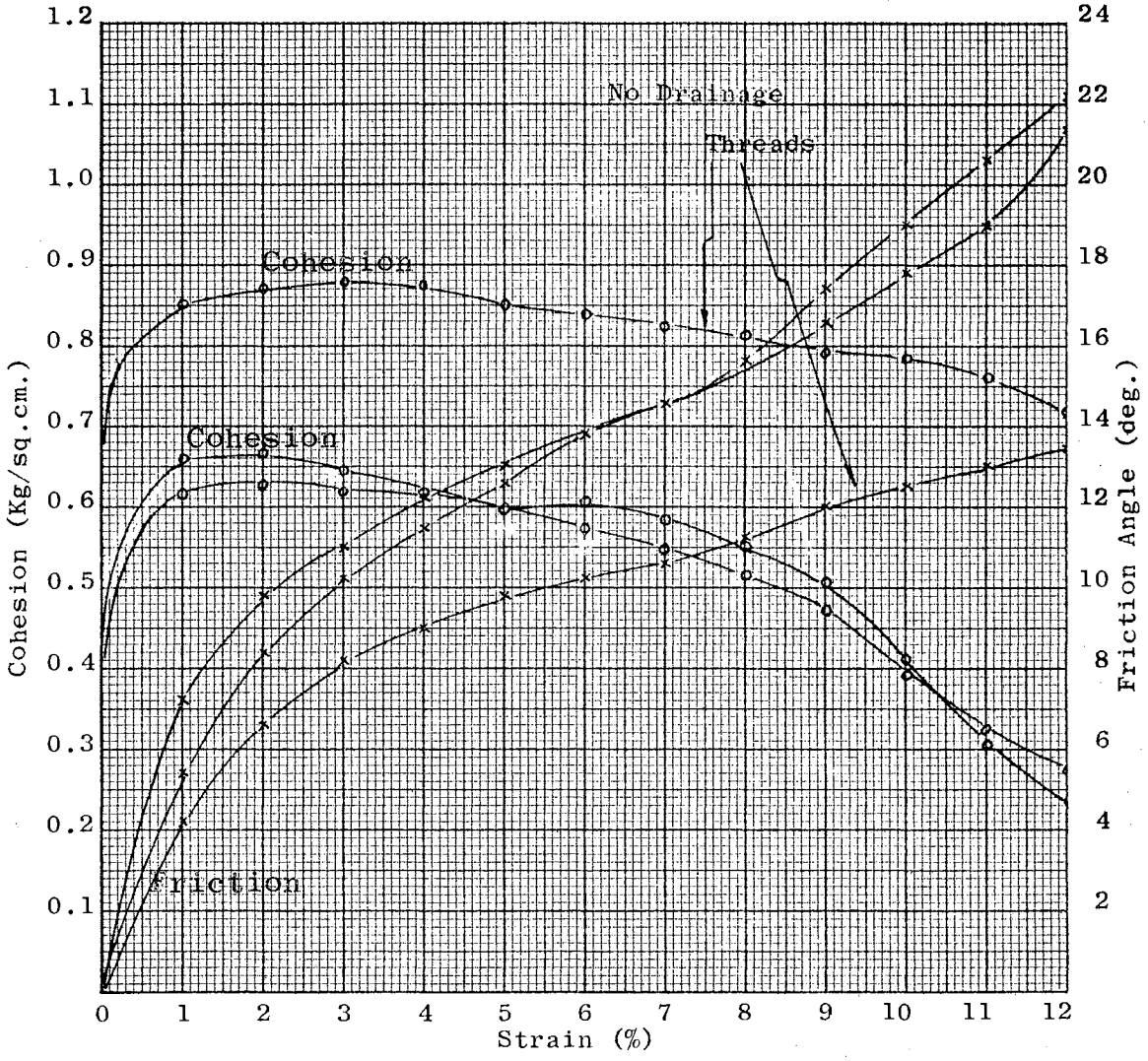

Fig. 54 - C AND ϕ VERSUS STRAIN - IS-L-2

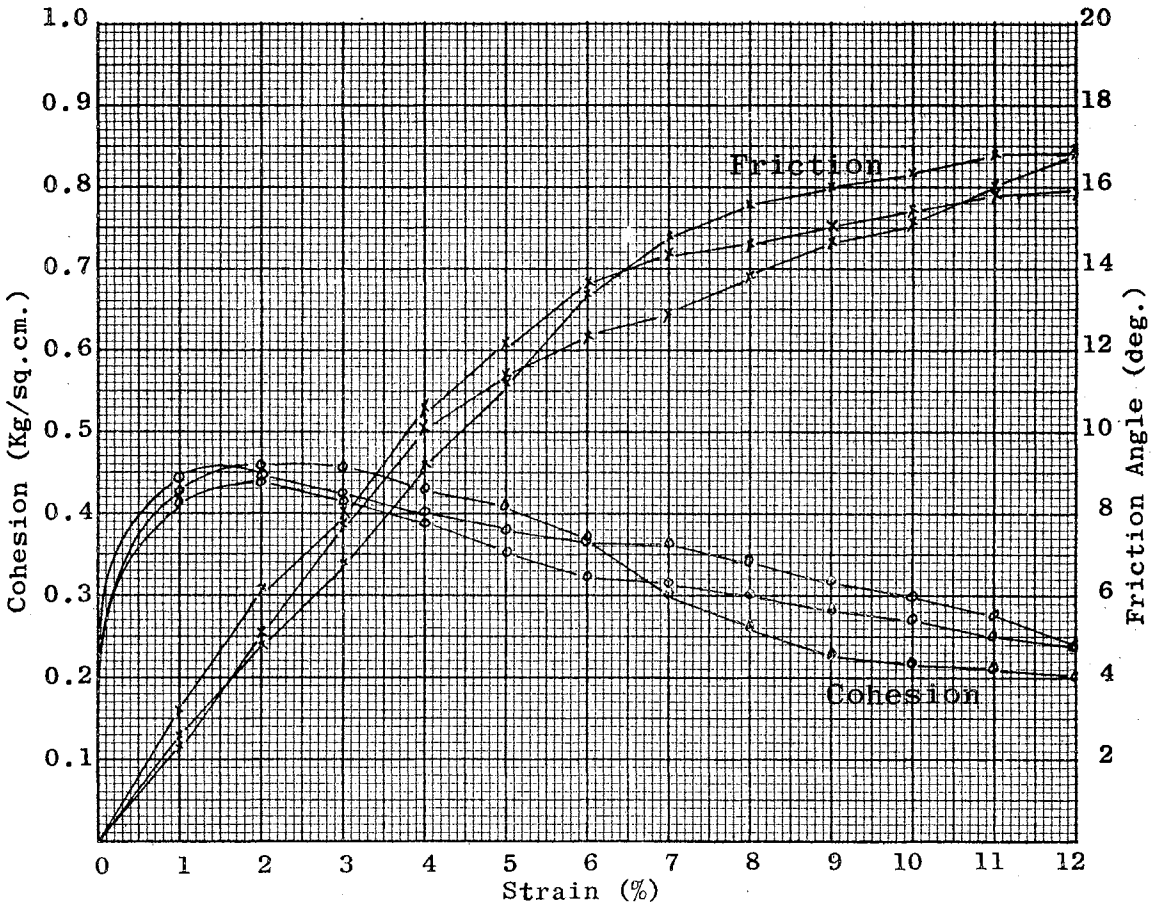

Fig. 55 - C AND ϕ VERSUS STRAIN - HC-H

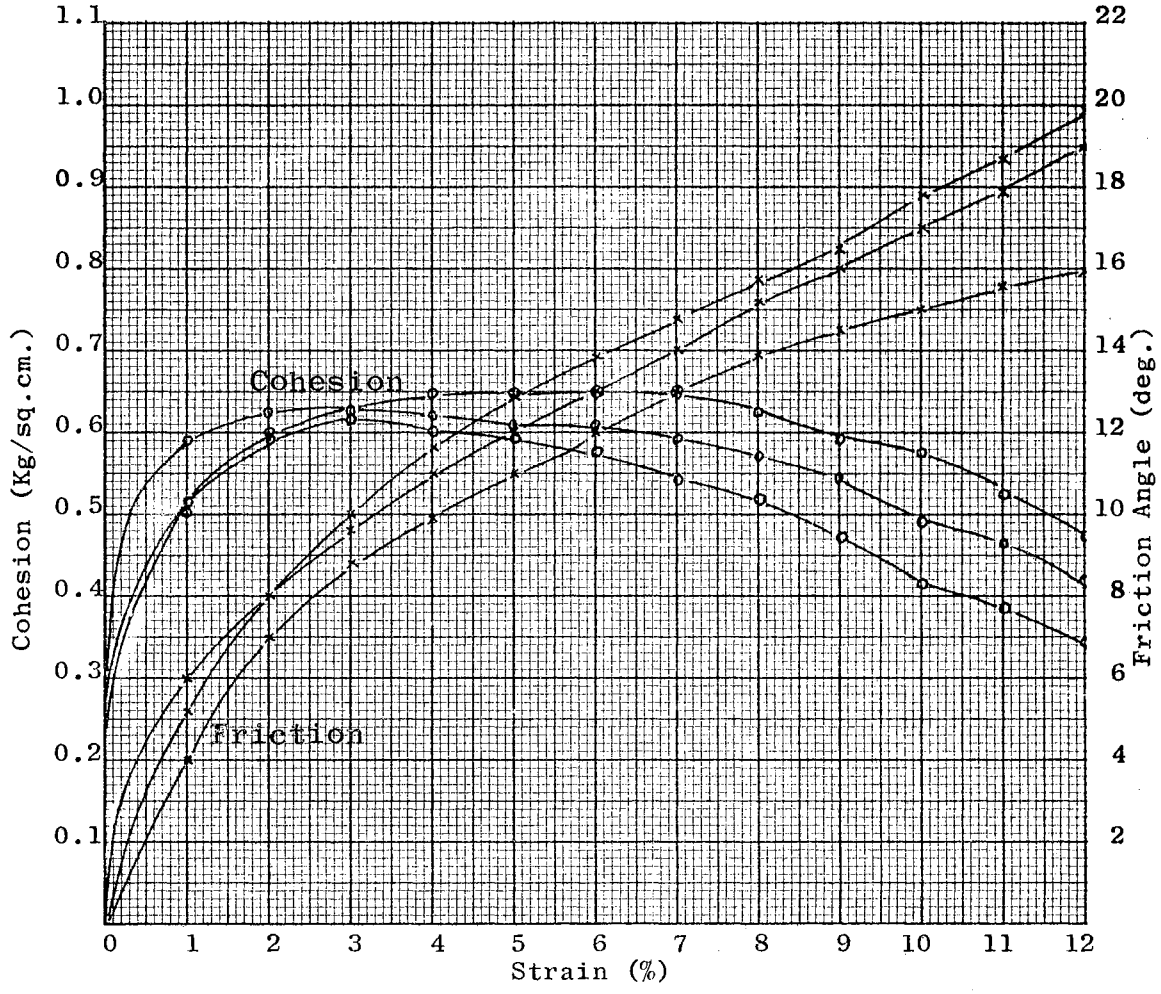

Fig. 56 - C AND ϕ VERSUS STRAIN - HC-M

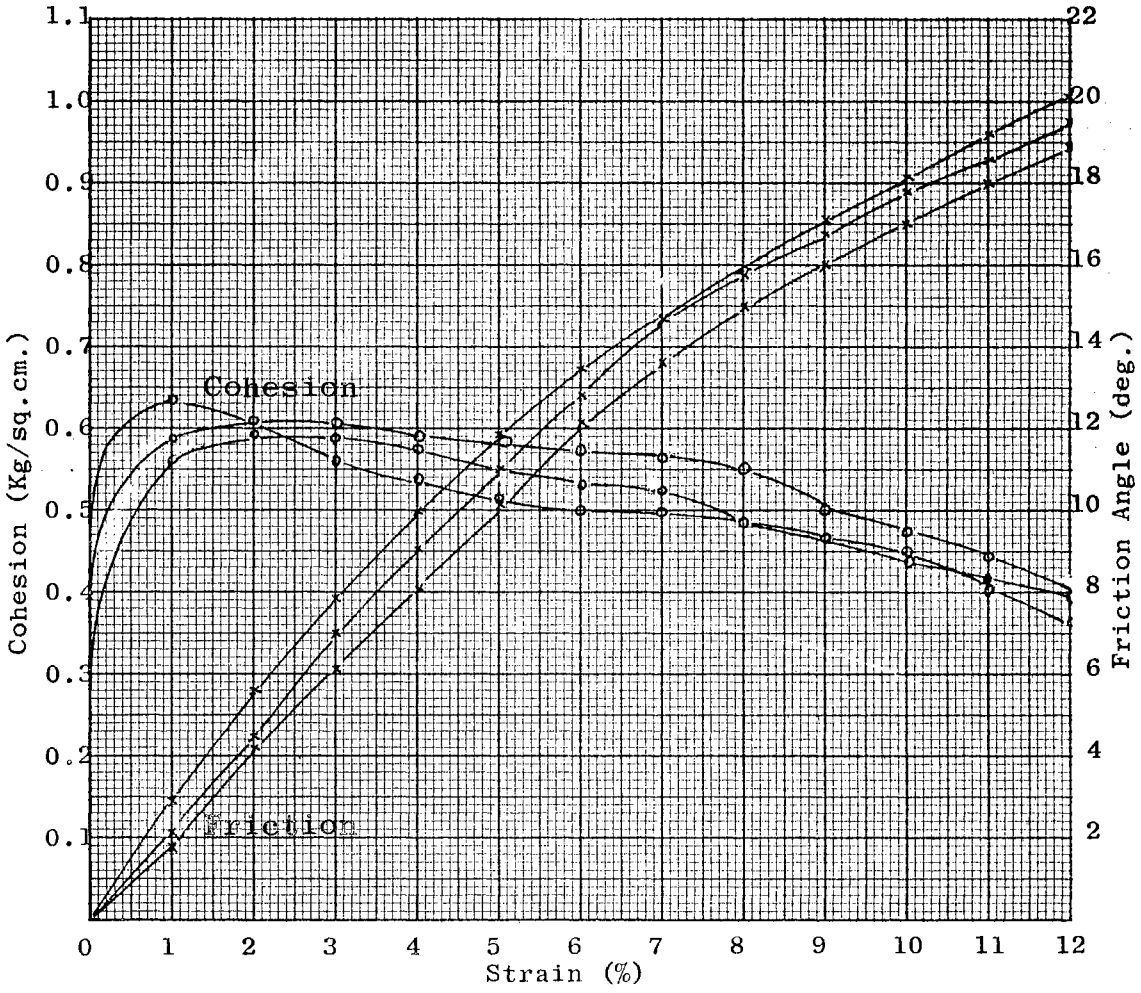

Fig. 57 - C AND ϕ VERSUS STRAIN - HC-L

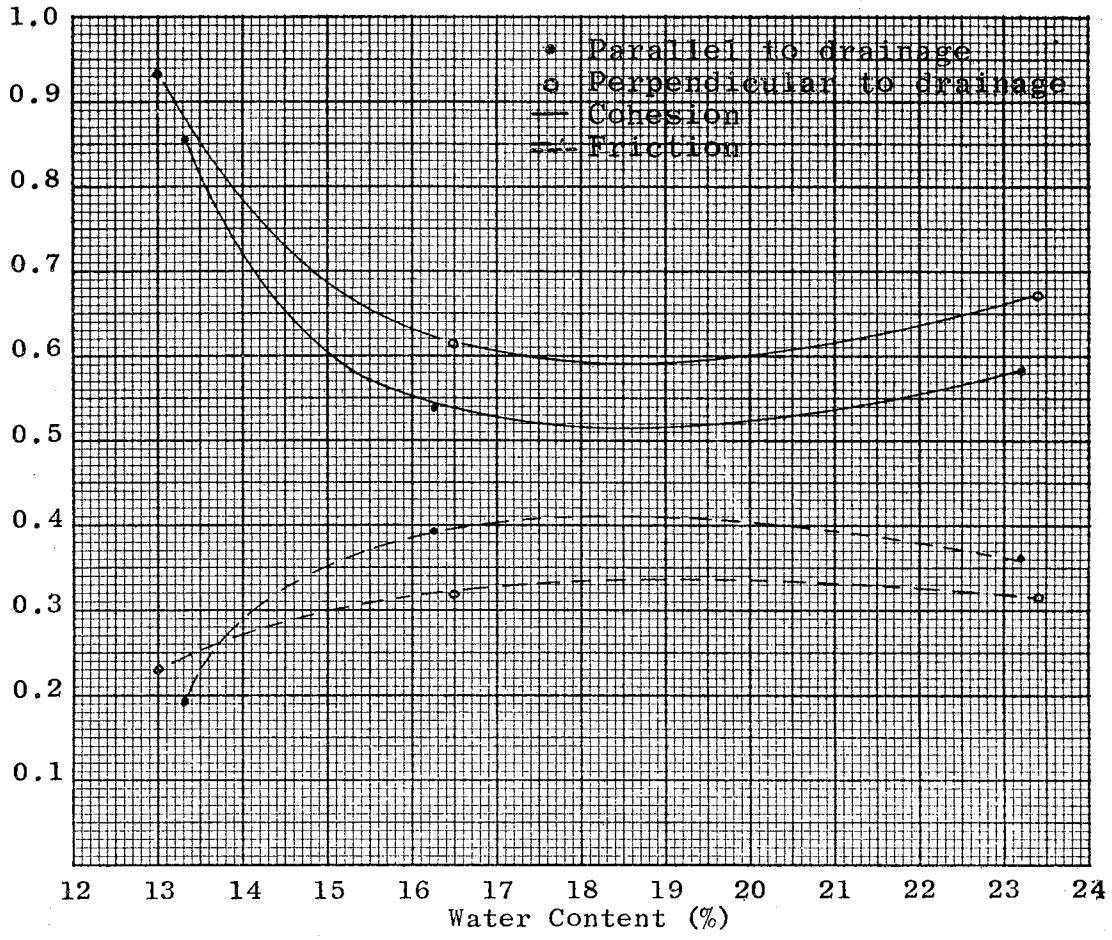

Fig. 58 - C AND ϕ VERSUS WATER CONTENT, Anisotropically Consolidated, 1% Strain

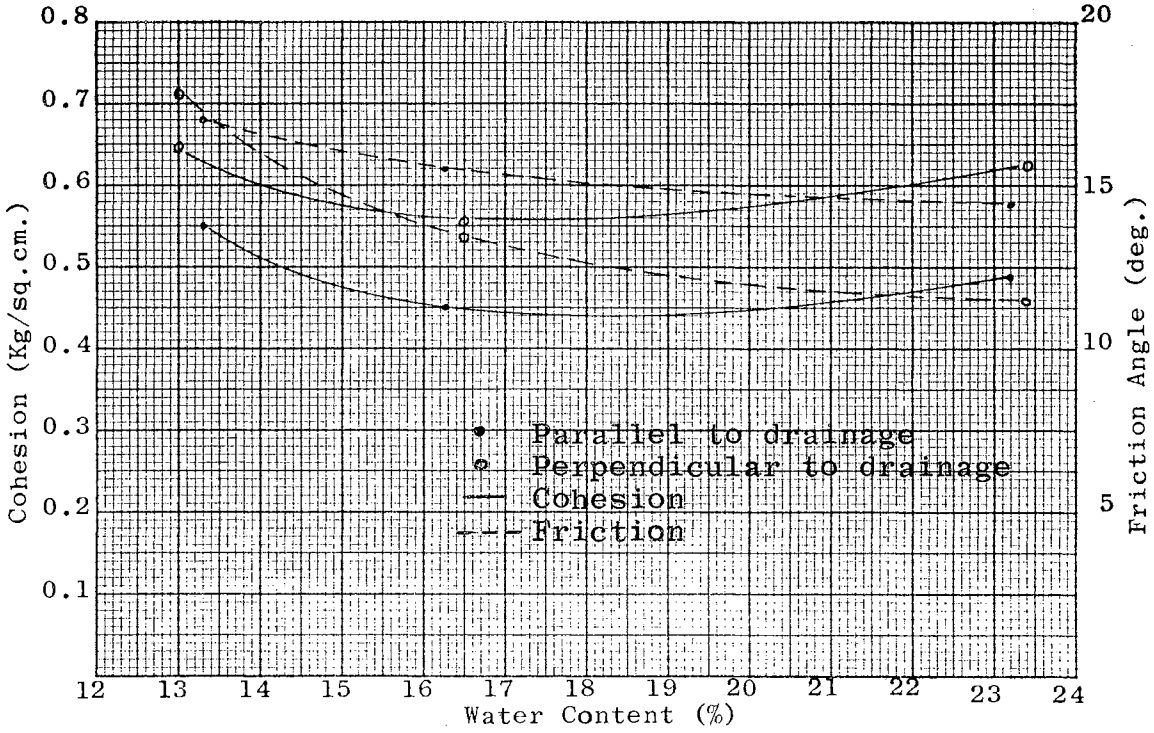

Fig. 59 - C AND ϕ VERSUS WATER CONTENT, Anisotropically Consolidated, 5% Strain

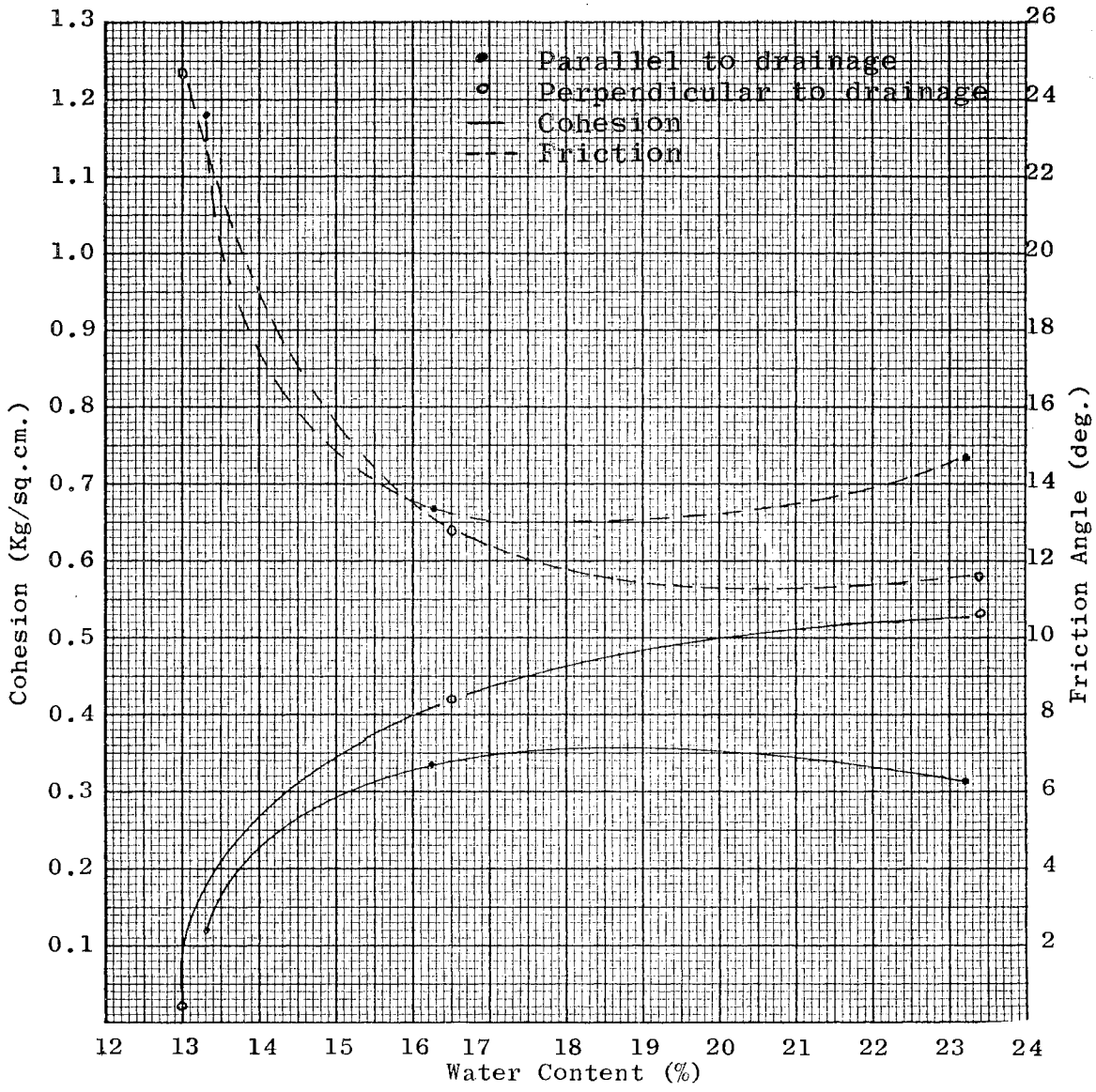

Fig. 60 - C AND ϕ VERSUS WATER CONTENT, Anisotropically Consolidated, 10% Strain

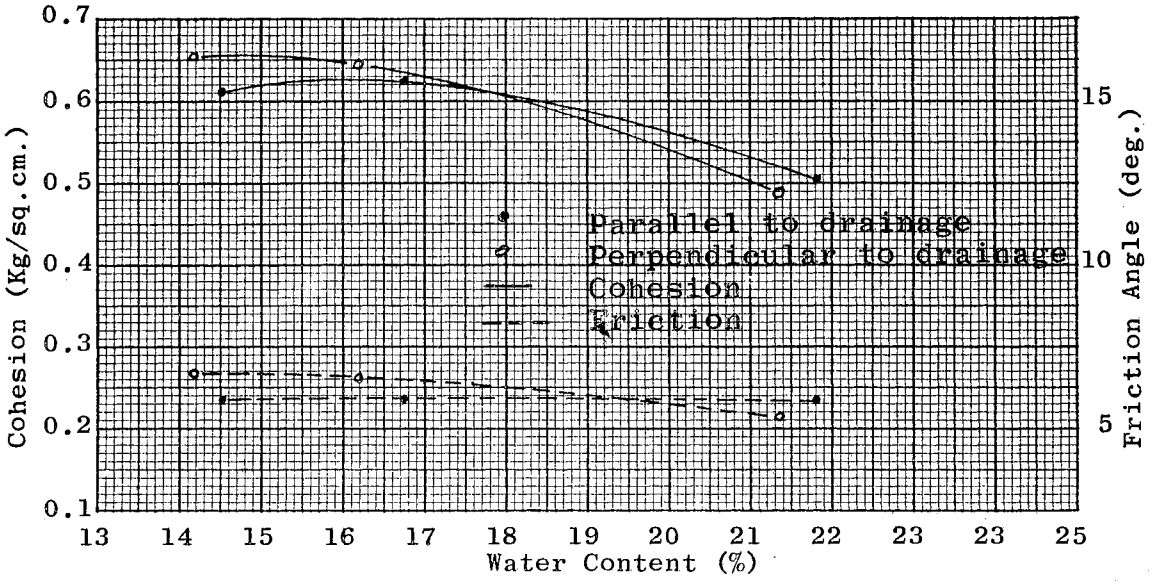

Fig. 61 - C AND ϕ VERSUS WATER CONTENT, Isotropically Consolidated, 1% Strain

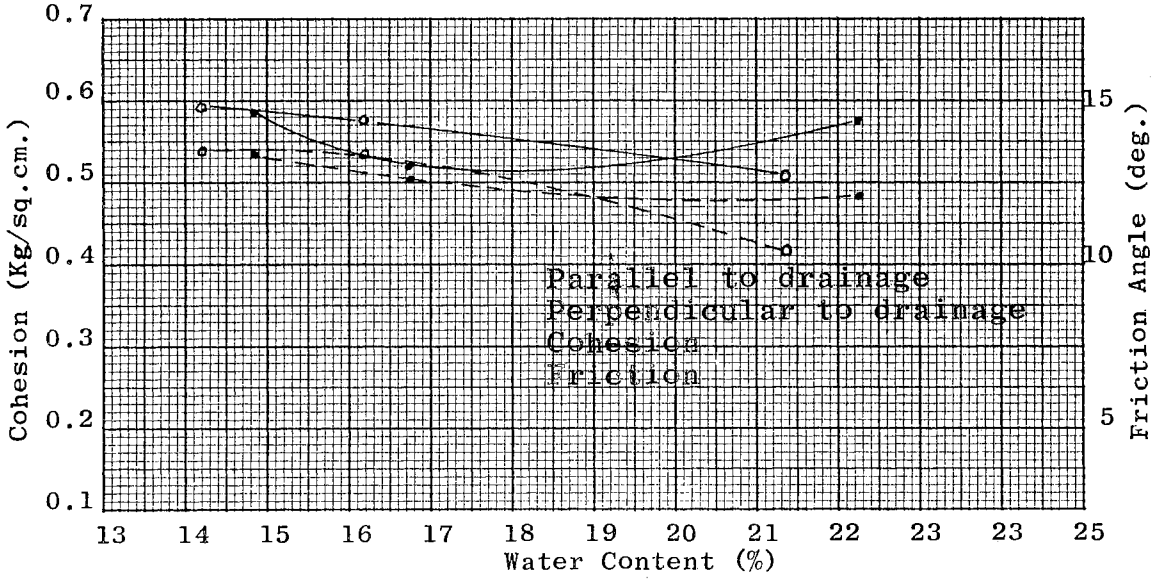

Fig. 62 - C AND ϕ VERSUS WATER CONTENT, Isotropically Consolidated, 5% Strain

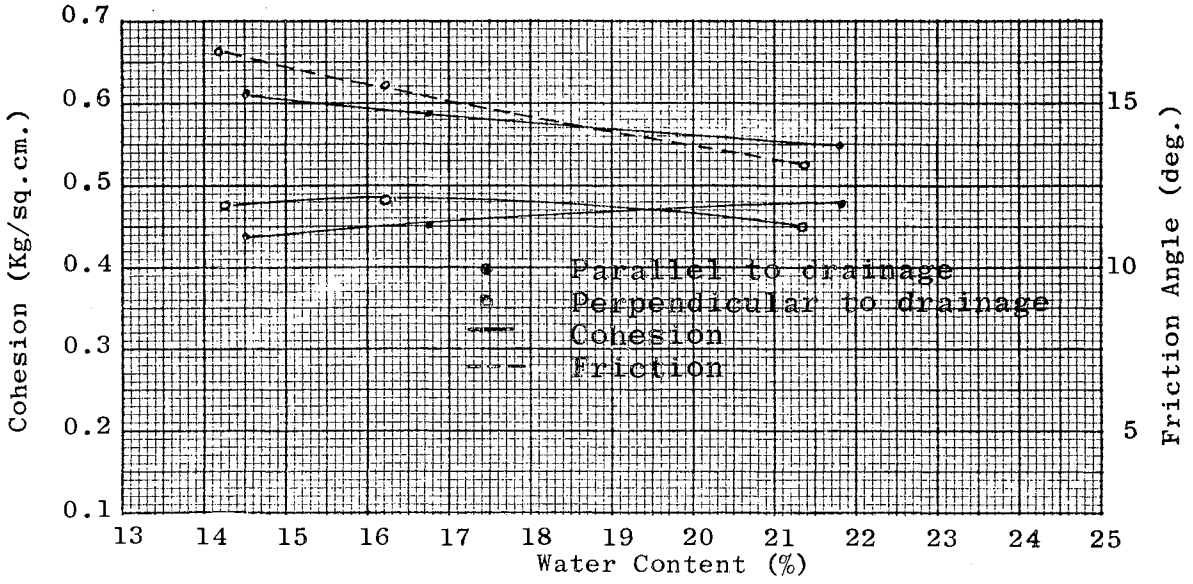

Fig. 63 - C AND Φ VERSUS WATER CONTENT, Isotropically Consolidated, 10% Strain

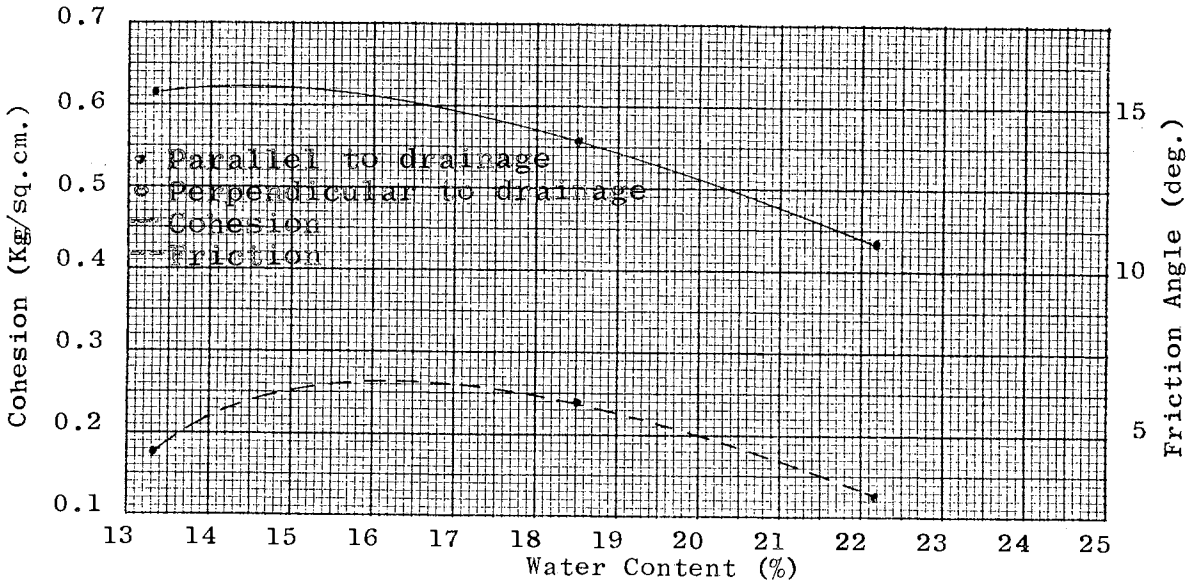

Fig. 64 - C AND Φ VERSUS WATER CONTENT, Compacted, 1% Strain

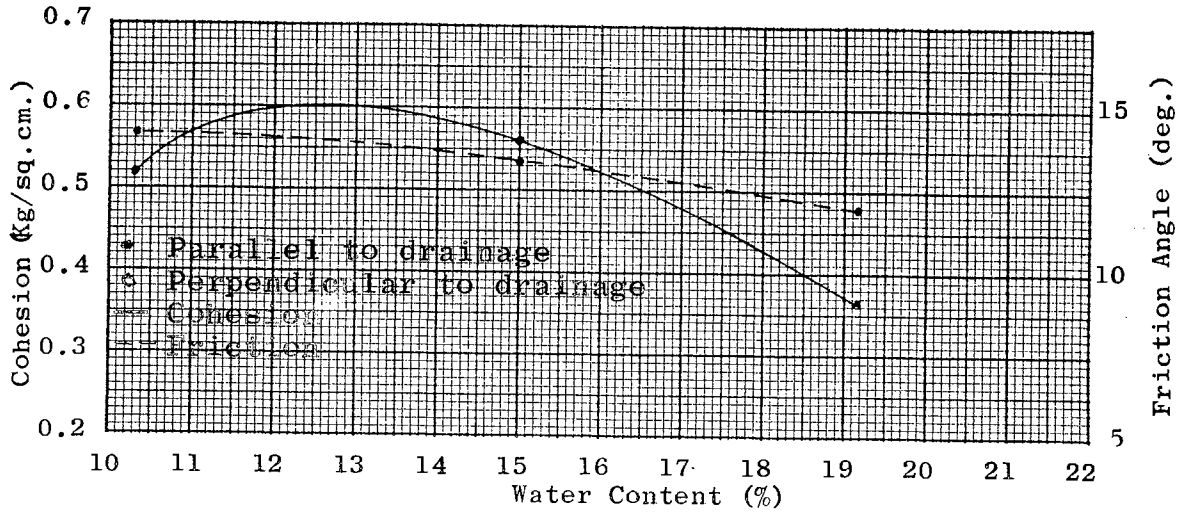

Fig. 65 - C AND ϕ VERSUS WATER CONTENT, Compacted, 5% Strain

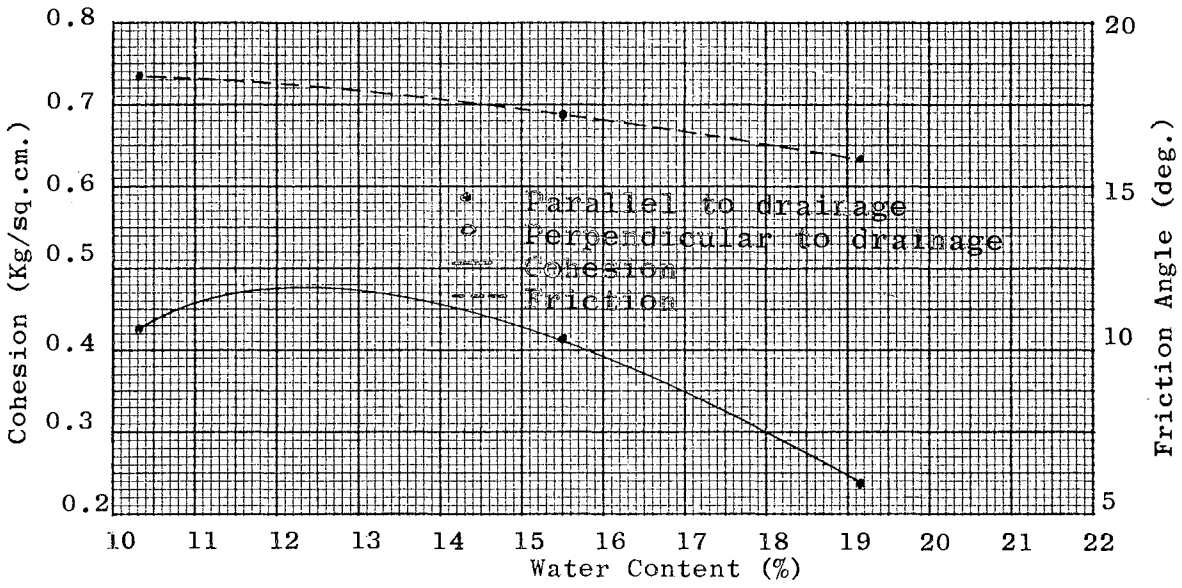

Fig. 66 - C AND ϕ VERSUS WATER CONTENT, Compacted, 10% Strain

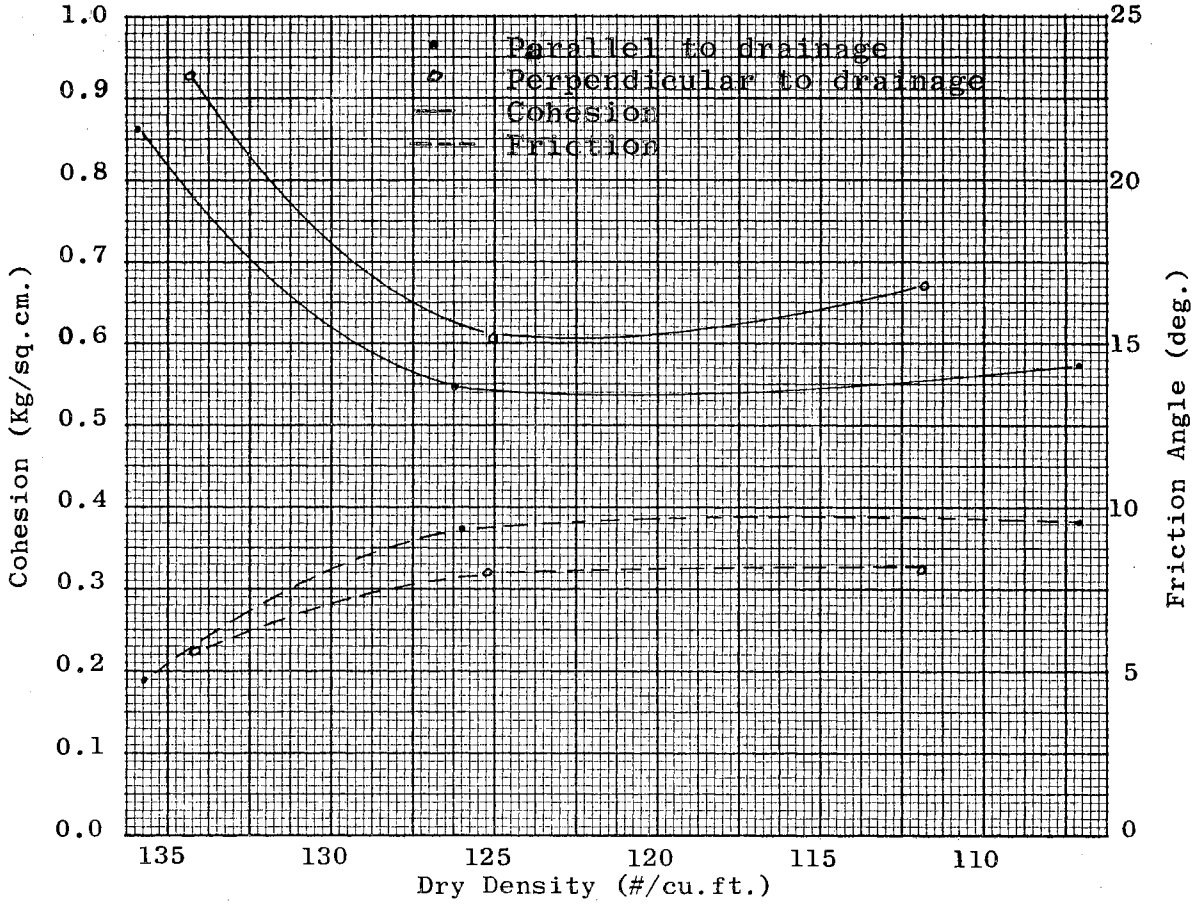

Fig. 67 - C AND ϕ VERSUS DRY DENSITY, Anisotropically Consolidated, 1% Strain

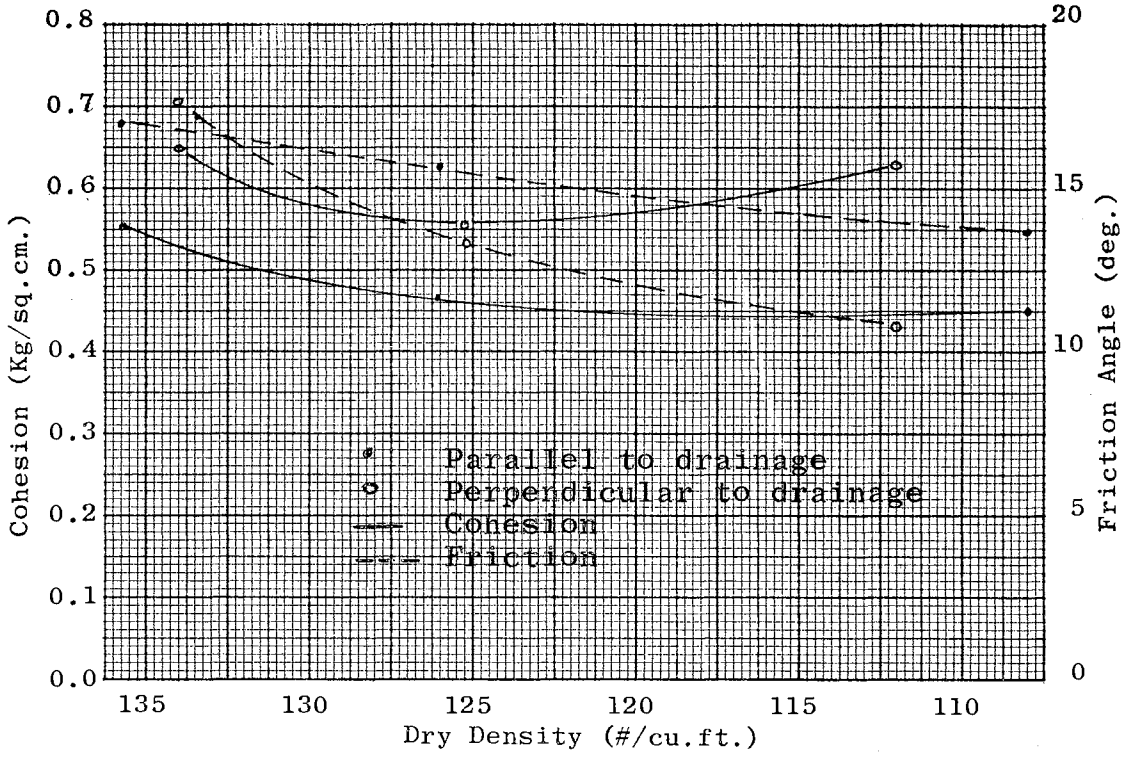

Fig. 68 - C AND ϕ VERSUS DRY DENSITY, Anisotropically Consolidated, 5% Strain

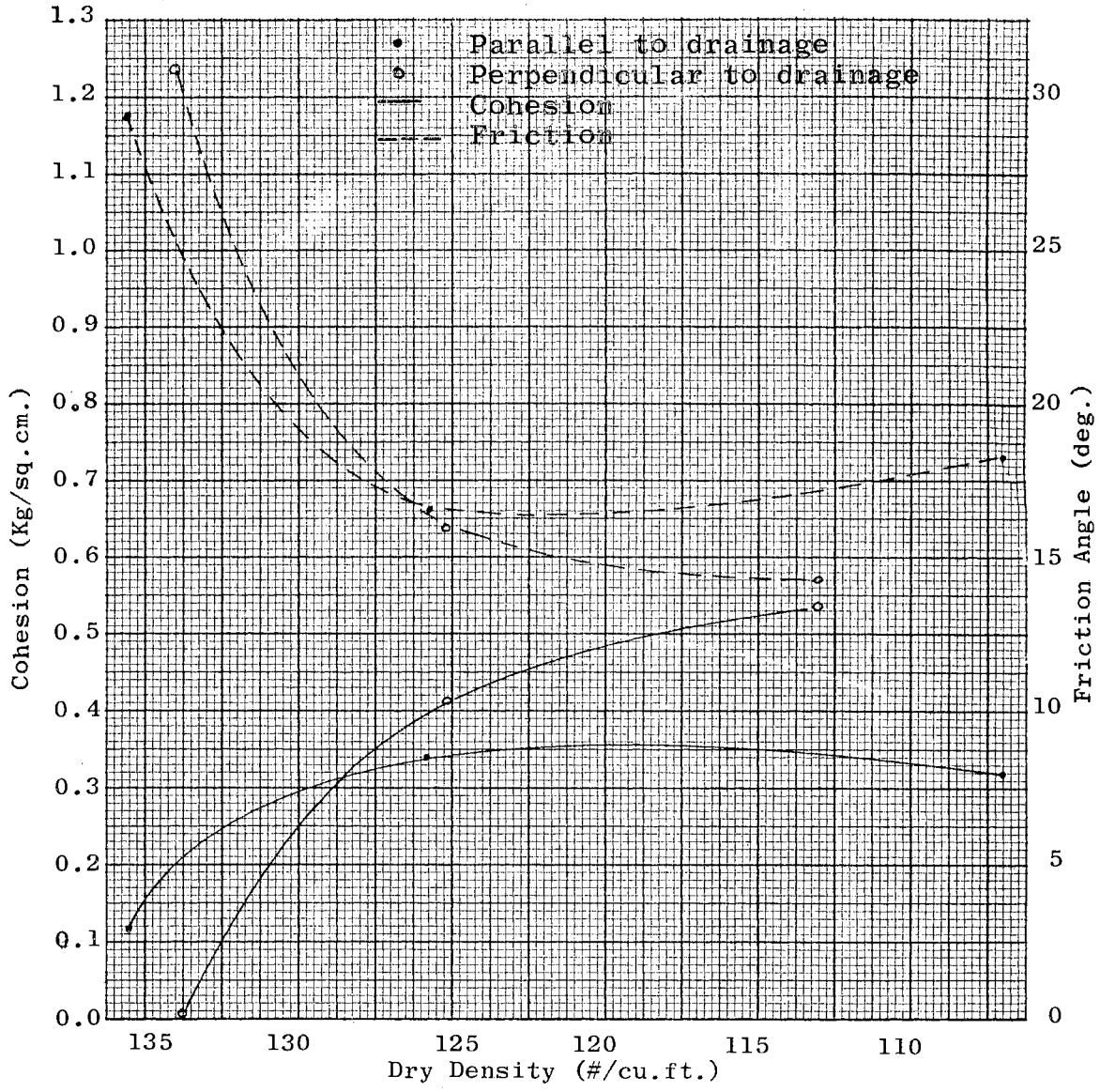

Fig. 69 - C AND ϕ VERSUS DRY DENSITY, Anisotropically Consolidated, 10% Strain

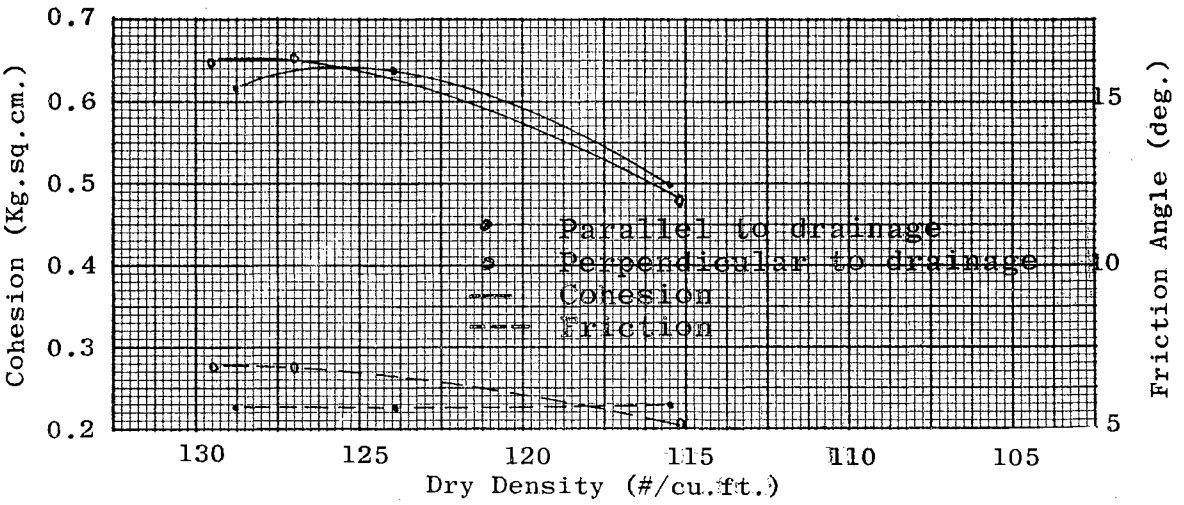

Fig. 70 - C AND ϕ VERSUS DRY DENSITY, Isotropically Consolidated, 1% Strain

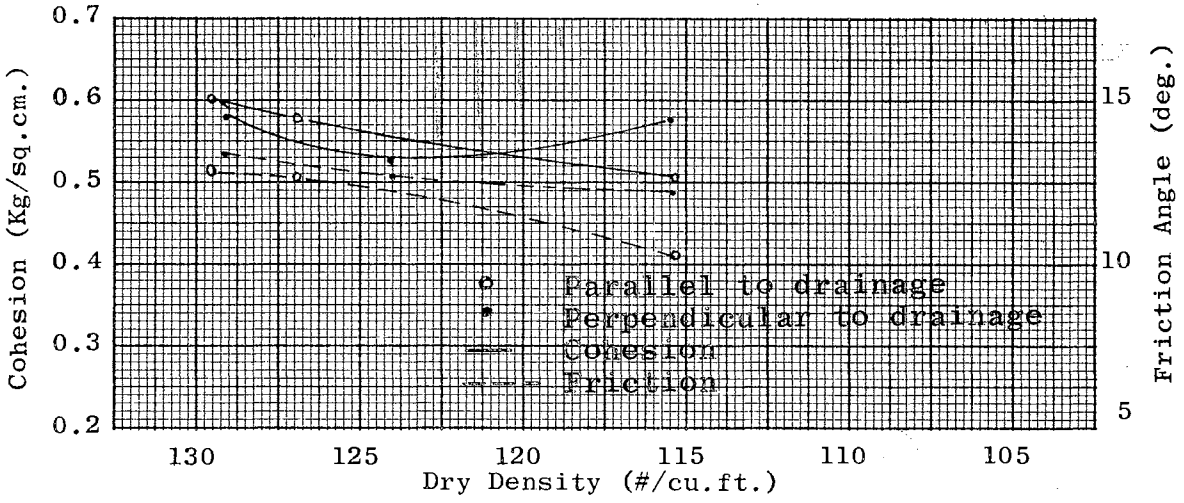

Fig. 71 - C AND ϕ VERSUS DRY DENSITY, Isotropically Consolidated, 5% Strain

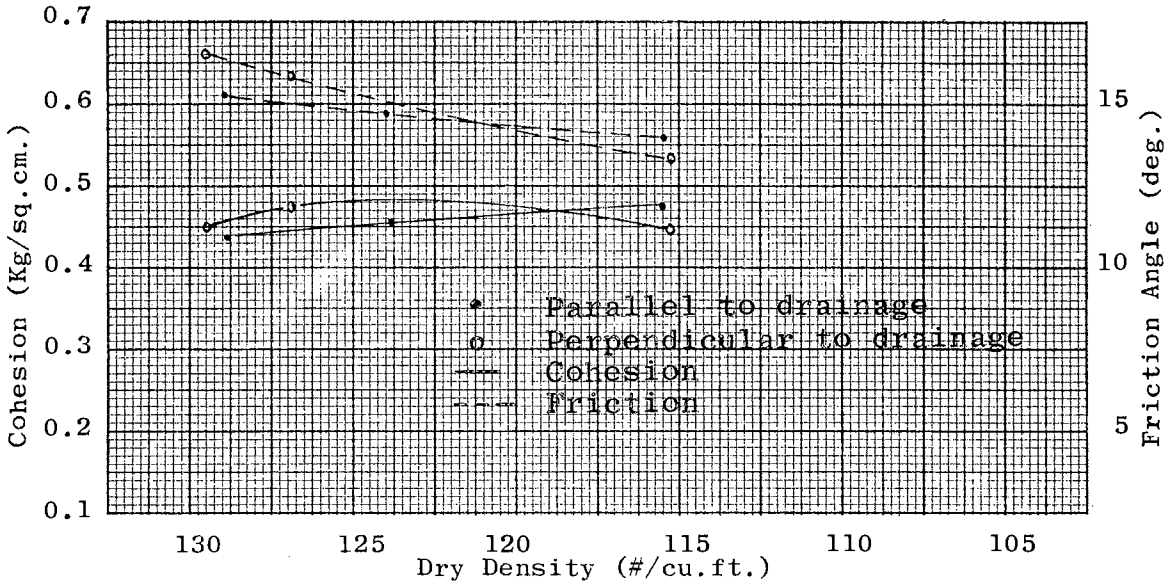

Fig. 72 - C AND ϕ VERSUS DRY DENSITY, Isotropically Consolidated, 10% Strain

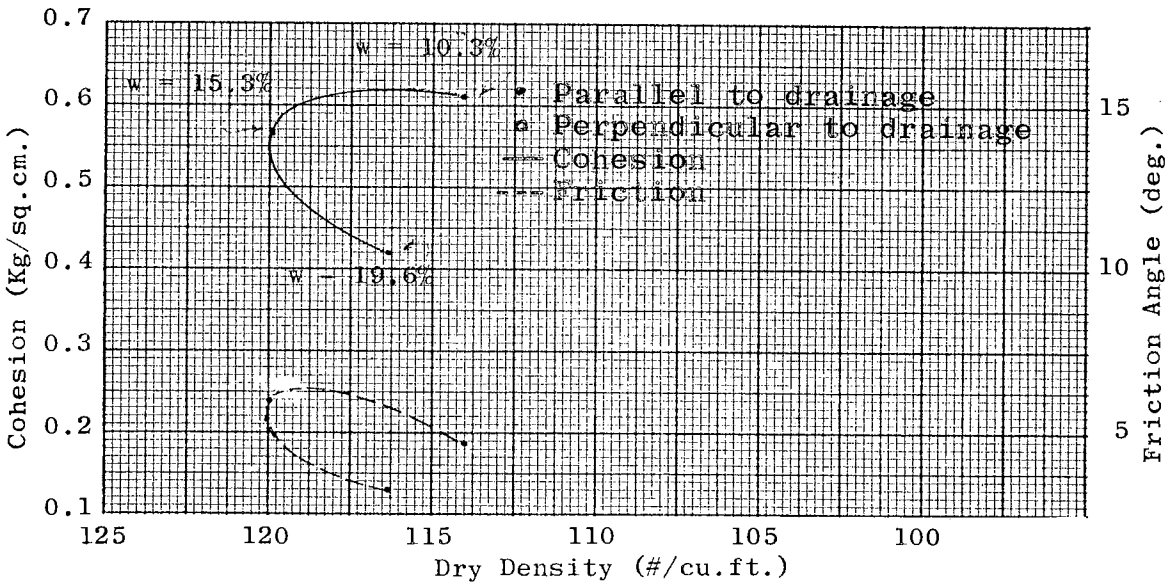

Fig. 73 - C AND ϕ VERSUS DRY DENSITY, Compacted, 1% Strain

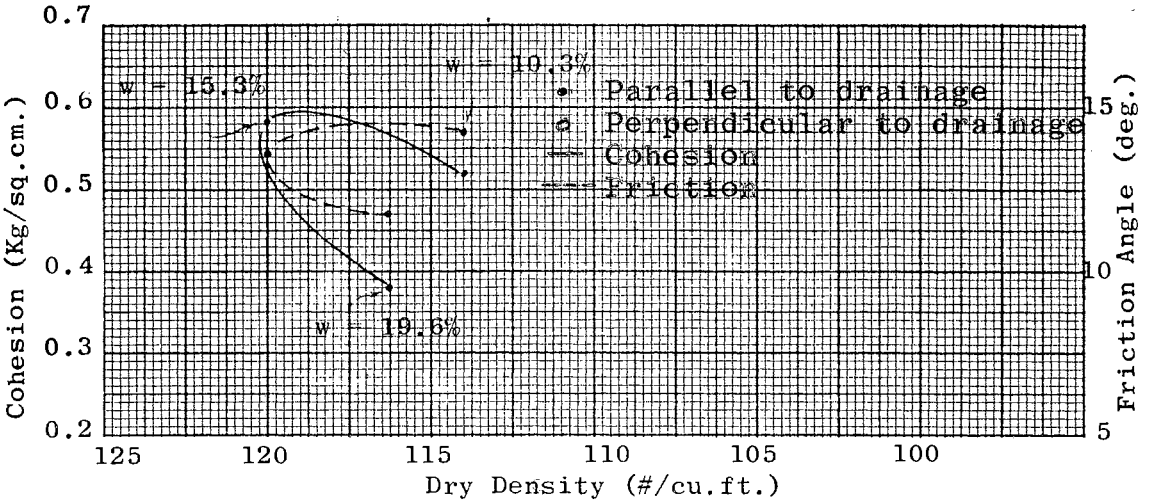

Fig. 74 - C AND ϕ VERSUS DRY DENSITY, Compacted, 5% Strain

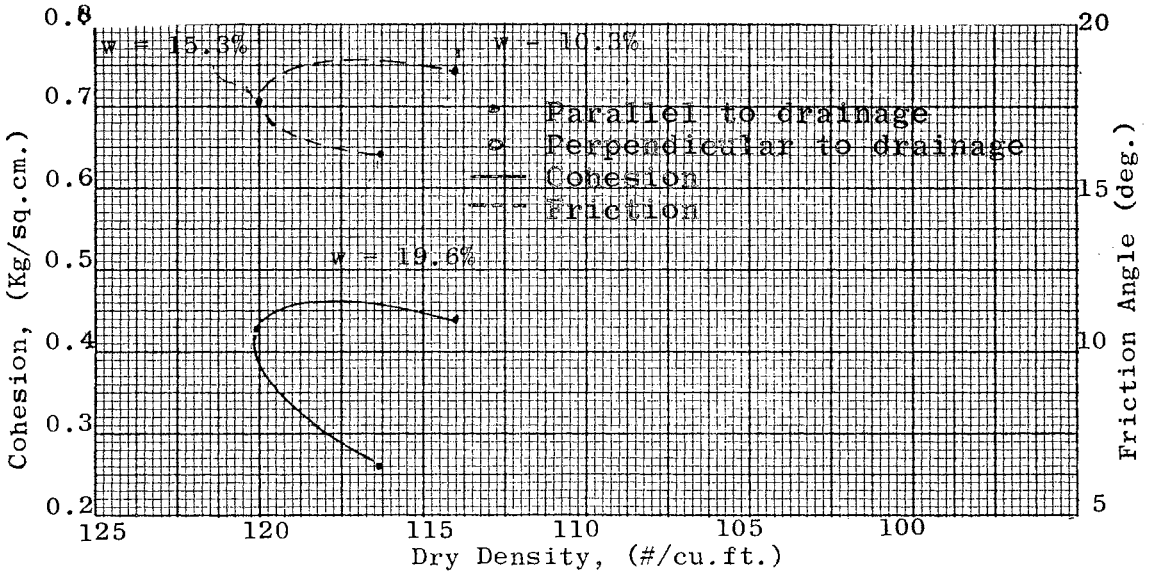

Fig. 75 - C AND ϕ VERSUS DRY DENSITY, Compacted, 10% Strain

VITA

T. J. Chung

Candidate for the Degree of

Doctor of Philosophy

Thesis: ANALYSIS OF COHESIVE AND FRICTIONAL RESISTANCE OF SOIL AS RELATED TO THE GEOMETRICAL CONFIGURATION OF THE PARTICLES

Major Field: Civil Engineering

Biographical:

Personal Data: Born in Sunchon, Korea, May 20, 1929, the son of Kutaek and Yona Chung.

Education: Graduated from Sunchon High School, Korea, in 1946; received the Professional Engineering Diploma from Seoul National University, in 1949; received the Master of Science degree from Oklahoma State University in 1962; completed requirements for the Doctor of Philosophy degree in August, 1964.

Professional Experience: Instructor of Engineering Topography in the Korean Military Academy from 1955 to 1958; Testing Engineer in Oklahoma Testing Laboratories, Summer, 1961; Structural Engineer with Hudgins, Thompson, Ball and Associates, Oklahoma City, Oklahoma, Summer, 1962; Graduate Assistant in the Civil Engineering Department of Oklahoma State University from September, 1961, to date.

Organizations: Associate member, Sigma Xi; member Chi Epsilon; Associate member, American Society of Civil Engineers.